Finding of New Functions of Heme Proteins Based on Crystal Structures

（結晶構造を基にしたヘムタンパク質の新規機能の創出）

Chikako SHIRATAKI

白瀧　千夏子

Contents

Chapter I *3*

General Introduction

Chapter II *34*

Aromatic Ring Hydroxylation by Myoglobin Mutants

Chapter III *59*

Capture of Artificial Metal Complexes by a Heme Acquisition Protein of *Pseudomonas aeruginosa* and Its Effect for Living Cells

Chapter IV *87*

Conclusion

Chapter I

General Introduction

1-1. Heme, a natural iron complex utilized in organisms

1-2. Myoglobin as a model protein of hemoproteins

1-3. Artificial metalloproteins constructed by the replacement of their prosthetic groups

1-4. Heme acquisition system in gram-negative bacteria

1-5. Summary and outlook

Chapter I. General Introduction

1-1. Heme, a natural iron complex utilized in organisms

Iron is an abundant transition metal on the earth and an essential nutrient for most living organisms as a cofactor of proteins involved in numerous metabolic pathways.[1-3] Heme, Fe-protoporphyrin IX, is one of most important metal complexes, which include an iron ion (Fig. 1-1). Heme serves as a prosthetic group of proteins (hemoproteins) that perform diverse functions such as oxygen storage and transport (e.g. myoglobin and hemoglobin),[4-7] gas sensing (e.g. FixL and CooA),[8-11] electron transfer (e.g. cytochrome b_5 and cytochrome *c*),[12-15] and catalysis (e.g. horseradish peroxidase, chloroperoxidase, cytochrome P450, catalase, and heme oxygenase)[16-26] (Fig. 1-2, 1-3). While myoglobin and hemoglobin do not have any catalytic function, cytochrome P450 and heme oxygenase catalyze monooxygenase reactions by generating active species using molecular oxygen. The reaction catalyzed by heme oxygenase is important for the degradation of heme to recover iron ions. A gas sensor protein, FixL expressed in *Bradyrhizobium japonicum* also binds molecular oxygen, but its function is neither the oxygen storage and transportation nor the catalyst. FixL senses the level of oxygen concentration to control its kinase activity. There are hemoproteins that sense not only the oxygen concentration but also carbon monoxide concentration. CooA expressed in *Rhodospirillum rubrum* is a CO-sensing transcriptional factor that controls expression of certain genes in response to CO concentration. In contrast to hemoproteins interacting with gaseous molecules, cytochrome b_5 and cytochrome *c* do not have a space for binding gaseous molecules to the heme iron and they serve as electron transfer proteins.

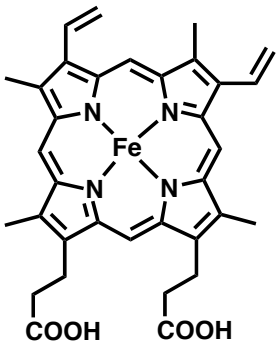

Fig. 1-1 Heme structure

In spite of diverse functions of hemoproteins, the heme serves as the sole active center of the hemoproteins. The intrinsic biological functions of the hemoproteins are governed by amino acids around the heme. Therefore, understanding the relationship between the structure of the hemoproteins and their function remains a significant challenge for the elucidation of the system of living organism and developing artificial metalloproteins for controlling functions.

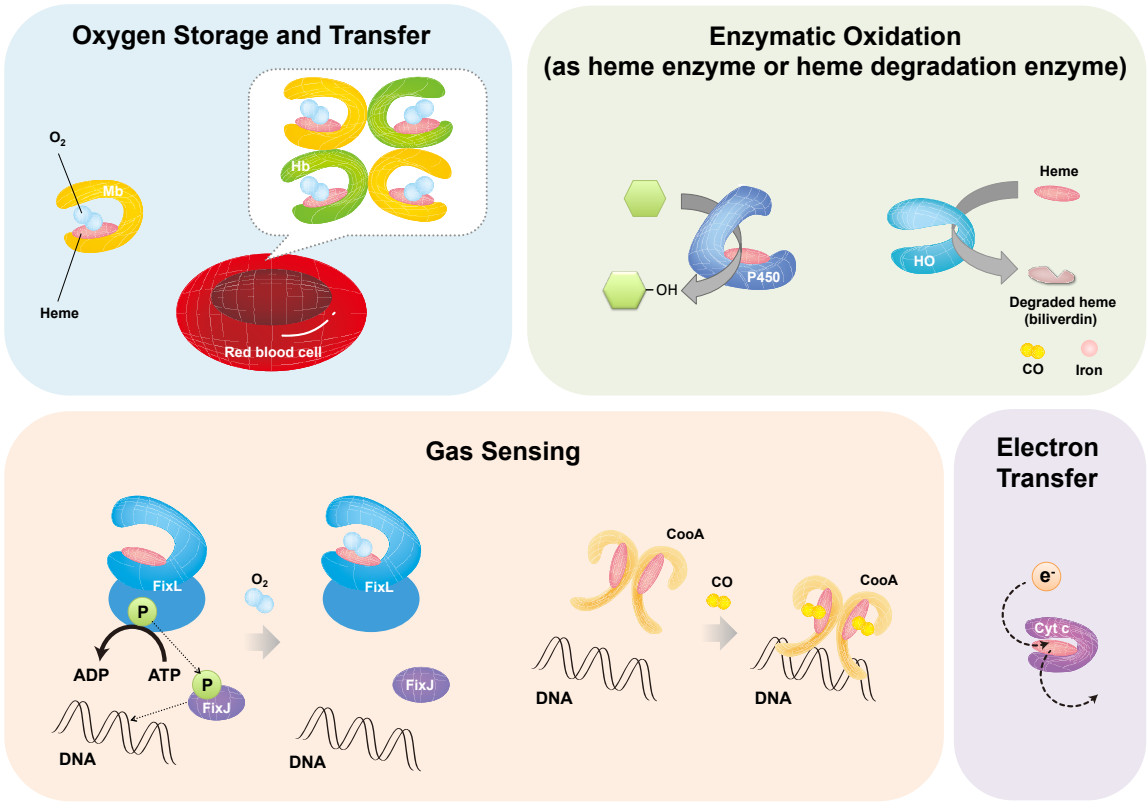

Fig. 1-2 Heme protein functions. Myoglobin (Mb) and hemoglobin (Hb) bind molecular oxygen on their heme iron atoms. Myoglobin storages oxygen in muscle. Hemoglobin also binds molecular oxygen and transports it using blood flow. Cytochrome P450 (P450) is a family of hemoenzymes that catalyze hydroxylation reactions. Heme oxygenase (HO) is an enzyme, which catalyzes heme degradation. FixL and CooA are responsible for gas sensing. Cytochrome *c* (Cyt *c*) is responsible for electron transfer.

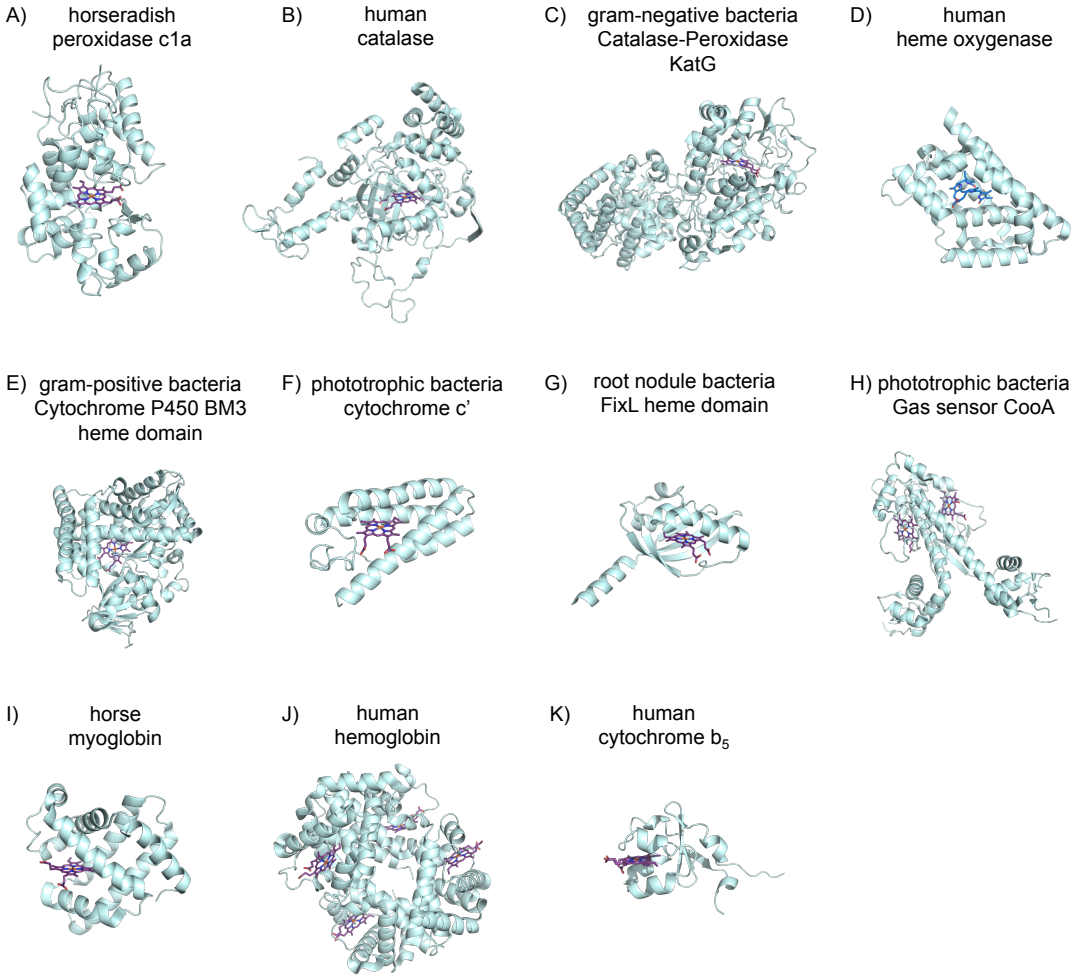

Fig. 1-3 Crystal structures of heme proteins. Light blue parts show amino acids of proteins. Purple sticks show the heme. A blue stick shows degraded heme by heme oxygenase. A) Horseradish peroxidase (PDB ID: 1ATJ), B) Catalase (PDB ID: 1DGB), C) Catalase-Peroxydase (PDB ID: 1MWV), D) Heme oxygenase (PDB ID: 1S8C), E) Cytochrome P450 (PDB ID: 2J1M), F) Cytochrome c (PDB ID: 1RCP), G) Heme domain of FixL (PDB ID: 1DP6), H) CooA (PDB ID: 1FT9), I) Myoglobin (PDB ID: 1WLA), J) Hemoglobin (PDB ID: 2HHB), K) Cytochrome b_5 (PDB ID: 3NER).

1-2. Myoglobin as a model protein of hemoproteins

Myoglobin is an oxygen storage protein found in muscle tissues. Myoglobin is a small (17 kDa) and well-characterized hemoprotein, which has been used as a structural and functional model for understanding roles of amino acid residues in an active site of hemoproteins (Fig. 1-4).[27-31] In 1958, Kendrew *et al*. determined the first crystal structure of sperm whale myoglobin by X-ray crystallography.[32] This protein has a typical globular frame and the iron of heme is coordinated to the proximal histidine (His93). Another histidine located in the distal side of heme (His-64) is not coordinated to the heme iron. This histidine located in the distal side of heme is important for the oxygen storage and has been evolutionally conserved. In general, myoglobin does not show any catalytic activity, however, by the replacement of amino acids in the distal side of the heme, myoglobin can catalyze peroxidase, catalase, and peroxygenase reactions.[33-35] For example, an artificial peroxidase was developed using myoglobin by reproducing the active site of peroxidases based on some crystal structures of peroxidases.[28] Peroxidases catalyze one-electron oxidation of various substrates and histidine in the distal side of the heme is important for the generation of active species using hydrogen peroxide as

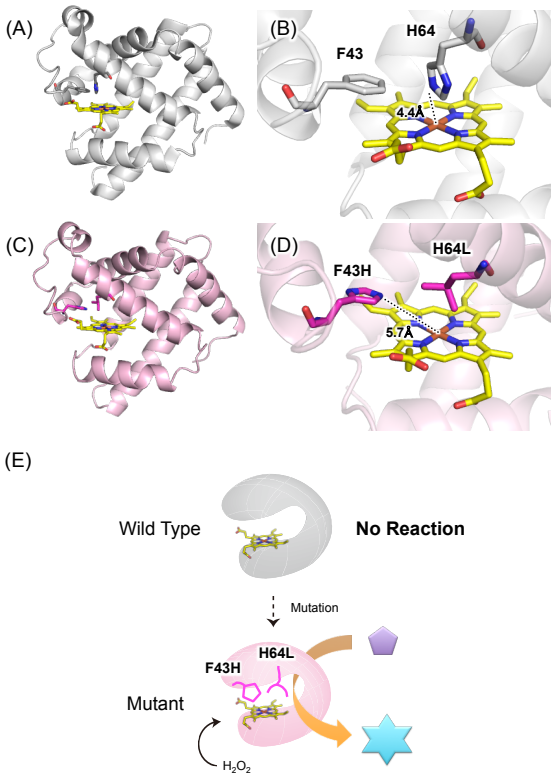

Fig. 1-4 Wild type and F43H/H64L mutant of myoglobin. A) A whole structure of wild type myoglobin (PDB ID: 1JP6), B) A close-up view of the active site of wild type myoglobin. C) A whole structure of F43H/H64L mutant (PDB ID: 1OFK), D) A close-up view of the active site of F43H/H64L myoglobin mutant. E) A cartoon image of mutation.

an oxidant (Fig. 1-5). The distal histidine is a critical residue for the peroxidase activity because it serves as a general acid-base catalyst for the generation of the active species, oxoferryl porphyrin π cation radical, so-called compound I.[36-38] (Fig. 1-6) The distal histidine first serves as a base to accelerate binding of hydrogen peroxide to the ferric heme iron. Subsequently, the same histidine with a proton facilitates heterolytic cleavage of the O-O bond of hydroperoxide bound to the heme. Myoglobin has the distal histidine, but it does not serve as a general acid-base catalyst. Crystal structures of myoglobin shows that the N_ε of the distal histidine is too close to the heme iron (4.4 Å, PDB ID: 1JP6, Fig. 1-4) compared with those of cytochrome *c* peroxidase (5.6 Å, PDB ID: 2CYP, Fig. 1-5) and horseradish peroxidase (5.6 Å, PDB ID: 1HCH, Fig. 1-5). The distance between the N_ε of the distal histidine and the heme iron is optimal for stabilizing the heme bound oxygen in myoglobin and thus it is not suitable for serving as a general acid-base catalyst. To further examine the relationship between the location of the distal histidine and the peroxidase activity of myoglobin, two sets of sperm whale myoglobin mutants, L29H/H64L and F43H/H64L (Fig. 1-4), were prepared by point mutagenesis.[28] His-64 was replaced with leucine to remove the original histidine that is too close to the heme iron and to construct a space for hydrogen peroxide binding. Subsequently, a histidine residue was placed at the position 29 or 43 and their catalytic activities were examined. F43H/H64L mutant showed one-electron oxidation activities (Fig. 1-7)[28] and this mutant also catalyzes sulfoxidation and epoxidation (Fig. 1-7).[29, 39, 40] The crystal structures of L29H/H64L and F43H/H64L showed that the distances between the distal histidine and the heme iron are 6.5 Å and 5.7 Å (Fig. 1-4), respectively. The F43H/H64L mutant reproduces the active site of peroxidases, while His-29 in L29H/H64L mutant was a bit far from the heme iron to serve as an acid-base catalyst. These results have encouraged many researchers to construct various myoglobin mutants.[41-47] Even aromatic C-H bond hydroxylation, which is a much more difficult oxidation reaction, was catalyzed by myoglobin mutants. Aromatic C-H bond hydroxylation is one of key oxidation reactions in organic synthesis and attractive

from the viewpoint of production of fine chemicals as well as drug intermediates. Xu *et al.* reported synthesis of indigo from indole with a series of H64D sperm whale

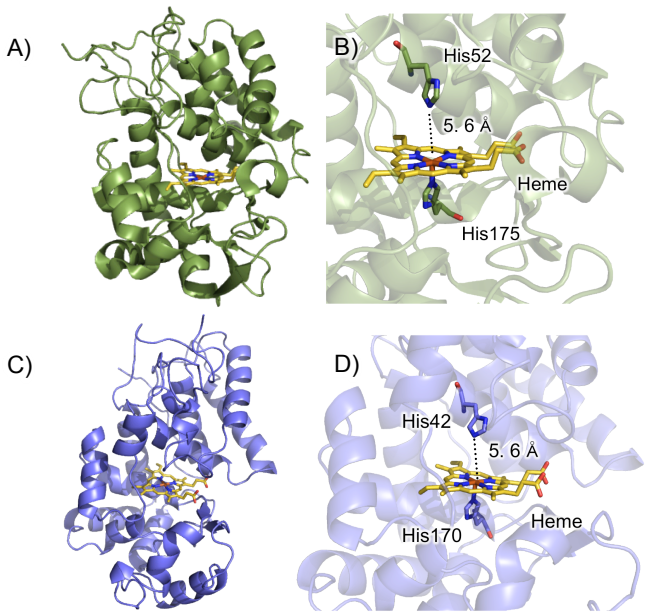

Fig. 1-5 Crystal structures of heme peroxidases. A, B) Cytochrome *c* peroxidase (PDB ID: 2CYP) and C, D) horseradish peroxidase (PDB ID: 1HCH). In the left column (A, C), overall structures are shown as a ribbon model. In the right column (B,D), close-up views of the active sites are shown. Histidines as well as ligands general acid-base catalysts are represented in stick models served in B) and D). Heme is also shown in the stick model in A)-D).

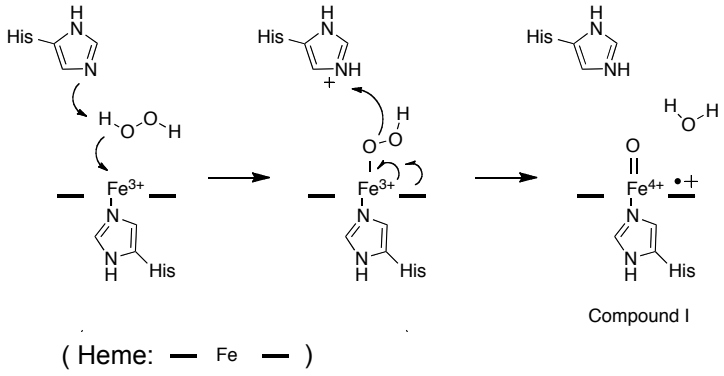

Fig. 1-6 A proposed reaction mechanism of Compound I formation. The distal histidine first serves as a base to deprotonate hydrogen peroxide. Subsequently, a protonated histidine serves as an acid to facilitate heterolytic cleavage of the O-O bond.

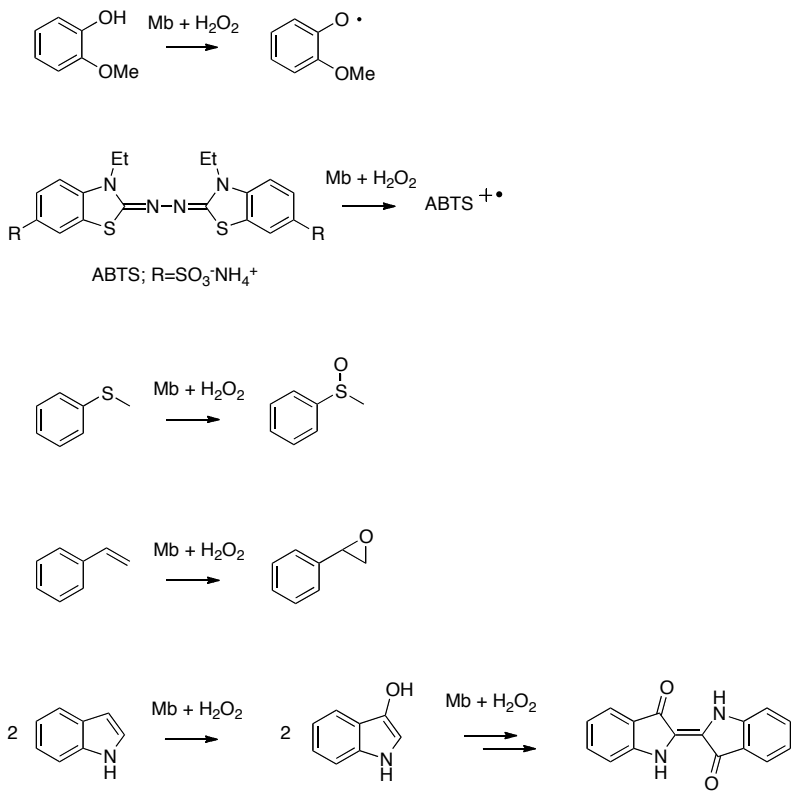

Fig. 1-7 Oxidation reactions catalyzed by myoglobin mutants (Mb).

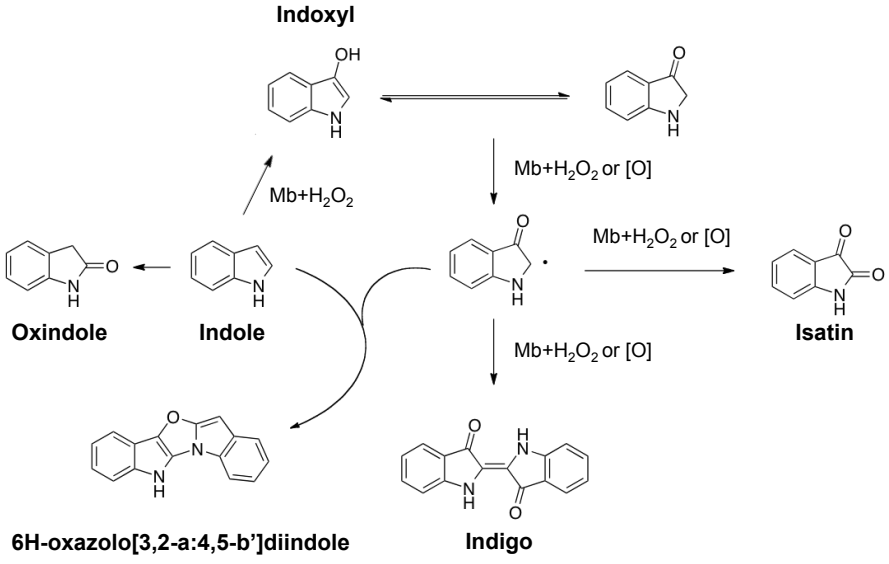

Fig. 1-8 A plausible reaction mechanism for the indigo formation from indole catalyzed by myoglobin mutants (Mb).[48]

myoglobin mutants (Fig. 1-8).[48] This reaction contains aromatic C-H bond hydroxylation, while the oxidized position was exclusively on the pyrrole ring of the indole. Although the H64D myoglobin mutant catalyzed the aromatic hydroxylation of indole, less reactive aromatic compounds such as ethylbenzene was not hydroxylated by this mutant.[49] Pfister *et al*. reported the hydroxylation of an aromatic ring at the C6 position of tryptophan 43 in the triple myoglobin mutant F43W/H64D/V68I (Fig. 1-9).[50] This is the first example of hydroxylation of less reactive aromatic compound by myoglobin mutants. This result suggested that fixation of substrate nearby the heme is one of important factors for the hydroxylation of inert substrates. In the reactions catalyzed by cytochrome P450s, their target substrates are generally fixed in the active site. Cytochrome P450 is a family of heme enzymes that catalyze monooxygenation of less reactive C-H bonds in conjunction with the biosynthesis of steroids, drug metabolism, and detoxification of xenobiotics. [51, 52] In cytochrome P450s, substrates are fixed by hydrogen bonding interaction as well as hydrophobic interaction to perform regio- and stereo- selective hydroxylation with high catalytic activity.

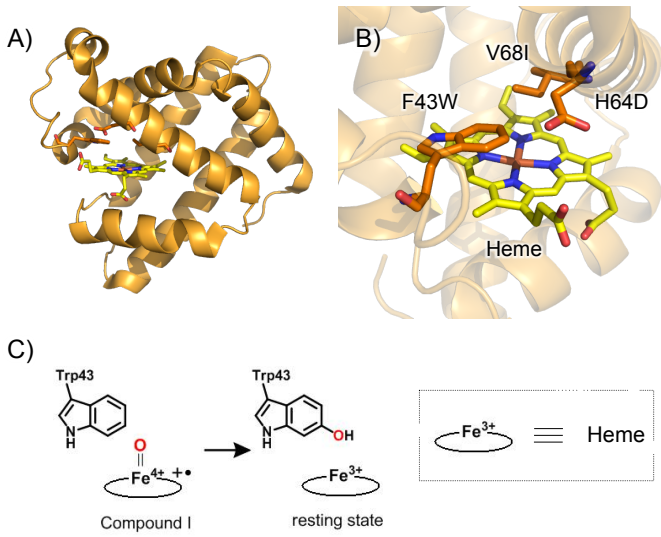

Fig. 1-9 An Overall structure of the sperm whale myoglobin F43W/H64D/V68I mutant (PDB ID: 2E2Y) A) and its active site B). The mutated amino acid residues and the heme are shown in stick models. The scheme of hydroxylation of the Trp-43 is shown in C).

For example, cytochrome P450BM3 catalyzes the hydroxylation of sub-terminal positions of fatty acids, where both arginine 47 and tyrosine 51 interact with the carboxylates of the fatty acids to fix them (Fig. 1-10).[53, 54] According to the strategy of P450s for monooxygenation of less reactive organic compounds, if one could construct a substrate binding site into myoglobin by point mutagenesis, some of resulting mutants of myoglobin would catalyze oxidation of less reactive substrates. Although P450s catalyze monooxygenation reactions, the reaction system is rather complicated mainly because of their multicomponent system. Construction of artificial P450s that catalyze monooxygenation of less reactive organic compound using myoglobin thus has been one of challenging research topics. To realize enzymatic hydroxylation of less reactive aromatic compound by myoglobin mutants, this author tried to construct a substrate-binding site into myoglobin by placing arginine residue, as is observed in P450BM3. The results concerning construction of a substrate-binding site in myoglobin are described in the chapter II.

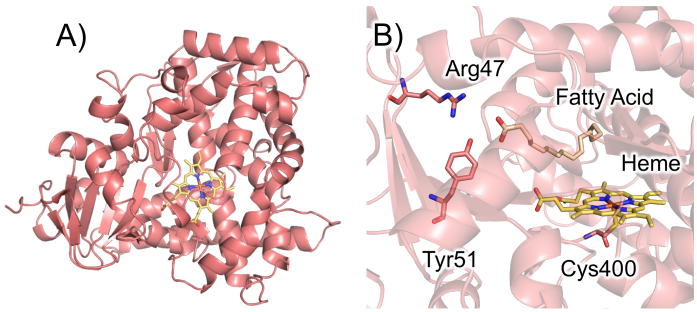

Fig. 1-10 The crystal structure of Cytochrome P450BM3 (PDB ID: 1FAG): A) an overall structure and B) the active site structure. Arg-47 (a key residue for substrate fixation), Tyr51 (another key residue for substrate fixation), heme, Cys400 (a ligand), and the fatty acid (substrate) are shown in stick models.

1-3. Artificial metalloproteins constructed by the replacement of their prosthetic groups

A large number of mutants of hemoproteins have been prepared to convert their functions. Replacement of the heme with an artificial prosthetic group is another way to drastically change their function and to create artificial metalloproteins (Fig. 1-11). A variety of reconstituted myoglobins with various synthetic metal complexes have been constructed.[49, 55-57] For example, Oohora *et al*. have prepared a myoglobin reconstituted with manganese porphycene.[58] They reported that the reconstituted wild type myoglobin by manganese porphycene catalyzes the hydrogen peroxide dependent hydroxylation of ethylbenzene to yield 1-phenylethanol as the sole product. Ibrahim *et al*. reported replacement of heme in the cytochrome c_{552} from *Thermus thermophilus* with zinc protoporphyrin IX. They demonstrated the reconstitution of *c*-type heme that is covalently connected to the cycteine residue of cytochrome *c*.[59] Hayashi *et al*. reported reconstituted cytochrome P450cam by an artificial heme without a carboxyl group, and they examined roles of a carboxyl group of the heme.[60] Ueno *et al*. reconstituted myoglobin and heme oxygenase with various Schiff-base metal complexes.[56, 61] Although a variety of reconstituted hemoproteins are reported thus far, the function of reconstituted proteins is basically limited to small improvement or affording new but low catalytic activities. Not only the construction of reconstituted hemoproteins including new methods for the reconstitution[62, 63] but also the development of multiple uses of reconstituted hemoproteins are also an important research topic in this field. For example, Olczak and coworkers reported antimicrobial activity of reconstituted hemoproteins with artificial

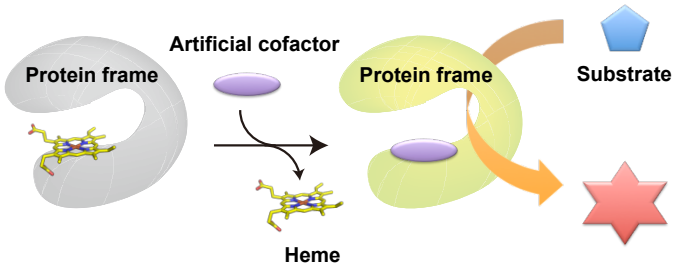

Fig. 1-11 A schematic representation of cofactor replacement of hemoprotein for creation of an artificial metalloenzyme. The heme is replaced with synthetic metal complex.

metalloporphyrins by using a bacterial heme acquisition protein.[64, 65]

1-4. Heme acquisition system in gram-negative bacteria

As described in the section 1-1, iron is an essential component for all living organisms. For example, *Escherichia coli* contains iron and the number is about 10^6 atoms per cell.[66, 67] In addition, it was reported that a similar amount of iron was found in other bacteria.[68] Although ferrous iron (Fe^{2+}) is soluble in water, it is easily oxidized to water-insoluble ferric iron (Fe^{3+}) under aerobic conditions. Iron chelators are valuable to solubilize ferric iron ion (Fe^{3+}). A great variety of bacteria, fungi and plants secret small iron chelate molecules called siderophores to acquire ferric iron in the environment (Fig. 1-12). The secreted siderophores capture iron ion and the resulting iron-siderophore complexes are taken up by bacteria through their specific outer membrane receptors.

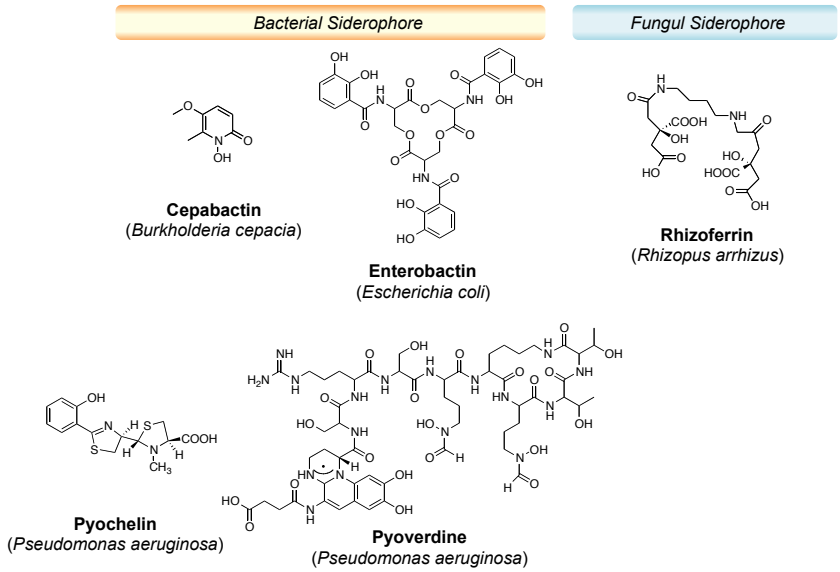

Fig. 1-12 Examples of siderophores of bacteria (left side) and fungi (right side).

Heme (Fig. 1-1) is found most abundantly in hemoglobin in the red blood cells. Old red blood cells are degraded in the spleen, and the released hemoglobin is separated into heme and polypeptide during this degradation process.[69] Free heme is

highly toxic to cells because it generates reactive oxygen species,[70, 71] organisms are equipped with systems to decompose the free heme. Heme oxygenase (Fig. 1-3) is an enzyme that catalyzes the regiospecific conversion of heme to a compound called biliverdin, carbon monoxide, and free iron.[72-76] Heme oxygenase is evolutionarily conserved enzymes, and it also presents in fish, higher plant, alga, and cyanobacteria.[77-80] Interestingly, in several pathogenic bacteria (e.g. *Pseudomonas aeruginosa*, *Neisseria meningitidis* and *Corynebacterium diphtheria*), heme oxygenase degrades heme from their hosts to get iron for their survival and proliferation.[81-86] The bacteria utilize heme of hosts as their iron sources the concentration of because free iron ions is quite limited in the animal bodies.[87, 88]

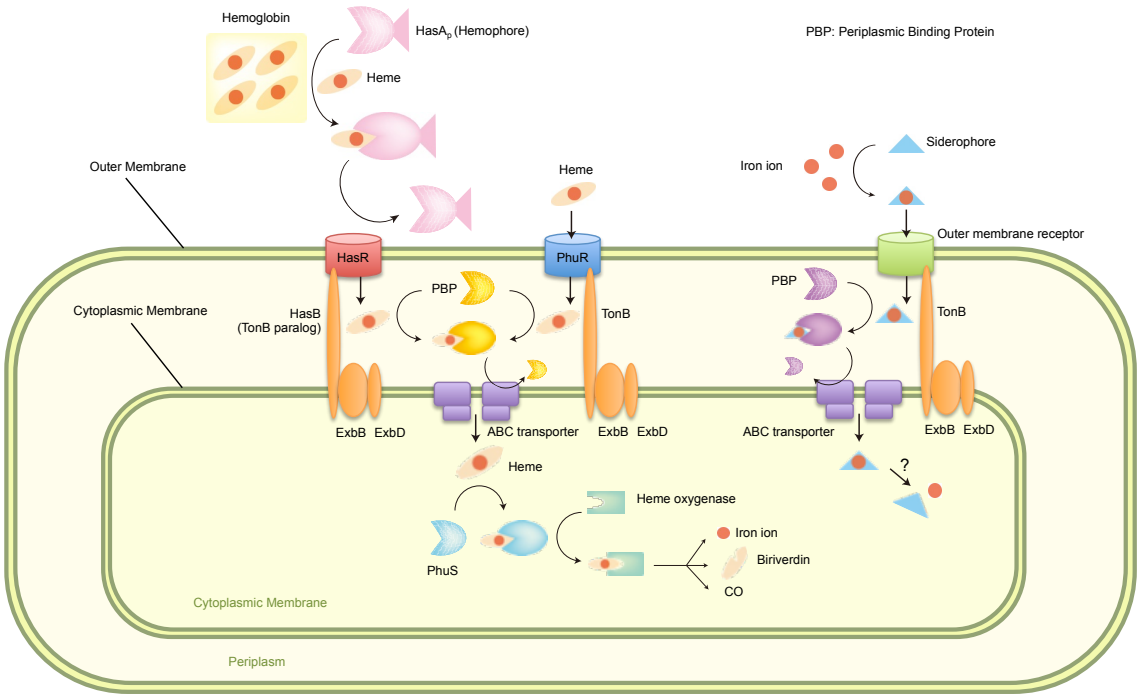

Fig. 1-13 Iron acquisition systems of *P. aeruginosa*. *P. aeruginosa* has two heme acquisition systems, Has system and Phu system. A acquired heme is degraded in cytoplasm by heme oxygenase, and then, iron ion is ejected. In addition, *P. aeruginosa* use siderophores to get iron ion in the environment.

An iron acquisition system called Has (Heme Acquisition System) has evolved in several Gram-negative pathogenic bacteria to acquire the heme and extract the iron (Fig. 1-13, 14, and 15).[89-94] Under iron limited conditions, the bacteria with the heme acquisition system secret a small soluble heme carrier protein, HasA (Fig. 1-14, 15). The HasA protein has been identified in *Serratia marcescence*, *Pseudomonas aeruginosa*, *Pseudomonas fluorescens*, *Yersinia pestis*, *Yersinia pseudotuberculosis*, *Erwinia carotovora* and *Pectobacterium carotovorum*.[95-101] In the extracellular medium, HasA either binds free heme or steals heme from host hemoproteins. The captured heme is transported to a bacterial membrane receptor, HasR.[102-104] The bacteria take up the heme through HasR. Subsequently, the heme is transported into the periplasm. Finally, the heme is degraded by heme oxygenase in the cytoplasm by which bacteria acquire iron ions.

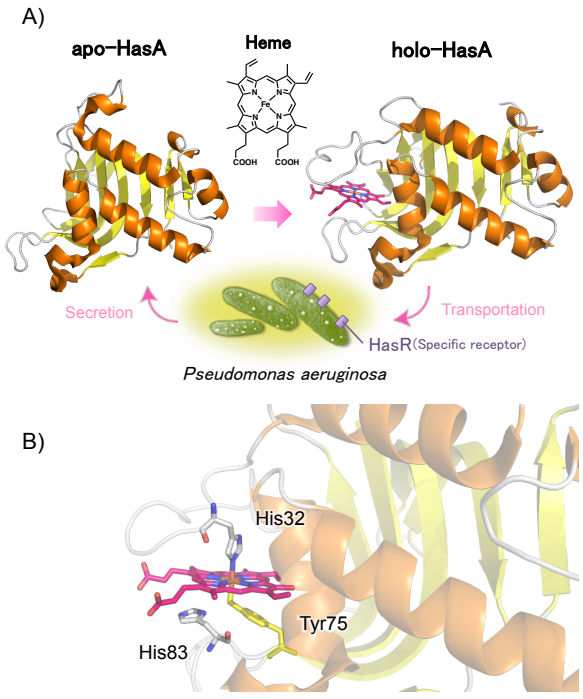

Fig. 1-14 The Has system in *P. aeruginosa*. A) Has system: Under iron-limited conditions, *P. aeruginosa* secrets apo-form hemophore, $HasA_p$. Therefore, this protein captures a heme and transports it to the specific membrane receptor, HasR. B) Specific three residues involved in the coordination of the heme by $HasA_p$.

The crystal structure of a heme-bound form of HasA from *S. marcescence* ($HasA_{sm}$) was first solved in 1999 (Fig. 1-16, 17).[105] The structure of holo-HasA revealed that the heme was located between two loops of HasA, and Tyr-75 and His-32 ligated the heme iron. The phenolate of Tyr-75 is also bounded to the N_δ atom of His-83 by a hydrogen bond. The structure of apo-HasA from the same bacterium was analyzed by NMR spectroscopy (Fig. 1-16).[106] The structural comparison of apo-HasA and holo-HasA suggested that the conformation of apo-HasA changes from open to closed conformation upon the heme binding. Wolff *et al*. proposed a two-step mechanism for the heme binding by HasA[106]: first, the binding pocket is opened and heme interacts with the loop including Tyr-75. Second, the pocket closes with a large shift of the loop including His-32. Experiments performed by Yukl *et al*. supports this hypothesis. They studied the kinetics of the heme acquisition with HasA from *P. aeruginosa* ($HasA_p$).[107] The binding of free hemin by $HasA_p$ was characterized by an initial rapid phase forming an intermediate prior to its further conversion to the final complex. This two-step process was also supported by the fact that the heme acquisition with an H32A mutant of $HasA_p$ showed only the rapid phase.

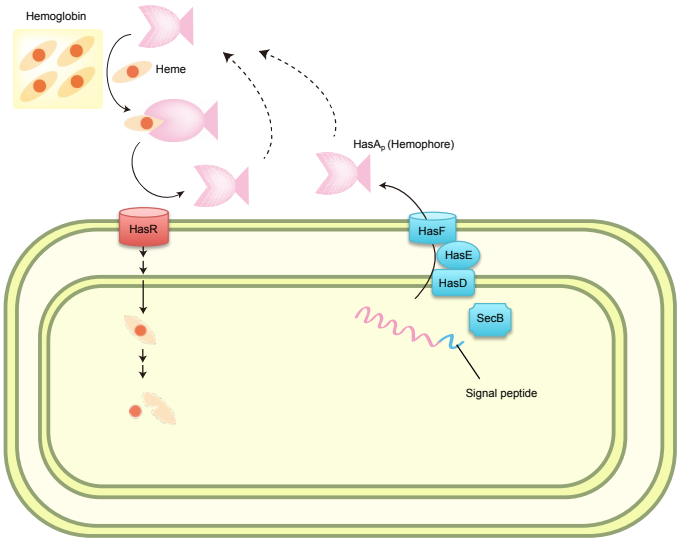

Fig. 1-15 The Has system in *P. aeruginosa*. SecB, a cytoplasmic Chaperone, helps folding of HasA. HasD, HasE, and HasF are responsible for secretion of HasA protein. HasA, shown as a pink fish figure, captures a heme from hemoglobin of a host. The transported heme from HasA passes through HasR. Finally, the heme is degraded in cytoplasm. The secreted HasA lacks its signal peptide.

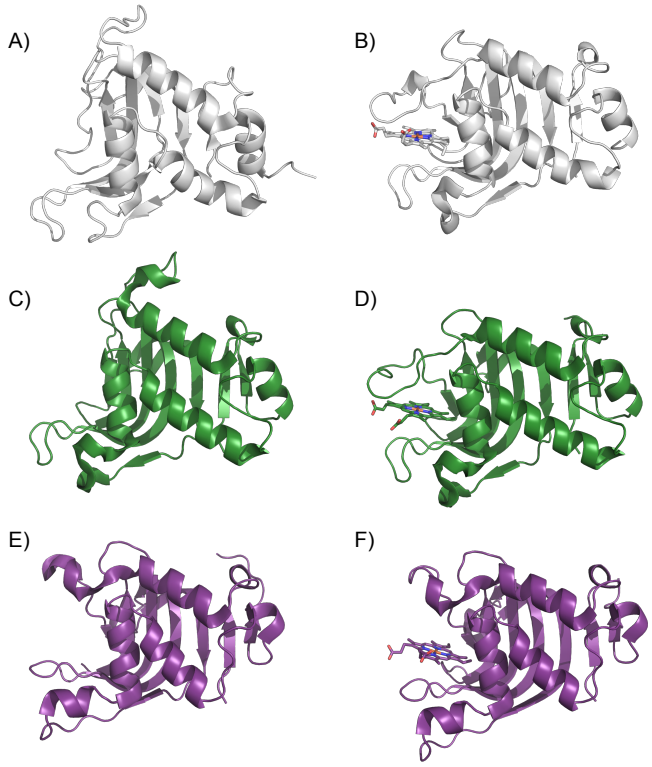

Fig. 1-16 Structures of various HasA proteins (PDB ID: 1ybj, 1y2v, 3mok, 3ell, 4jer, 4jet). A), C), E) are apo-forms, and B), D), F) are holo-forms. A) An NMR structure of apo-HasA from *S. marcescens,* B) a crystal structure of holo-HasA from *S. marcescens*. C) and D) show crystal structures of HasA from *P. aeruginosa*. E) and F) Crystal structures of HasA from *Y. pestis*.

The crystal structures of holo- and apo- HasA from *P. aeruginosa* ($HasA_p$) were solved in 2009 and 2010, respectively (Fig. 1-16, 1-18).[108, 109] The structure of holo-$HasA_p$ is essentially identical to holo-HasA from *S. marcescence* ($HasA_{sm}$) (Fig. 1-17). The crystal structures of HasA-HasR complexes with or without heme were reported in 2009 (Fig. 1-19).[103] The structure of HasR from *S. marcescence* resembles siderophore receptors of gram-negative bacteria (Fig. 1-20). In their report, importance of the isoleucine besides the captured heme is suggested for heme transportation (Fig. 1-21). The heme transfer from HasA to its specific membrane receptor HasR is believed to be driven by protein-protein interaction that makes it possible to transport heme from HasA with a higher heme-affinity to HasR with a lower heme-affinity.[104] Recently,

Caillet-Saguy *et al*. examined roles of axial ligands of HasA at a heme release process in 2012.[110, 111] Their experiments showed that the HasA-HasR complexation is critical for the heme transportation from HasA to HasR.

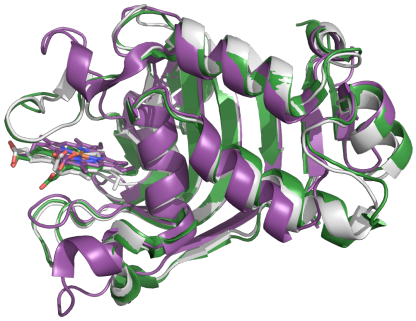

Fig. 1-17 Superimposed crystal structures of holo-HasA (PDB ID: 1ybj, 3mok, 4jet). White structure shows HasA from *S. marcescens*. Green structure shows HasA from *P. aeruginosa*. Purple structure shows HasA from *Y. pestis*.

Heme acquisition systems including Has system resembles iron acquisition system that utilize siderophores as an iron chelator. As was mentioned previously, the structure of HasR from *S. marcescence* is similar to various siderophore receptors. Several bacteria use both siderophore systems and heme acquisition systems to survive. *P. aeruginosa* has both the Has system and a Phu system as heme acquisition systems,[89] and this bacterium also use siderophores, e.g. pyochelin and pyoverdine (Fig. 1-12, 1-13)[93]. *E. coli* uses enterobactine as a siderophore (Fig. 1-12). In addition, *Escherichia coli* has a Chu system as a heme acquisition system.[112] In the Phu system and Chu system, heme is imported directory into outer membrane receptors without hemophore proteins. *Porphyromonas gingivalis* has a heme acquisition system in which HmuY serves as hemophore (Fig. 1-22).[113] Not only gram-negative bacteria, but also gram-positive bacteria have heme acquisition systems. *Staphylococcus aureus* has an Isd system as a heme acquisition system (Fig. 1-23).[114, 115] Gram-positive bacteria have no outer membrane, and uptake of heme involves membrane anchored binding proteins. Heme binding domains of such anchored proteins, IsdH and IsdB serve as hemophore (Fig. 1-24).[116-118] The little conformational changes due to heme binding was observed with IsdH and IsdB. It is interesting to note here that HasA from *P. aeruginosa* and HasA from *S. marcescence* are accompanied by the conformational changes upon binding of the heme (Fig. 1-16, 1-18), whereas HasA from *Y. pestis* does not show such conformational change (Fig.

1-16).[100]

The crystal structures of the holo-forms of $HasA_p$ and $HasA_{sm}$ showed that the captured heme molecules are highly exposed to a solvent; not only two propionate groups but also the edges of three pyrrole rings can be seen from outside. This unique binding fashion of HasA suggests that HasA proteins could accommodate the metal complexes having different structures from heme. Because apo-HasA exhibits "open conformation" with large rearrangement of the loop containing His-32, even bulky metal complexes could be received in the heme binding pocket of HasA. In this research, it is shown that the hemophore from *P. aeruginosa* can capture several metal complexes without heme frame. Furthermore, the effects of $HasA_p$ containing artificial metal complexes against living *P. aeruginosa* are also examined. Accordingly, we found HasA capturing an artificial metal complex inhibits bacterial heme acquisition through Has proteins.

P. aeruginosa is a well-known pathogen due to appearance of multi-drug resistant *P. aeruginosa* (Fig. 1-25), which is a serious social problem in hospitals. Creation of novel bacteria elimination system without the use of pre-existing antibiotics would contribute to solve the problem of multi-drug resistant *P. aeruginosa*.

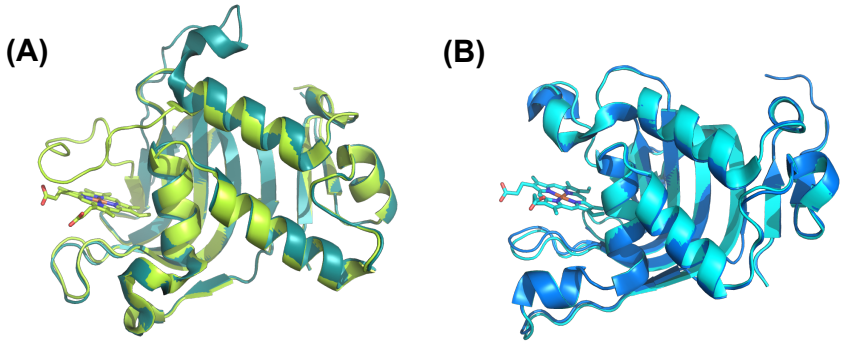

Fig. 1-18 Comparison of crystal structures between apo-forms (dark colors) and holo-forms (light colors). A) shows crystal structures of HasA from *P. aeruginosa* (PDB ID: 3MOK, 3ELL). B) shows crystal structures of HasA from *Y. pestis* (PDB ID: 4JER, 4JET).

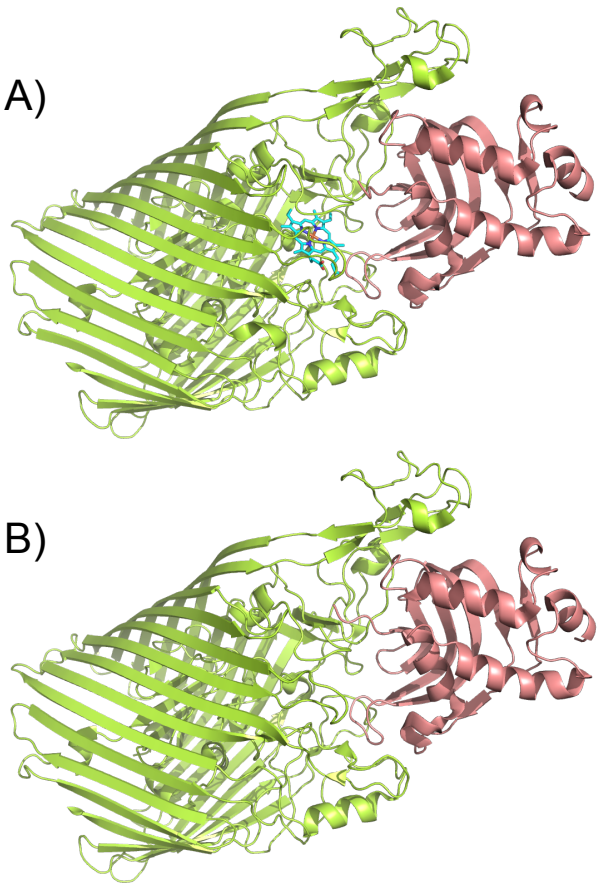

Fig. 1-19 Crystal structure of complexes of A) HasA and HasR with heme (PDB ID: 3CSL), B) HasA and HasR (PDB ID: 3CSN). Pink ribbon model shows HasA. Green ribbon model shows HasR. Cyan stick model in A) shows heme.

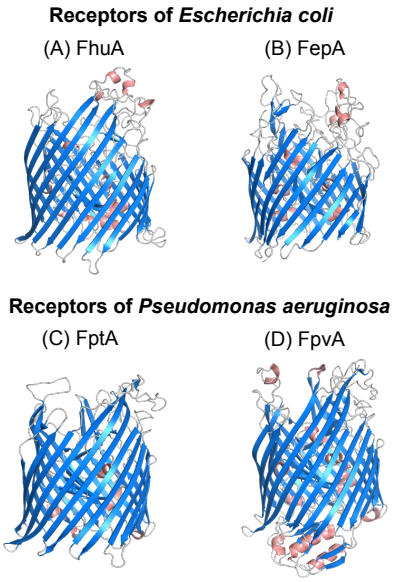

Fig. 1-20 Outer membrane receptors for siderophores of gram-negative bacteria. A) FhuA: a ferrichrome receptor of *E. coli*. B) FepA is a ferric enterobactine receptor of *E. coli*. C) FptA: a ferric pyochelin receptor of *P. aeruginosa*. D) FpvA: a ferric pyoverdine receptor of *P. aeruginosa*.

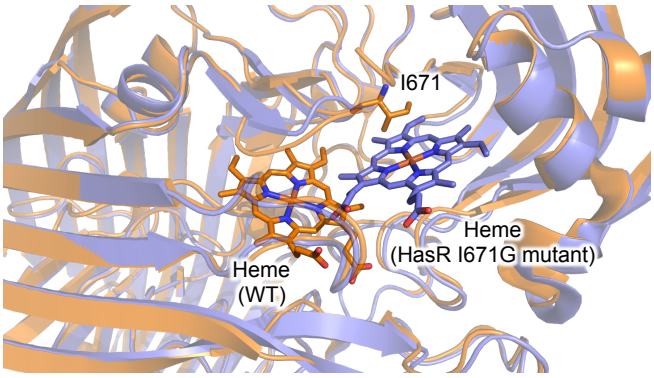

Fig. 1-21 Close up views of the heme binding site of wild type HasR (depicted in orange, PDB ID: 3CSL) and HasR I671G mutant (depicted in purple, PDB ID: 3DDR). The 671st amino acids of wild type HasR is shown as a stick model.

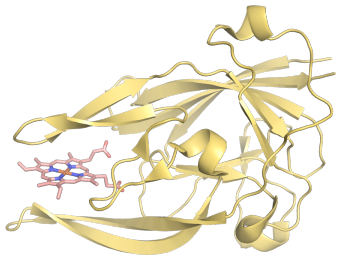

Fig. 1-22 Crystal structure of HmuY monomer (PDB ID: 3H8T). The protein frame by amino acids is shown a yellow ribbon model. The heme is shown as a pink stick model.

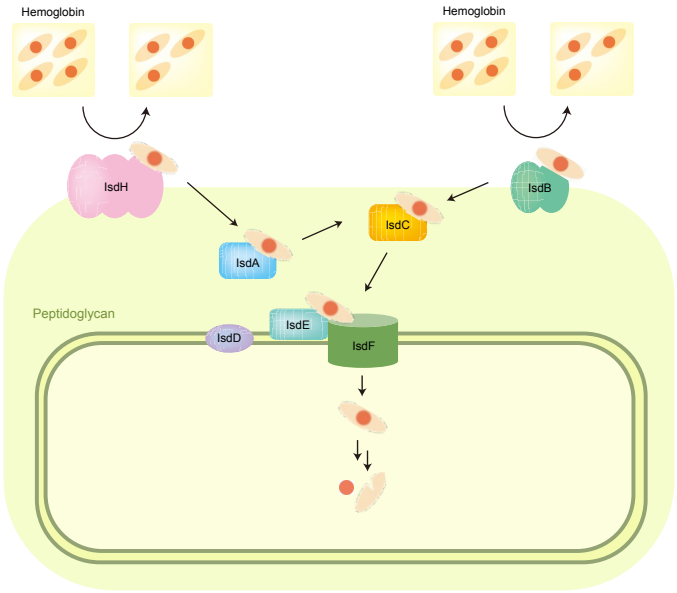

Fig. 1-23 Isd system of *S. aureus*. Heme from host is imported into a cell by cell-surface receptors IsdH and IsdB. Subsequently, the heme is transported by IsdA and IsdC in cell wall. The carried heme to IsdE by IsdC passes through the plasma membrane receptor IsdF. The heme iron is extracted by enzymes in cytoplasm. The IsdD function is unknown.

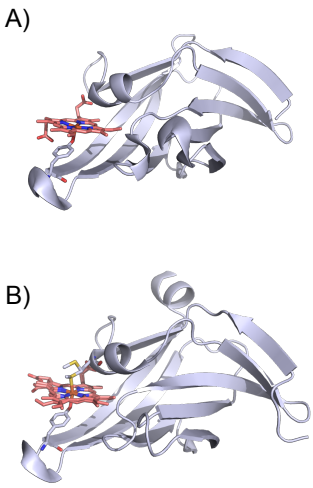

Fig. 1-24 Heme binding domains of A) IsdH (PDB ID: 2Z6F) and B) IsdB (PDB ID: 3RTL). Heme and ligands are shown as stick models.

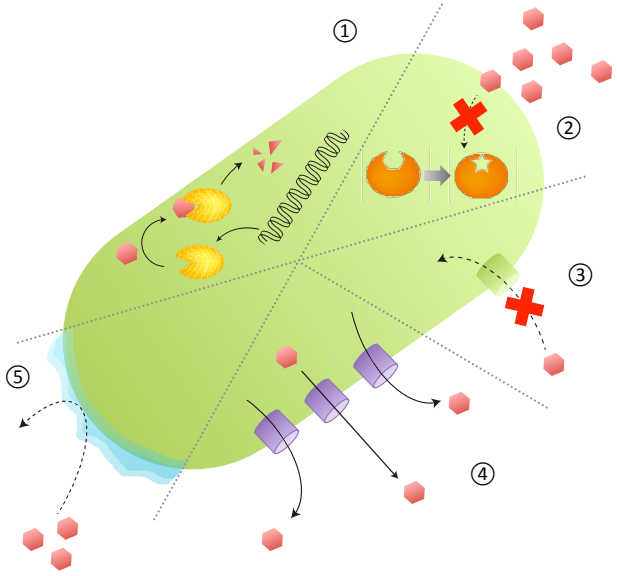

Fig. 1-25 A cartoon image of the multi-drug resistant *P. aeruginosa*:

1. Drug molecules are modified or degraded by enzymes.[119] 2. Mutational change of DNA gyrase prevents binding of antibiotics.[120] 3. Loss of D2 porin, a channel protein on the outer membrane, causes inhibition of drug influx.[121] 4. Antibiotic is eliminated by multidrug efflux pumps.[122, 123] 5. Antibiotic penetration is inhibited by biofilm.[124] Multidrug resistance often reflects not one but a combination of resistance mechanisms.

1-5. Summary and outlook

Heme, an iron-containing cofactor, is essential for hemoproteins as the prosthetic group to perform a wide variety of biological functions. Myoglobin is one of the most intensively studied hemoproteins. Myoglobin has been studied not only for understanding its biological functions, but also for utilizing myoglobin as a model framework for the protein engineering studies to probe the structure-function relationships of heme enzymes. In chapter II, the construction of myoglobin mutants for hydrogen peroxide-dependent aromatic C-H bond hydroxylation by rational design of the active site of myoglobin is described. H64D and H64D/V68I mutants of myoglobin catalyze the hydroxylation of 1-methoxynaohthalene. In this reaction, a blue compound so-called Russig's blue was prepared by myoglobin mutants (Fig. 1-26). Moreover, construction of a substrate-binding site was also carried out to increase the hydroxylation activity of myoglobin mutants. The author engaged in rational design of the myoglobin active site to introduce a substrate binding site. An arginine residue was inserted into myoglobin mutant as a substrate binding site for substrates having a carboxylate group. Interestingly, the H64D/T67R/V68I myoglobin mutant catalyze an enantioselective hydroxylation of *(S)*-naproxen.

Heme is utilized as not only a reaction center of hemoproteins, but also an iron source of organisms. Because free iron ion is limited in vertebrate hosts, pathogenic

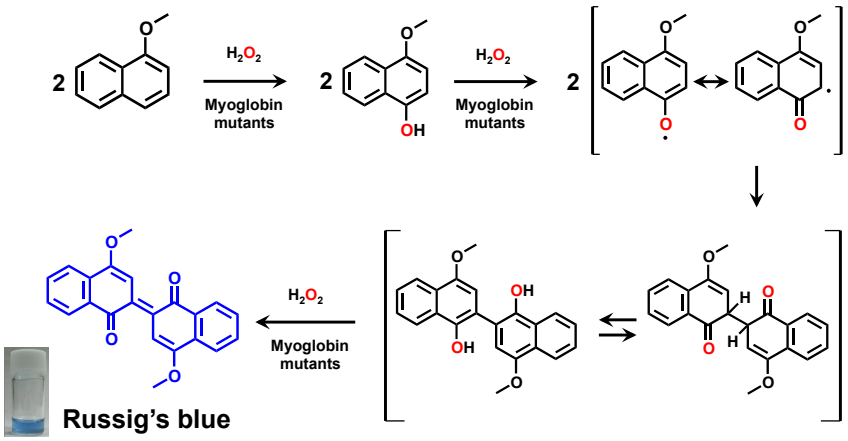

Fig. 1-26 Russig's blue formation by myoglobin mutants.

bacteria have developed various ways to get the iron from hemoproteins of hosts. *P. aeruginosa*, which is one of Gram-negative pathogens, secrets a heme-binding protein, $HasA_p$ in iron-limited conditions. This hemophore protein captures heme and transports it to the specific membrane receptor, HasR. The unique heme binding fashion of HasA suggests that HasA can bind various metal complexes other than heme. In chapter III, the author investigated whether $HasA_p$ can capture artificial metal complexes having different structures from heme. Three crystal structures, $HasA_p$ with Fe-mesoporphyrin IX, Fe-salophen and Fe-phthalocyanine revealed little perturbation of the overall structure compared with $HasA_p$ harboring heme. Furthermore, effects of $HasA_p$ containing artificial metal complexes on the growth of *P. aeruginosa* were examined. $HasA_p$ harboring Fe-phthalocyanine inhibited heme acquisition even in the presence of $HasA_p$ containing heme as an iron source.

Finally, the summary and perspective of this thesis are described in chapter IV.

References

[1] S. C. Andrews, A. K. Robinson, F. Rodriguez-Quinones, *FEMS Microbiol. Rev.* **2003**, *27*, 215-237.

[2] F. G. Mutti, *Bioinorg. Chem. Appl.* **2012**.

[3] E. I. Solomon, A. Decker, N. Lehnert, *Proc. Natl. Acad. Sci. USA* **2003**, *100*, 3589-3594.

[4] M. F. Perutz, *Trends Biochem. Sci.* **1989**, *14*, 42-44.

[5] J. B. Wittenberg, B. A. Wittenberg, *Annu. Rev. Biophys. Biophys. Chem.* **1990**, *19*, 217-241.

[6] M. L. Anson, A. E. Mirsky, *Physiol. Rev.* **1930**, *10*, 506-546.

[7] M. F. Perutz, *Annu. Rev. Biochem.* **1979**, *48*, 327-386.

[8] J. L. Pellequer, R. Brudler, E. D. Getzoff, *Curr. Biol.* **1999**, *9*, R416-R418.

[9] M. F. Perutz, M. Paoli, A. M. Lesk, *Chem. Biol.* **1999**, *6*, R291-R297.

[10] K. R. Rodgers, *Curr. Opin. Chem. Biol.* **1999**, *3*, 158-167.

[11] W. N. Lanzilotta, D. J. Schuller, M. V. Thorsteinsson, R. L. Kerby, G. P. Roberts, T. L. Poulos, *Nat. Struct. Biol.* **2000**, *7*, 876-880.

[12] H. R. Bosshard, M. W. Davidson, D. B. Knaff, F. Millett, *J. Biol. Chem.* **1986**, *261*, 190-193.

[13] G. Vergeres, L. Waskell, *Biochimie* **1995**, *77*, 604-620.

[14] M. J. Rodriguez-Maranon, F. Qiu, R. E. Stark, S. P. White, X. Zhang, S. I. Foundling, V. Rodriguez, C. L. Schilling, 3rd, R. A. Bunce, M. Rivera, *Biochemistry* **1996**, *35*, 16378-16390.

[15] F. Millett, M. A. Miller, L. Geren, B. Durham, *J. Bioenerg. Biomembr.* **1995**, *27*, 341-351.

[16] I. S. Isaac, J. H. Dawson, *Essays Biochem.* **1999**, *34*, 51-69.

[17] H. M. Jouve, P. Andreoletti, P. Gouet, J. Hajdu, J. Gagnon, *Biochimie* **1997**, *79*, 667-671.

[18] A. Deisseroth, A. L. Dounce, *Physiol. Rev.* **1970**, *50*, 319-375.

[19] A. V. Pandey, C. E. Fluck, *Pharmacol. Ther.* **2013**, *138*, 229-254.

[20] E. G. Hrycay, S. M. Bandiera, *Arch. Biochem. Biophys.* **2012**, *522*, 71-89.

[21] S. P. de Visser, *Adv. Inorg. Chem.* **2012**, *64*, 1-31.

[22] T. L. Poulos, *Arch. Biochem. Biophys.* **2010**, *500*, 3-12.

[23] G. Battistuzzi, M. Bellei, C. A. Bortolotti, M. Sola, *Arch. Biochem. Biophys.* **2010**, *500*, 21-36.

[24] L. E. Otterbein, M. P. Soares, K. Yamashita, F. H. Bach, *Trends Immunol.* **2003**, *24*, 449-455.

[25] M. Sono, M. P. Roach, E. D. Coulter, J. H. Dawson, *Chem. Rev.* **1996**, *96*, 2841-2887.

[26] N. C. Veitch, *Phytochemistry* **2004**, *65*, 249-259.

[27] S. Ozaki, T. Matsui, M. P. Roach, Y. Watanabe, *Coord. Chem. Rev.* **2000**, *198*, 39-59.

[28] T. Matsui, S. Ozaki, E. Liong, G. N. Phillips, Y. Watanabe, *J. Biol. Chem.* **1999**, *274*, 2838-2844.

[29] S. Ozaki, T. Matsui, Y. Watanabe, *J. Am. Chem. Soc.* **1997**, *119*, 6666-6667.

[30] S. Adachi, S. Nagano, K. Ishimori, Y. Watanabe, I. Morishima, T. Egawa, T. Kitagawa, R. Makino, *Biochemistry* **1993**, *32*, 241-252.

[31] S. I. Ozaki, M. P. Roach, T. Matsui, Y. Watanabe, *Acc. Chem. Res.* **2001**, *34*, 818-825.

[32] J. C. Kendrew, G. Bodo, H. M. Dintzis, R. G. Parrish, H. Wyckoff, D. C. Phillips, *Nature* **1958**, *181*, 662-666.

[33] Y. Goto, T. Matsui, S. Ozaki, Y. Watanabe, S. Fukuzumi, *J. Am. Chem. Soc.* **1999**, *121*, 9497-9502.

[34] S. I. Rao, A. Wilks, P. R. O. Demontellano, *J. Biol. Chem.* **1993**, *268*, 803-809.

[35] S. Kato, T. Ueno, S. Fukuzumi, Y. Watanabe, *J. Biol. Chem.* **2004**, *279*, 52376-52381.

[36] Y. Watanabe, *J. Biol. Inorg. Chem.* **2001**, *6*, 846-856.

[37] M. Wirstam, M. R. A. Blomberg, P. E. M. Siegbahn, *J. Am. Chem. Soc.* **1999**, *121*, 10178-10185.

[38] A. N. P. Hiner, E. L. Raven, R. N. F. Thorneley, F. Garcia-Canovas, J. N. Rodriguez-Lopez, *J. Inorg. Biochem.* **2002**, *91*, 27-34.

[39] S. Ozaki, I. Hara, T. Matsui, Y. Watanabe, *Biochemistry* **2001**, *40*, 1044-1052.

[40] S. Ozaki, H. J. Yang, T. Matsui, Y. Goto, Y. Watanabe, *Tetrahedron Asymmetry* **1999**, *10*, 183-192.

[41] J. Du, M. Sono, J. H. Dawson, *Coord. Chem. Rev.* **2011**, *255*, 700-716.

[42] S. Ozaki, Y. Ishikawa, *React. Kinet. Catal. L.* **2006**, *89*, 21-28.

[43] Y. W. Lin, S. S. Dong, J. H. Liu, C. M. Nie, G. B. Wen, *J. Mol. Catal. B-Enzym.* **2013**, *91*, 25-31.

[44] S. Bagchi, B. T. Nebgen, R. F. Loring, M. D. Fayer, *J. Am. Chem. Soc.* **2010**, *132*, 18367-18376.

[45] R. Roncone, E. Monzani, M. Murtas, G. Battaini, A. Pennati, A. M. Sanangelanton, S. Zuccotti, M. Bolognesi, L. Casella, *Biochem. J.* **2004**, *377*, 717-724.

[46] H. J. Yang, T. Matsui, S. Ozaki, S. Kato, T. Ueno, G. N. Phillips, S. Fukuzumi, Y. Watanabe, *Biochemistry* **2003**, *42*, 10174-10181.

[47] T. Matsui, S. Ozaki, Y. Watanabe, *J. Am. Chem. Soc.* **1999**, *121*, 9952-9957.

[48] J. Xu, O. Shoji, T. Fujishiro, T. Ohki, T. Ueno, Y. Watanabe, *Catal. Sci. Technol.* **2012**, *2*, 739-744.

[49] T. Matsuo, K. Fukumoto, T. Watanabe, T. Hayashi, *Chemistry-an Asian Journal* **2011**, *6*, 2491-2499.

[50] T. D. Pfister, T. Ohki, T. Ueno, I. Hara, S. Adachi, Y. Makino, N. Ueyama, Y. Lu, Y. Watanabe, *J. Biol. Chem.* **2005**, *280*, 12858-12866.

[51] A. P. Li, D. L. Kaminski, A. Rasmussen, *Toxicology* **1995**, *104*, 1-8.

[52] S. Kille, F. E. Zilly, J. P. Acevedo, M. T. Reetz, *Nat. Chem.* **2011**, *3*, 738-743.

[53] T. W. B. Ost, C. S. Miles, J. Murdoch, Y. F. Cheung, G. A. Reid, S. K. Chapman, A. W. Munro, *FEBS Lett.* **2000**, *486*, 173-177.

[54] H. Y. Li, T. L. Poulos, *Nat. Struct. Biol.* **1997**, *4*, 140-146.

[55] H. Sato, T. Hayashi, T. Ando, Y. Hisaeda, T. Ueno, Y. Watanabe, *J. Am. Chem. Soc.* **2004**, *126*, 436-437.

[56] T. Ueno, M. Ohashi, M. Kono, K. Kondo, A. Suzuki, T. Yamane, Y. Watanabe, *Inorg. Chem.* **2004**, *43*, 2852-2858.

[57] I. Hamachi, S. Shinkai, *Eur. J. Org. Chem.* **1999**, 539-549.

[58] K. Oohora, Y. Kihira, E. Mizohata, T. Inoue, T. Hayashi, *J. Am. Chem. Soc.* **2013**, *135*, 17282-17285.

[59] S. M. Ibrahim, H. Nakajima, T. Ohta, K. Ramanathan, N. Takatani, Y. Naruta, Y. Watanabe, *Biochemistry* **2011**, *50*, 9826-9835.

[60] K. Harada, K. Sakurai, K. Ikemura, T. Ogura, S. Hirota, H. Shimada, T. Hayashi, *J. Am. Chem. Soc.* **2008**, *130*, 432-+.

[61] T. Ueno, N. Yokoi, M. Unno, T. Matsui, Y. Tokita, M. Yamada, M. Ikeda-Saito,

H. Nakajima, Y. Watanabe, *Proc. Natl. Acad. Sci. USA* **2006**, *103*, 9416-9421.

[62] N. Kawakami, O. Shoji, Y. Watanabe, *ChemBioChem* **2012**, *13*, 2045-2047.

[63] V. S. Lelyveld, E. Brustad, F. H. Arnold, A. Jasanoff, *J. Am. Chem. Soc.* **2011**, *133*, 649-651.

[64] T. Olczak, D. Maszczak-Seneczko, J. W. Smalley, M. Olczak, *Arch. Microbiol.* **2012**, *194*, 719-724.

[65] H. Wojtowicz, M. Bielecki, J. Wojaczynki, M. Olczak, J. W. Smalley, T. Olczak, *Metallomics* **2013**, *5*, 343-351.

[66] S. Semsey, A. M. C. Andersson, S. Krishna, M. H. Jensen, E. Masse, K. Sneppen, *Nucleic Acids Res.* **2006**, *34*, 4960-4967.

[67] T. Nunoshiba, F. Obata, A. C. Boss, S. Oikawa, T. Mori, S. Kawanishi, E. Yamamoto, *J. Biol. Chem.* **1999**, *274*, 34832-34837.

[68] M. A. Rouf, *J. Bacteriol.* **1964**, *88*, 1545-&.

[69] C. Porth, *Essentials of Pathophysiology: Concepts of Altered Health States* **2010**, *Chapter 13*, 279-298.

[70] S. Kumar, U. Bandyopadhyay, *Toxicol. Lett.* **2005**, *157*, 175-188.

[71] S. R. Robinson, T. N. Dang, R. Dringen, G. M. Bishop, *Redox Rep.* **2009**, *14*, 228-235.

[72] M. Unno, T. Matsui, M. Ikeda-Saito, *J. Inorg. Biochem.* **2012**, *113*, 102-109.

[73] M. D. Maines, P. E. M. Gibbs, *Biochem. Biophys. Res. Commun.* **2005**, *338*, 568-577.

[74] N. Hill-Kapturczak, S. H. Chang, A. Agarwal, *DNA Cell Biol.* **2002**, *21*, 307-321.

[75] T. Yoshida, G. Kikuchi, *J. Biol. Chem.* **1978**, *253*, 4224-4229.

[76] R. Gozzelino, V. Jeney, M. P. Soares, *Annu. Rev. Pharmacol. Toxicol.* **2010**, *50*, 323-354.

[77] D. Wang, X. P. Zhong, Z. X. Qiao, J. F. Gui, *J. Exp. Biol.* **2008**, *211*, 2700-2706.

[78] S. I. Beale, J. Cornejo, *Arch. Biochem. Biophys.* **1984**, *235*, 371-384.

[79] C. T. Migita, X. H. Zhang, T. Yoshida, *Eur. J. Biochem.* **2003**, *270*, 687-698.

[80] S. J. Davis, S. H. Bhoo, A. M. Durski, J. M. Walker, R. D. Vierstra, *Plant Physiol.* **2001**, *126*, 656-669.

[81] C. Wandersman, P. Delepelaire, *Annu. Rev. Microbiol.* **2004**, *58*, 611-647.

[82] W. M. Zhu, A. Wilks, I. Stojiljkovic, *J. Bacteriol.* **2000**, *182*, 6783-6790.

[83] M. Ratliff, W. M. Zhu, R. Deshmukh, A. Wilks, I. Stojiljkovic, *J. Bacteriol.* **2001**, *183*, 6394-6403.

[84] M. P. Schmitt, *J. Bacteriol.* **1997**, *179*, 838-845.

[85] W. M. Zhu, D. J. Hunt, A. R. Richardson, I. Stojiljkovic, *J. Bacteriol.* **2000**, *182*, 439-447.

[86] C. Wandersman, I. Stojiljkovic, *Curr. Opin. Microbiol.* **2000**, *3*, 215-220.

[87] J. M. McCord, *J. Nutr.* **2004**, *134*, 3171S-3172S.

[88] S. Osaki, D. A. Johnson, E. Frieden, *J. Biol. Chem.* **1966**, *241*, 2746-2751.

[89] U. A. Ochsner, Z. Johnson, M. L. Vasil, *Microbiol.* **2000**, *146*, 185-198.

[90] S. Cescau, H. Cwerman, S. Letoffe, P. Delepelaire, C. Wandersman, F. Biville, *BioMetals* **2007**, *20*, 603-613.

[91] C. Wandersman, P. Delepelaire, *Mol. Microbiol.* **2012**, *85*, 618-631.

[92] C. Wandersman, I. Stojiljkovic, *Curr. Opin. Microbiol.* **2000**, *3*, 215-220.

[93] P. Cornelis, J. Dingemans, *Front. Cell. Infect. Microbiol.* **2013**, *3*.

[94] T. E. Clarke, L. W. Tari, H. J. Vogel, *Curr. Top. Med. Chem.* **2001**, *1*, 7-30.

[95] A. Idei, E. Kawai, H. Akatsuka, K. Omori, *J. Bacteriol.* **1999**, *181*, 7545-7551.

[96] S. Letoffe, K. Omori, C. Wandersman, *J. Bacteriol.* **2000**, *182*, 4401-4405.

[97] S. Letoffe, V. Redeker, C. Wandersman, *Mol. Microbiol.* **1998**, *28*, 1223-1234.

[98] J. M. Ghigo, S. Letoffe, C. Wandersman, *J. Bacteriol.* **1997**, *179*, 3572-3579.

[99] S. Letoffe, J. M. Ghigo, C. Wandersman, *Proc Natl Acad Sci U S A* **1994**, *91*, 9876-9880.

[100] R. Kumar, S. Lovell, H. Matsumura, K. P. Battaile, P. Moenne-Loccoz, M. Rivera, *Biochemistry* **2013**, *52*, 2705-2707.

[101] M. S. Rossi, J. D. Fetherston, S. Letoffe, E. Carniel, R. D. Perry, J. M. Ghigo, *Infect. Immun.* **2001**, *69*, 6707-6717.

[102] S. Letoffe, C. Deniau, N. Wolff, E. Dassa, P. Delepelaire, A. Lecroisey, C. Wandersman, *Mol. Microbiol.* **2001**, *41*, 439-450.

[103] S. Krieg, F. Huche, K. Diederichs, N. Izadi-Pruneyre, A. Lecroisey, C. Wandersman, P. Delepelaire, W. Welte, *Proc Natl Acad Sci U S A* **2009**, *106*, 1045-1050.

[104] N. Izadi-Pruneyre, F. Huche, G. S. Lukat-Rodgers, A. Lecroisey, R. Gilli, K. R. Rodgers, C. Wandersman, P. Delepelaire, *J. Biol. Chem.* **2006**, *281*,

25541-25550.

[105] P. Arnoux, R. Haser, N. Izadi, A. Lecroisey, M. Delepierre, C. Wandersman, M. Czjzek, *Nat. Struct. Biol.* **1999**, *6*, 516-520.

[106] N. Wolff, N. Izadi-Pruneyre, J. Couprie, M. Habeck, J. Linge, W. Rieping, C. Wandersman, M. Nilges, M. Delepierre, A. Lecroisey, *J. Mol. Biol.* **2008**, *376*, 517-525.

[107] E. T. Yukl, G. Jepkorir, A. Y. Alontaga, L. Pautsch, J. C. Rodriguez, M. Rivera, P. Moenne-Loccoz, *Biochemistry* **2010**, *49*, 6646-6654.

[108] A. Y. Alontaga, J. C. Rodriguez, E. Schonbrunn, A. Becker, T. Funke, E. T. Yukl, T. Hayashi, J. Stobaugh, P. Monne-Loccoz, M. Rivera, *Biochemistry* **2009**, *48*, 96-109.

[109] G. Jepkorir, J. C. Rodriguez, H. Rui, W. Im, S. Lovell, K. P. Battaile, A. Y. Alontaga, E. T. Yukl, P. Moenne-Loccoz, M. Rivera, *J. Am. Chem. Soc.* **2010**, *132*, 9857-9872.

[110] C. Caillet-Saguy, M. Piccioli, P. Turano, G. Lukat-Rodgers, N. Wolff, K. R. Rodgers, N. Izadi-Pruneyre, M. Delepierre, A. Lecroisey, *J. Biol. Chem.* **2012**, *287*, 26932-26943.

[111] C. Caillet-Saguy, M. Piccioli, P. Turano, G. Lukat-Rodgers, N. Wolff, K. R. Rodgers, N. Izadi-Pruneyre, M. Delepierre, A. Lecroisey, *J. Biol. Chem.* **2013**, *288*, 2190-2190.

[112] A. G. Torres, P. Redford, R. A. Welch, S. M. Payne, *Infect. Immun.* **2001**, *69*, 6179-6185.

[113] H. Wojtowicz, T. Guevara, C. Tallant, M. Olczak, A. Sroka, J. Potempa, M. Sola, T. Olczak, F. X. Gomis-Ruth, *PLoS Path.* **2009**, *5*.

[114] A. W. Maresso, O. Schneewind, *BioMetals* **2006**, *19*, 193-203.

[115] N. T. Vu, Y. Moriwaki, J. M. M. Caaveiro, T. Terada, H. Tsutsumi, I. Hamachi, K. Shimizu, K. Tsumoto, *Protein Sci.* **2013**, *22*, 942-953.

[116] M. Watanabe, Y. Tanaka, A. Suenaga, M. Kuroda, M. Yao, N. Watanabe, F. Arisaka, T. Ohta, I. Tanaka, K. Tsumoto, *J. Biol. Chem.* **2008**, *283*, 28649-28659.

[117] R. M. Pilpa, S. A. Robson, V. A. Villareal, M. L. Wong, M. Phillips, R. T. Clubb, *J. Biol. Chem.* **2009**, *284*, 1166-1176.

[118] C. F. M. Gaudin, J. C. Grigg, A. L. Arrieta, M. E. P. Murphy, *Biochemistry*

2011, *50*, 5443-5452.

[119] G. D. Wright, *Adv. Drug Del. Rev.* **2005**, *57*, 1451-1470.

[120] K. Drlica, X. Zhao, *Microbiol. Mol. Biol. Rev.* **1997**, *61*, 377-392.

[121] J. Ishii, T. Nakae, *FEMS Microbiol. Lett.* **1996**, *136*, 85-90.

[122] L. J. V. Piddock, *Nat. Rev. Microbiol.* **2006**, *4*, 629-636.

[123] H. P. Schweizer, *Gen. Mol. Res.* **2003**, *2*, 48-62.

[124] P. S. Stewart, *Int. J. Med. Microbiol.* **2002**, *292*, 107-113.

Chapter II

Aromatic Ring Hydroxylation by Myoglobin Mutants

Chapter II. Aromatic Ring Hydroxylation by Myoglobin Mutants

Introduction

Myoglobin is a small hemoprotein (17 kDa) with an oxygen storage function in muscle tissue.[1-9] Myoglobin has been used as structural and functional models of other heme proteins/enzymes to understand structure and function relationship of heme proteins/enzymes, because a practical amount of myoglobin including its mutants can be obtained using a typical *Escherichia coli* gene-expression system. Furthermore, relatively easy preparation of high-quality crystals of myoglobin for X-ray crystal structure analysis makes myoglobin one of practical model proteins for studies on molecular engineering of proteins (Fig. 2-1).[5, 9] Myoglobin thus has been engineered to perform peroxidase, catalase, peroxygenase, and nitric oxide reductase activities by replacing amino acids in the active-site of myoglobin to mimic the active site of other heme proteins.[10-15] In fact, the location of the distal histidine (His-64) of myoglobin is optimized as an oxygen storage function (Fig. 2-2A) and thus not suitable for the generation of the active species so-called Compound I (iron oxoferryl porphyrin π-cation radical) that is responsible for the oxidation reactions catalyzed by horseradish peroxidase, chloroperoxidase, KatG, catalase, and cytochrome P450s.[16-26] The location

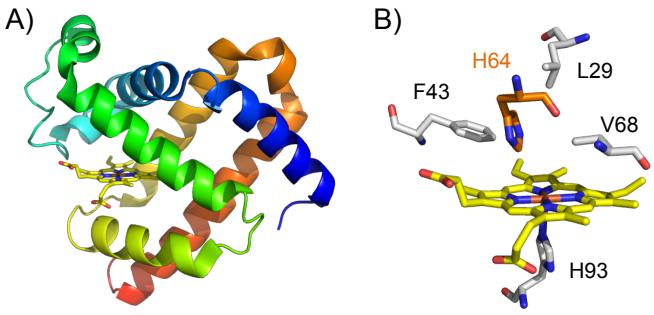

Fig. 2-1 A crystal structure of wild type sperm whale myoglobin (PDB ID: 1DUK). A) Whole structure, B) Close-up view of the active site of wild type myoglobin.

of amino acid residues in peroxidases providing a general acid-base function has been well studied and recognized to be very important for the generation of compound I. On the basis of the distal histidine relocation studies together with the replacement of amino acids to create a space for the access of hydrogen peroxide and substrates (Fig. 2-2B), it was demonstrated that even myoglobin can catalyze peroxidase as well as peroxygenase reactions, while myoglobin basically does not have any enzymatic activities.[10, 27] A variety of myoglobin mutants which shows enzymatic reactions of horseradish peroxidase, catalase, and chloroperoxidase were prepared. For example, a H64D/V68I mutant of myoglobin showed peroxidase and peroxygenase activities; one electron oxidation of ABTS, sulfoxidation of thioanisole, and epoxidation of styrene are catalyzed by the mutant.[28, 29] The aromatic ring hydroxylation of indole is also catalyzed by a series of myoglobin mutants developed based on the H64D/V68I mutant, whereas the position hydroxylated was limited to the pyrrole ring of indole.[30] While it has been believed that the proximal thiolate ligation observed in chloroperoxidase and cytochrome P450s is critical for the oxidation of less-reactive aromatic rings, the phenyl ring of tryptophan placed in the heme pocket (Trp-43 in the F43W/H64D/V68I mutant) was efficiently hydroxylated by the myoglobin mutant (Fig. 2-3).[31] This result indicates that myoglobin compound I is able to proceed cytochrome P450 type reactions, even though their proximal ligand is histidine. In addition, this result shows that substrate fixation at an appropriate position near the active species is critical to perform hydroxylations of less-reactive C-H bonds. This conclusion is supported by the fact that most cytochrome P450s appropriately fix their substrates near by the heme iron. For example, the crystal structure of palmitoleic acid bound form of P450BM3, a fatty acid hydroxylase, shows that the palmitoleic acid is fixed by the interaction of the carboxylate group of fatty acid with Tyr-51 as well as Arg-47 of P450BM3 located at the entrance of the substrate (Fig. 2-4).[32, 33] These results encouraged this author to develop myoglobin mutants that efficiently catalyze a hydroxylation reaction of aromatic rings by constructing a substrate binding site at the surface of the H64D/V68I

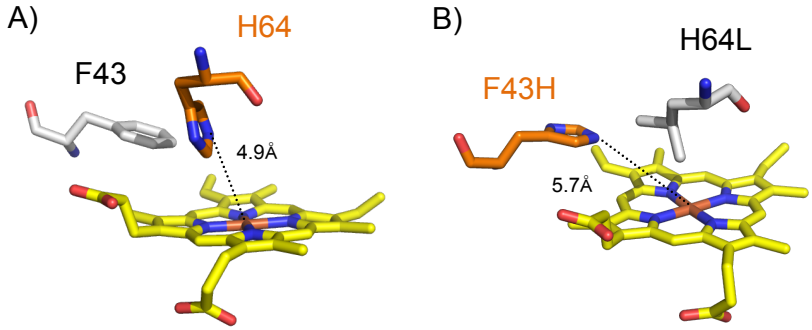

Fig. 2-2 The crystal structure of active sites of A) wild type sperm whale myoglobin (PDB ID: 1DUK), B) F43H/H64L sperm whale myoglobin mutant, which has enzymatic activities due to the replaced histidine (PDB ID: 1OFK).

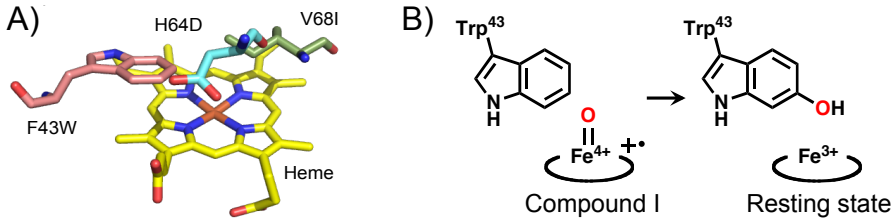

Fig. 2-3 A) A close-up view of the active site in myoglobin F43W/H64D/V68I mutant (PDB ID: 2E2Y). B) Hydroxylation position of the inserted Tryptophan at position 43. Heme is shown as a circle.

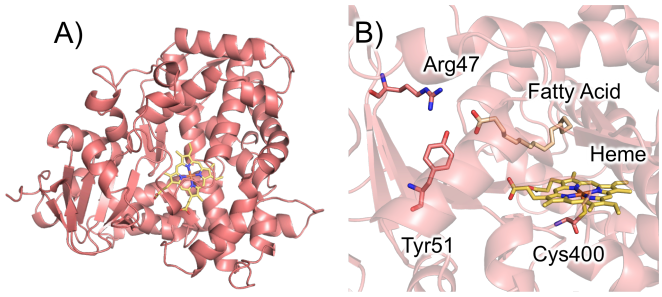

Fig. 2-4 The crystal structure of Cytochrome P450BM3 (PDB ID: 1FAG): A) Overall structure and B) active site structure. The Arg47 (a key residue for substrate fixation), Tyr51 (another key residue for substrate fixation), heme, Cys400 (a ligand), and a fatty acid (a substrate) are shown as stick models.

mutant of myoglobin. The author decided to introduce an arginine residue into the H64D/V68I myoglobin mutant to fix substrates having a carboxyl group by an electro static interaction and prepared a H64D/T67R/V68I mutant. This mutant with an arginine residue can be regarded as a model of P450BM3. In addition, the author also decided to develop a colorimetric assay system based on the stepwise oxidation of methoxynaphthalene for the evaluation of an enzymatic activity of myoglobin mutants. During the course of our studies on the foreign substrates hydroxylation by myoglobin mutants, we found a blue color product formation in the oxidation reaction of the derivative of methoxynaphthalene by H_2O_2-dependent cytochrome P450s. The product was finally identified as Russig's blue. This finding strongly suggested that methoxynaphthalene and its derivatives could be used as a substrate for colorimetric assay of enzymatic oxidation activities. In this chapter, the aromatic ring hydroxylation of methoxynaphthalene and naproxen by myoglobin mutants was described. To examine the effect of an arginine residue as a substrate-binding site for the fixation of substrate with a carboxyl group, the catalytic activities of both the H64D/V68I and the H64D/T67R/V68I mutants toward naproxen were examined. Furthermore, the catalytic activities toward (*R*)-naproxen and (*S*)-naproxen were also compared to further evaluate the substrate binding to the H64D/T67R/V68I myoglobin mutant.

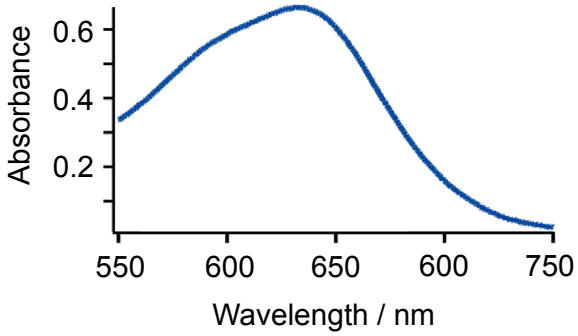

Fig. 2-5 UV-vis spectrum of Russig's blue in chloroform. A reaction mixture of 1-methoxynaphthalene oxidation by myoglobin mutant was extracted with chloroform.

Result and Discussion

Aromatic hydroxylation of 1-methoxynaphthalene by myoglobin mutants

Initially, the author examined whether 1-methoxynapthalene was oxidized by the H64D mutant of myoglobin by monitoring the color change of the reaction mixture. When hydrogen peroxide was added to the reaction mixture as an oxidant, the color of a reaction mixture turned to blue. The blue product was extracted with chloroform. The UV-vis spectrum of the extract with absorption maximum at 634.5 nm was identical to that obtained by using cytochrome $P450_{BS\beta}$[34, 35] that gave 4,4'-dimethoxy-[2,2']-binaphthalenylidene-1,1'-dion called Russig's blue, which has a strong absorption at a visible region due to its extended π system (Fig. 2-5).[36, 37] The MALDI-TOF-mass spectrum of the blue product obtained using the H64D mutant showed a peak at *m/z* 345.13 $[M+H]^+$, which accords well with that calculated for Russig's blue (calcd. exact mass for $C_{22}H_{16}O_2$ 344.11), indicating that the H64D mutant of myoglobin catalyzes the hydroxylation of 1-methoxynapthalene and the subsequent oxidation of 4-methoxy-1-naphthol gave Russig's blue. A plausible reaction mechanism for the formation of Russig's blue is shown in Figure 2-6.

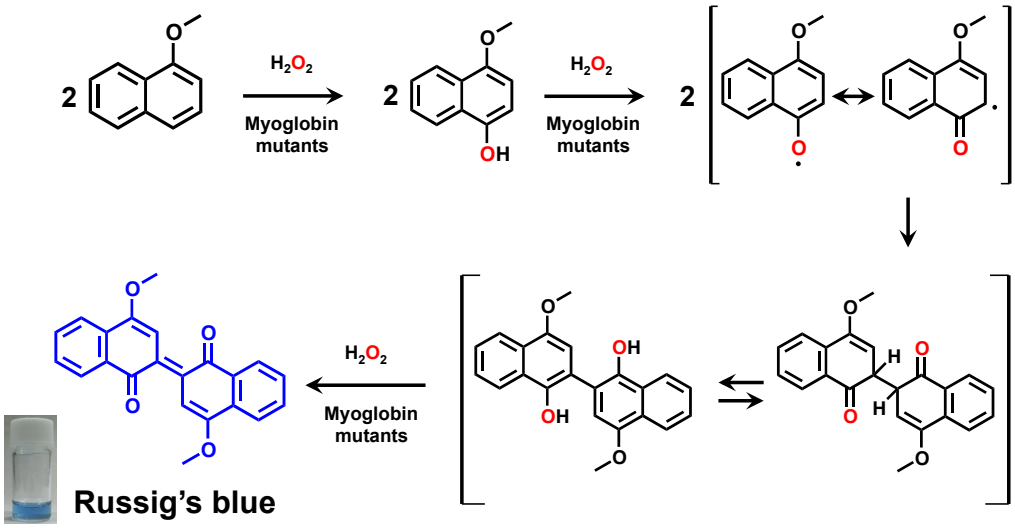

Fig. 2-6 A plausible reaction mechanism for Russig's blue formation.

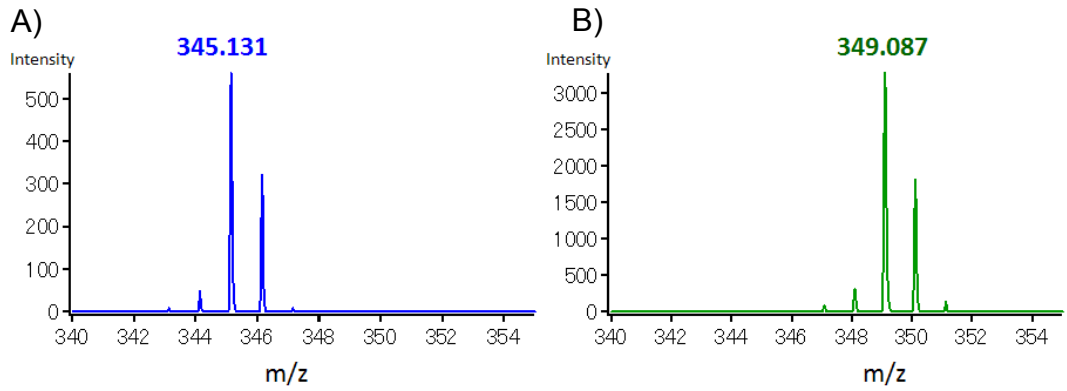

Fig. 2-7 MALDI-TOF-MS spectra of the extracted Russig's Blue prepared by myoglobin H64D mutant. A) The spectrum of the product obtained with $H_2{}^{16}O_2$. B) The spectrum of the product obtained with $H_2{}^{18}O_2$.

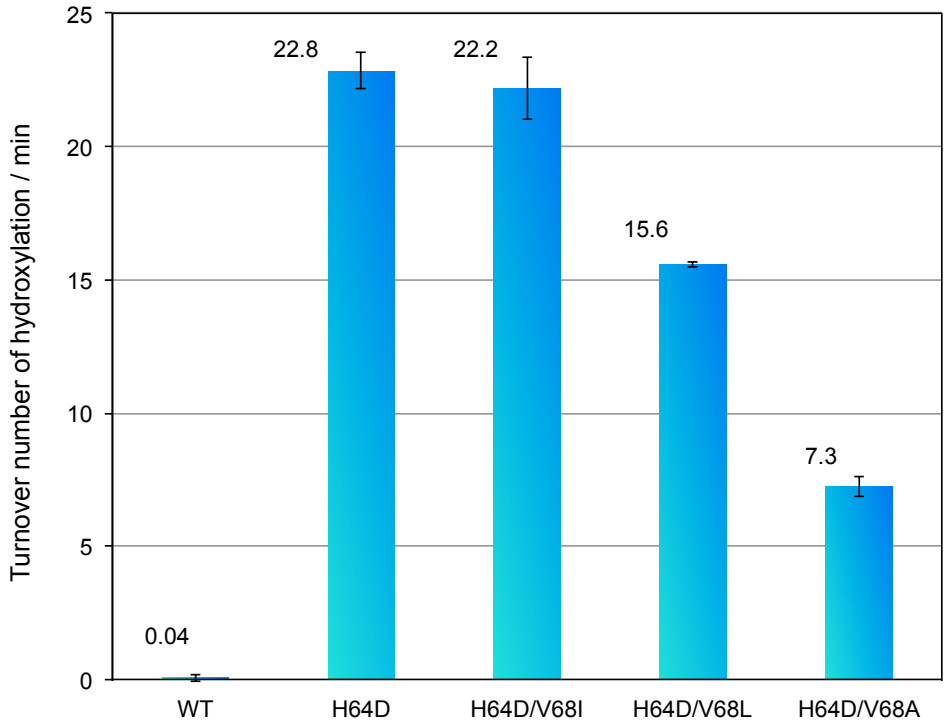

Fig. 2-8 Aromatic ring hydroxylation activities of a series of H64D myoglobin mutants for 1-methoxynaphthalene.

The hydroxylation of 1-methoxynaphthalene at its 4-position followed by a one-electron-oxidation reaction of 4-methoxy-1-naphthol and subsequent radical coupling reaction affords Russig's blue. This reaction mechanism is supported by the reaction using ^{18}O-labeled hydrogen peroxide. The MALDI-TOF-mass spectrum of Russig's blue obtained with $H_2{}^{18}O_2$ showed a peak at *m/z* 349.09 $[M+H]^+$ (calcd. exact mass for $C_{22}H_{16}{}^{18}O_2{}^{16}O^2$ 348.11), suggesting that the ^{18}O atom from hydrogen peroxide is inserted to 1-methoxynaphthalene via compound I (Fig. 2-7). The clear color change due to the hydroxylation of substrate allows us to monitor the progress of the reaction by UV-vis spectroscopy and to estimate catalytic activity of myoglobin mutants without use of HPLC, GC, and NMR. The initial tune over rate for the hydroxylation by a series of H64D mutants of myoglobin are estimated from the absorption change and shown in Figure 2-8. The catalytic activities of a series of H64D mutants for 1-methoxynaphthalene hydroxylation are dependent on the amino acid at the position of 68 and the H64D and H64D/V68I mutants are equally active. The 68 position appears to

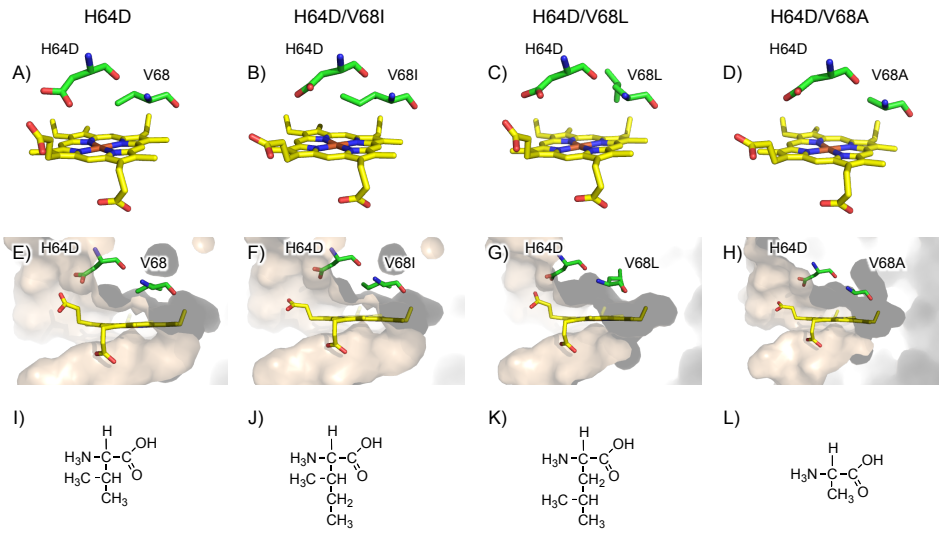

Fig. 2-9 The simulated structures of a series of H64D myoglobin mutants A, E) H64D, B, F) H64D/V68I, C, G) H64D/V68L, and D, H) H64D/V68A. These structures were calculated by Insight II. The residues of position 64 and 68 are shown by stick models. Heme is also shown by stick models. The chemical structure of inserted amino acids are also shown. I) valine, J) isoleucine, K) leucine, and L) alanine.

be important for the access and/or fixation of 1-methoxynaphthalene (Fig. 2-10). It is noteworthy to mention here that the catalytic activities of myoglobin mutants in 1-methoxynaphthalene and styrene correlate quite well (Fig. 2-10), indicating that 1-methoxynaphthalene is useful to estimate monooxygenation activities.

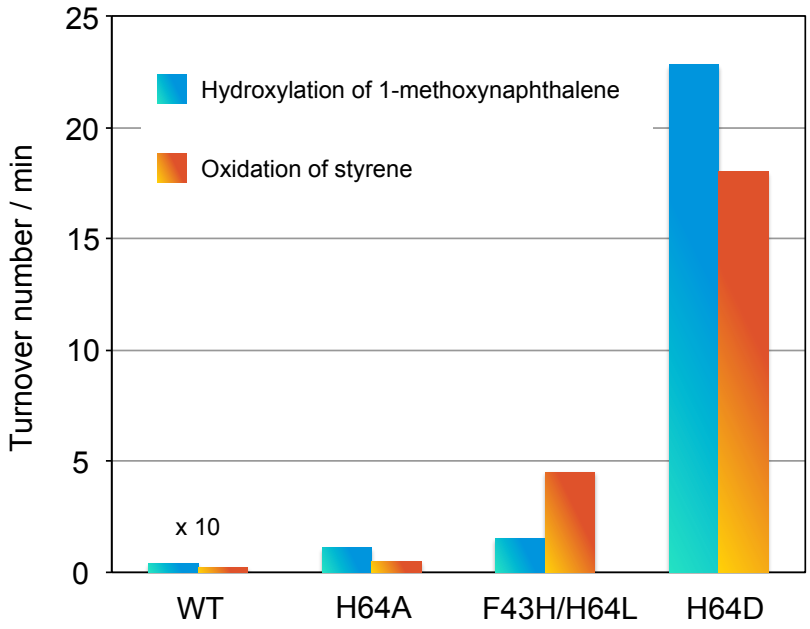

Fig. 2-10 Comparison of the activities of Russig's blue formation and those stylene oxidation catalyzed by myoglobin mutants. In the case of the F43H/H64L mutant, the initial turnover rate of the styrene epoxidation is shown in the previous reports.[12, 38, 39]

(*R*) and (*S*)-Naproxen hydroxylation by myoglobin mutants

(*S*)-naproxen is a non-steroidal anti-inflammatory drug,[40] which includes 2-methoxynaphthalene as its partial structure. Since (*S*)-naproxen is available as a commonly-used drug, it is not so expensive in spite of its chiral structure. Because the enzymatic hydroxylation of 1-methoxynaphthalene by myoglobin mutants affords Russig's blue, the author expected that (*S*)-naproxen with a partial structure of 2-methoxynaphthalene can be also a substrate of myoglobin mutants, thus, their catalytic activities for aromatic hydroxylation were examined. As expected, the oxidation of (*S*)-naproxen by the H64D/V68I mutant, which showed high hydroxylation

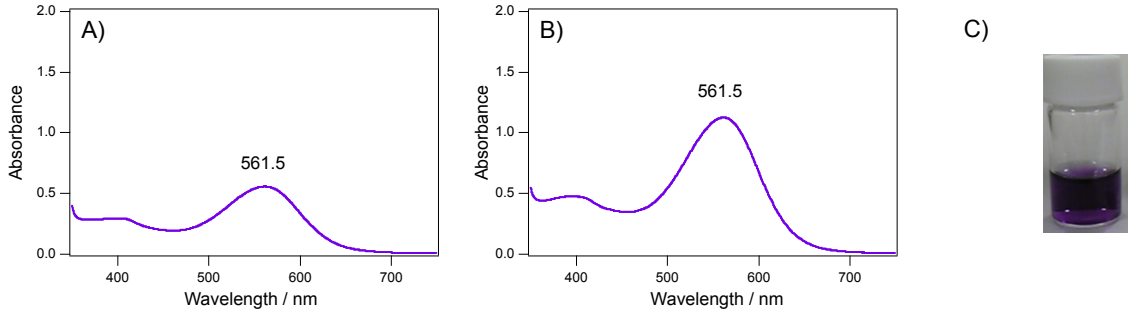

Fig. 2-11 UV-Vis spectra of (*S*)-naproxen reaction mixtures of oxidation by A) by H64D/V68I myoglobin mutant, B) H64D/T67R/V68I mutant. The reaction time was 30 minutes. C) A picture of reaction mixture of (*S*)-naproxen oxidation by myoglobin mutant.

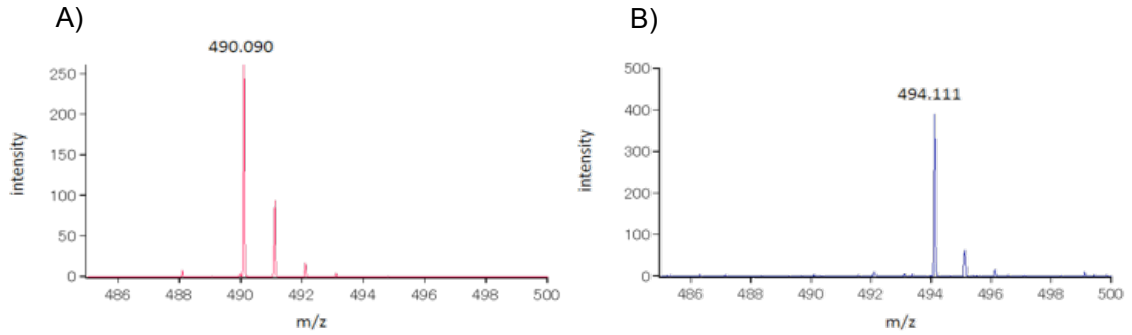

Fig. 2-12 MALDI-TOF-MS spectra of the extracted reaction mixture of (*S*)-naprxen oxidation by H64D/T67R/V68I myoglobin mutant. A) The spectrum of the product obtained with $H_2{}^{16}O_2$. B) The spectrum of the product obtained with $H_2{}^{18}O_2$.

activity for 1-methoxynaphtahlene, gave a purple product with UV-vis absorption maxima at 560 nm (Fig. 2-11). The molecular weight of the product measured by MALDI-TOF-MS (*m/z* 490.090 $[M+H]^+$) (Fig. 2-12A) suggests a dimer of (*S*)-naproxen with an extended π-system that is similar to Russig's blue. It was confirmed that two ^{18}O atoms are inserted into the product using $H_2{}^{18}O_2$. (*m/z* 494.111$[M+H]^+$, Fig. 2-12B). A plausible reaction mechanism for the oxidation of (*S*)-naproxen is shown in Fig. 2-13. It is noteworthy to mention here that the solubility of the final product obtained from

(*S*)-naproxen is much better than that of Russig's blue. The carboxylate of (*S*)-naproxen contributes to improve the solubility of the final product. This carboxylate can be also used to evaluate an effect of substrate binding to enzyme upon catalytic activity. The binding of (*S*)-naproxen would be enhanced by the electrostatic interaction of its carboxylate with positively charged amino acids such as arginine, as is observed in P450BM3; i.e., in which the carboxylate of fatty acids interacts with Arg-47 on the surface of P450BM3. Indeed, it was reported that the arginine of T67R mutant of myoglobin stabilizes the binding of ligand molecules bearing a carboxyl group to the iron center.[41] The crystal structure of the H64D/T67R/V68I mutant of myoglobin showed that an arginine residue is located close to the heme (Fig. 2-14).[42] Therefore, the arginine of H64D/T67R/V68I was expected to serve as a binding site for substrates having a carboxylate including (*S*)-naproxen. The time course of absorption change at 560nm due to the oxidation of (*S*)-naproxen by the H64D/T67R/V68I was examined and compared with that of H64D/V68I (Fig. 2-15). The oxidation of (*S*)-naproxen catalyzed by H64D/T67R/V68I was faster than that catalyzed by H64D/V68I, suggesting that the Arg-67 serves as a substrate-binding site.

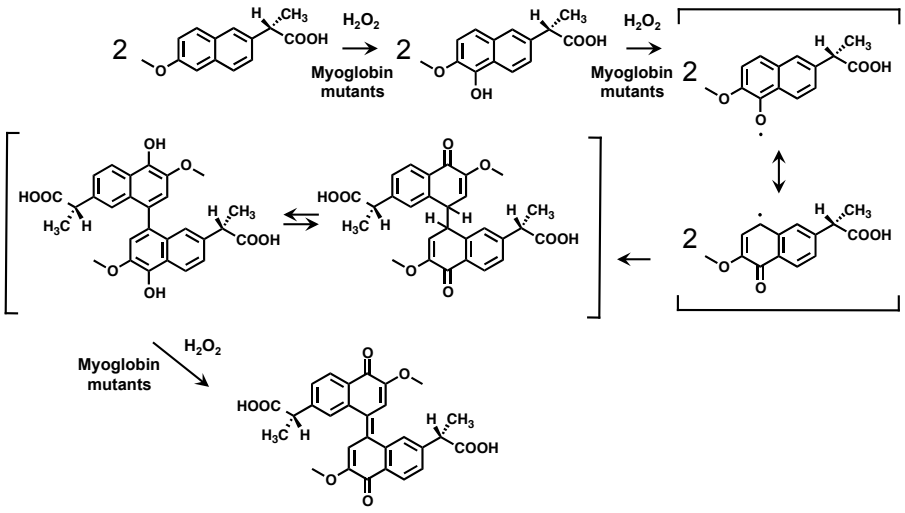

Fig. 2-13 A plausible reaction scheme of (*S*)-naproxen oxidation. The exact mass of the expected final compound is 488.15, and its calculated molecular weight is 488.49.

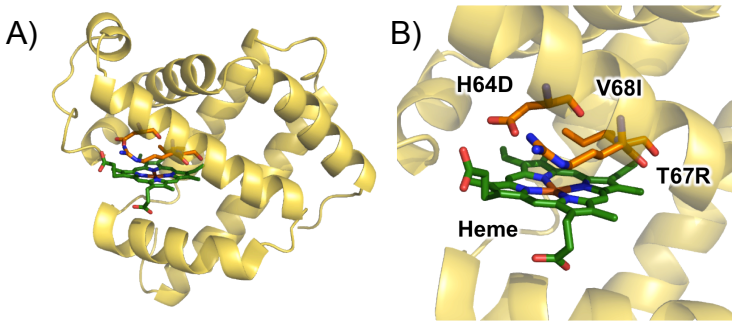

Fig. 2-14 A crystal structure of myoglobin H64D/T67R/V68I mutant. A) Whole structure, B) Close-up view of the active site of the myoglobin mutant.

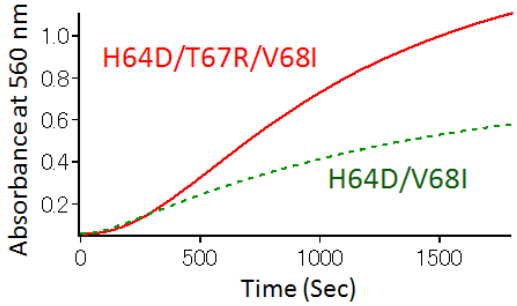

Fig. 2-15 Time course of absorbance at 560 nm during the (*S*)-naproxen oxidation by myoglobin H64D/T67R/V68I mutant (red, a solid line) and H64D/V68I mutant (green, a dashed line). UV-Vis spectra of samples after these time course measurements are shown in Fig. 2-11.

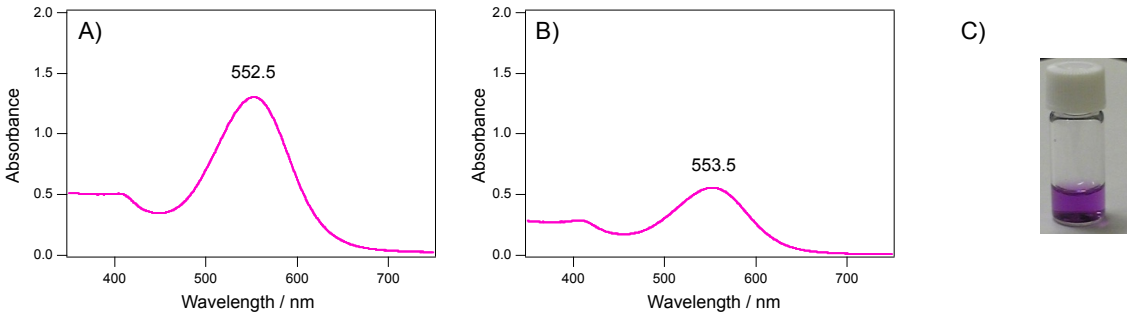

Fig. 2-16 UV-Vis spectra of 2-methoxynaphthalene reaction mixtures of oxidation by A) by H64D/V68I myoglobin mutant, B) H64D/T67R/V68I mutant. The reaction time was 30 minutes. C) A picture of reaction mixture of 2-methoxynaphthalene oxidation by myoglobin mutant.

Interestingly, 2-methoxynaphtalen hydroxylation by the H64D/T67R/V68I mutant proceeds slower than (*S*)-naproxen, while the catalytic activity of the H64D/V68I mutant for 2-methoxynaphtalen hydroxylation was larger than (*S*)-naproxen (Fig. 2-16, 2-17), suggesting the H64D/T67R/V68I mutant is suitable for the hydroxylation of substrates with carboxylic acid. A possible interaction between the carboxylic acid of substrate and the Arg-67 of myoglobin mutant appears to improve the catalytic activity. The binding constants of (*S*)-naproxen against the H64D/T67R/V68I and H64D/V68I mutants were estimated by the UV-vis titration experiment to examine an effect of the Arg-67 upon the substrate binding. The binding constant of (*S*)-naproxen against the H64D/T67R/V68I (0.12 mM^{-1}) is, however, smaller than that against H64D/V68I. Similarly, the Michaelis-Menten constant (K_m) for the H64D/T67R/V68I is larger compared with that for the H64D/V68I (Fig. 2-18, 2-19, Table 2-1). The Hill coefficient values of both myoglobin mutants were estimated to be around 1.0 showing no cooperative effect in the naproxen hydroxylation (Fig. 2-20, Table 2-1). These results suggest that the Arg-67 may not contribute to fixation of (*S*)-naproxen, but it may be involve in controlling the orientation of (*S*)-naproxen, which accelerates the hydroxylation of aromatic ring (the rate-determining step). This is supported by the facts that a clear difference was observed in its catalytic activity between the (*S*)-naproxen oxidation and (*R*)-naproxen oxidation by the H64D/T67R/V68I. The H64D/T67R/V68I mutant showed higher oxidation activity for (*S*)-naproxen than (*R*)-naproxen (Fig. 2-21). In sharp contrast, the H64D/V68I mutant showed the same oxidation profile irrespective of the chirality of naproxen. Although the catalytic activities of the H64D/T67R/V68I for (*S*)-naproxen and (*R*)-naproxen oxidation were small, the author believes that (*S*)-naproxen and (*R*)-naproxen can be used as a set of substrate for a facile screening of chiral selectively in oxidation by enzymes.

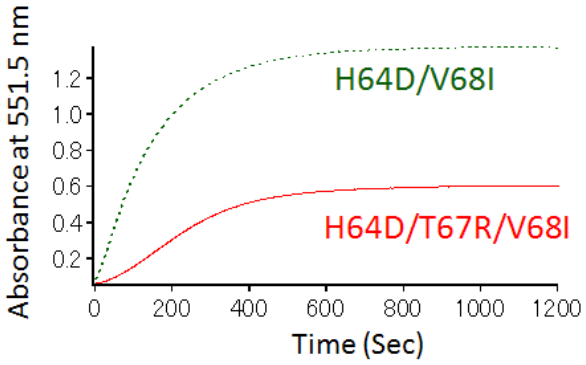

Fig. 2-17 Time course of absorbance at 551.5 nm during the 2-methoxynaphthalene oxidation by myoglobin H64D/T67R/V68I mutant (red, a solid line) and H64D/V68I mutant (green, a dashed line). UV-Vis spectra of samples after these time course measurements are shown in Fig. 2-16.

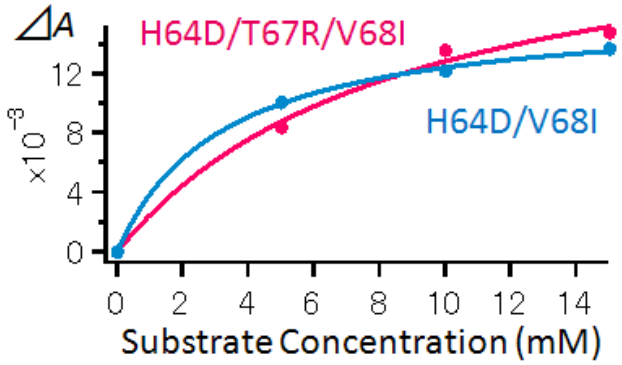

Fig. 2-18 Binding curves of myoglobin mutants (Pink line: H64D/T67R/V68I, Blue line: H64D/V68I) to (*S*)-naproxen. The vertical axis shows difference of the absorbance at 560 nm after oxidation reaction.Points represent experimental spectral data (Abs. at 560 nm) and the solid curve represents the fit with eq. 1.

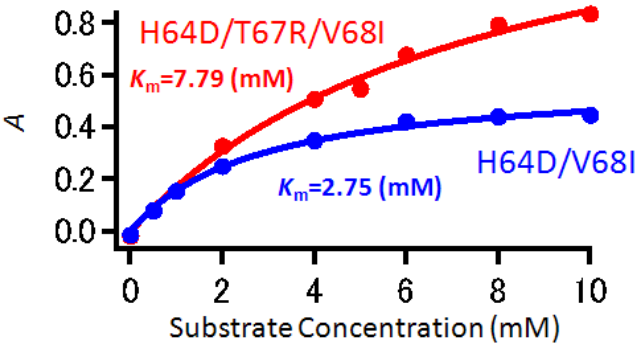

Fig. 2-19 The purple product formation by myoglobin mutant (Red: H64D/T67R/V68I, Blue: H64D/V68I) dependent (*S*)-naproxen oxidation. The vertical axis shows absorbance at 560 nm after oxidation reaction. The horizontal axis shows substrate concentration. Points represent experimental spectral data (Abs. at 560 nm) and the solid curve represents the fit with eq. 3.

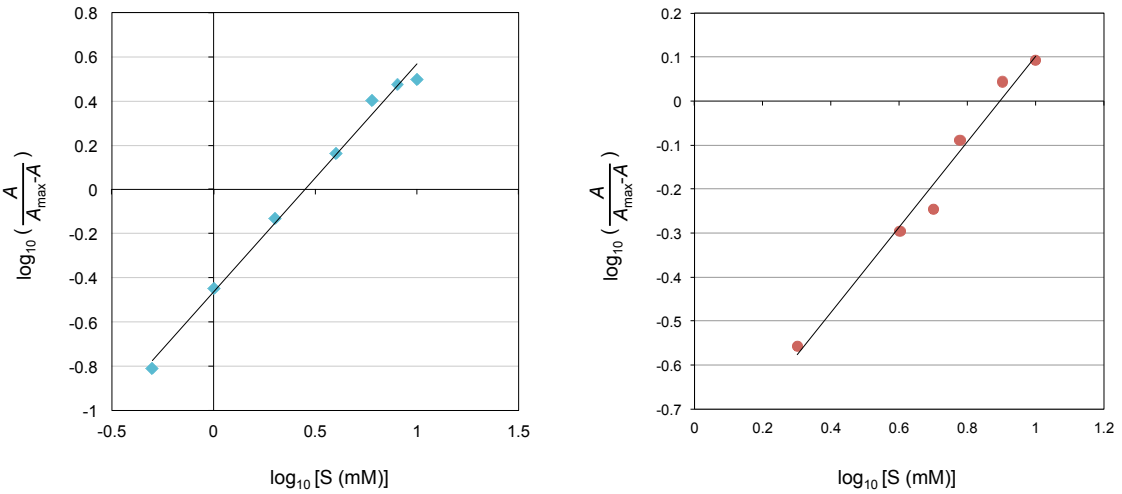

Fig. 2-20 Cooperativity in the oxidation of the (*S*)-naproxen by myoglobin H64D/V68I mutant (left side) and H64D/T67R/V68I mutant (right side) supported by H_2O_2 and in the binding of (*S*)-naproxen. The rates of the purple product formation were fitted to an equation (eq. 4) based on Hill equation (eq. 5). The Hill coefficients were estimated from the slop of the plots.

Table 2-1 Kinetic constants for purple product formation by (*S*)-naproxen oxidation with myoglobin mutants and hydrogen peroxide.

Coupling Constant

Mb mutant	Chi Square	K_{11} (mM^{-1})	ε_{11}	[Mb] (mM)
H64D/V68I	9.28E-08	0.31	3.29	0.005
H64D/T67R/V68I	8.64E-07	0.12	8.33	0.029

Michaelis Constant

Mb mutant	Chi Square	A_{max}	K_m (mM)
H64D/V68I	0.0009	0.59	2.75
H64D/T67R/V68I	0.0041	1.51	7.79

Hill Coefficient

Mb mutant	Hill coefficient
H64D/V68I	1.031
H64D/T67R/V68I	0.969

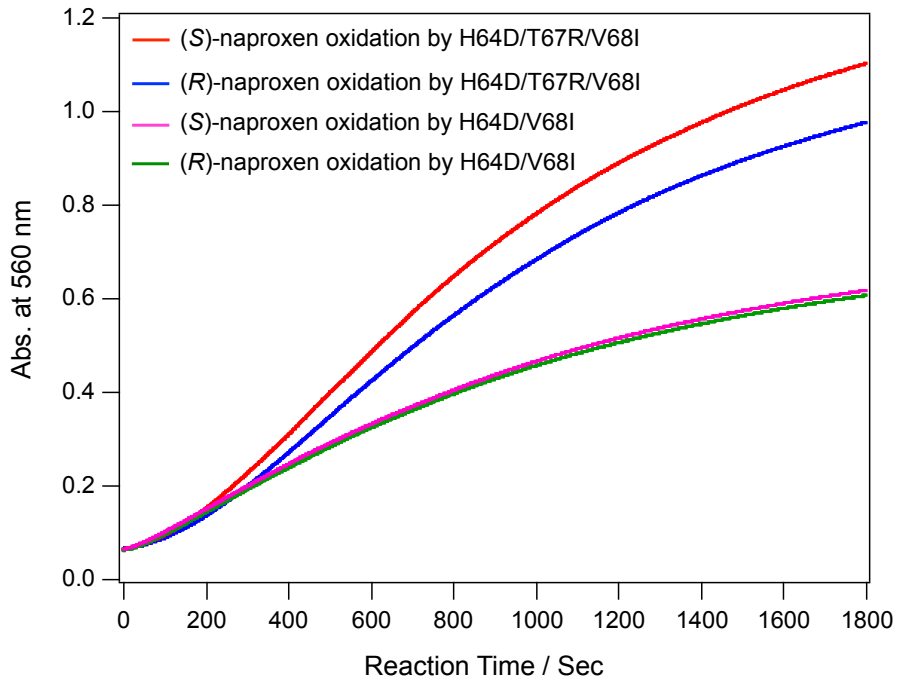

Fig. 2-21 Time course of the oxidation reaction of naproxen by myoglobin mutants. Red line is the time course of the (*S*)-naproxen oxidation by H64D/T67R/V68I mutant. Blue line is the time course of (*R*)-naproxen by H64D/T67R/V68I mutant. Pink line is the time course of the (*S*)-naproxen oxidation by H64D/V68I mutant. Green line is the time course of (*R*)-naproxen by H64D/V68I mutant.

Conclusion

The author has reported here that the aromatic hydroxylation of 1-methoxynaphthalene is catalyzed by sperm whale myoglobin mutants using hydrogen peroxide as an oxidant. Its activities can be estimated by monitoring a color change due to the Russig's blue formation. The initial turnover rates were 23 min^{-1} and 22 min^{-1} in the cases of H64D and H64D/V68I, respectively. H64D/T67R/V68I myoglobin mutant catalyzes naproxen effectively compared with H64D/V68I mutant. Interestingly, H64D/T67R/V68I myoglobin mutant oxidized the (*S*)-naproxen more efficiently compared with (*R*)-naproxen. These results suggest that the inserted arginine residue contributes to control the orientation of naproxen in the heme vicinity. This is the first example of chirality selective aromatic hydroxylation by a myoglobin mutant. The naproxen oxidation is a useful reaction for estimating the hydroxylation activity of enzymes without the use of HPLC, gas chromatography, and NMR measurements.

Material and Methods

Chemicals

All chemicals were purchased from commercial sources and used without further purification. Hydrogen peroxide, 1-methoxynaphthalene, and (*S*)-(+)-naproxen were obtained from Wako Pure Chemical Industries (Osaka, Japan). 2-methoxynaphthalene was obtained from Tokyo Chemical Industry (Japan). Dithranol and (*R*)-(-)-6-methoxy-alpha-methyl-2-napthaleneacetic acid (naproxen) were obtained from Sigma-Aldrich (USA). $H_2{}^{18}O_2$ was purchased from ICON (Isotope) Services (Summit, NJ, USA).

Instruments

UV-vis spectra were recorded on a Shimadzu UV-2400 PC spectrophotometer. Matrix-assisted laser deposition ionization (MALDI) time-of-flight (TOF) mass

spectrometry was performed using a Bruker Daltonics Ultraflex III MALDI-TOF mass spectrometer.

Protein Expression and Purification

The preparation and purification of H64D, H64D/V68I, H64D/V68L and H64D/V68A mutants were reported previously.[29, 43, 44] The H64D/T67R/V68I myoglobin mutant was constructed using a polymerase chain reaction-based cassette mutagenesis technique developed by Mr. Takahiro Ohki who had belonged to the author's research group at Nagoya University. The primer used for the mutation at the 107 position in wild type myoglobin gene was reported previously.[41]

Mutants were expressed in *Escherichia coli* strain TB-1 and purified according to a reported procedure with some modifications.[12, 28, 29] Briefly, an 18 L culture of the *E. coli* cells was grown at 37 ^{o}C in LB medium in the presence of ampicillin (100 mg/L), harvested in the late log phase, lysed, and sonicated on ice. Cell debris was removed by centrifugation (4 ^{o}C, 17500 rpm, 30 min), and the supernatant was fractionated by ammonium sulfate precipitation. The precipitate was dissolved in a minimum amount of potassium phosphate buffer (15 mM, pH 6.0), followed by dialysis against the same buffer. The dialyzed solution was applied to a CM-52 ion exchange column (5 x 40 cm) equilibrated with the same buffer. Once the sample is submitted on the top of the column, it is washed by the same buffer, fresh eluting solvent is added to the top with a linear gradient from 15 mM potassium phosphate buffer (pH6.0) to 40 mM (pH 9.0). The sample was applied on a Sephadex G-75 gel filtration column (4.6 x 100 cm) equilibrated with 50 mM potassium phosphate buffer (pH 7.0), and eluted with the same buffer for further purification of myoglobin mutants. Concentration of Myoglobin mutants was determined by a pyridine hemochrome method. The purified protein was frozen with liquid nitrogen and stored at -80 ^{o}C until used.

Catalytic activity assay of myoglobin mutants to 1-methoxynaphthalene

The reaction was carried out in 50 mM potassium phosphate buffer (pH 7.0) containing 0.5 of mM 1-methoxynapthalene, 10% EtOH, and 3.6 μM of myoglobin mutants in a final volume of 1 mL at room temperature for 1 minute. The reaction was initiated by the addition of 100 mM hydrogen peroxide (final concentration of 1 mM). After the reaction for 1 minute, the reaction mixture was extracted with 1 mL chloroform. The catalytic activities of the myoglobin mutants for 1-methoxynaphthalene were determined by monitoring the absorbance at 634.5 nm in chloroform.[45] The molar absorption coefficient of Russig's blue at 634.5 nm was determined using a purified sample ($\varepsilon_{634.5}$ = 1.8 x 10^4 $M^{-1}cm^{-1}$). The reaction was repeated at least three times and the averages of the initial turnover rate are summarized.

MALDI-TOF-MS spectral measurement of produced Russig's blue

The oxidation was carried out in 50 mM potassium phosphate buffer (pH 7.0) containing 0.5 mM of 1-methoxynapthalene, 10% EtOH, and 3.6 μM of a myoglobin H64D mutant. After enzymatic 1-methoxynaphthalene oxidation by a series of myoglobin mutants, the reaction mixture was extracted with chloroform. The extracted compounds and dithranol as a matrix were applied on a plate and a MALDI-TOF-MS spectrum was measured in a positive ion mode.

Comparison of oxidation efficiency between (S)-naproxen and 2-methoxynapthalene

The reaction was carried out in 50 mM potassium phosphate buffer (pH 7.0) containing 10 mM of substrate, 10% EtOH, and 3.0 μM of myoglobin mutants in a final volume of 3 mL at room temperature. After addition of 100 mM of hydrogen peroxide (final concentration of 1 mM), the time course of absorbance change at 560.0 nm was recorded for 30 minute. After the reaction, the UV-vis spectrum of the reaction mixture was measured. The cell temperature in the UV-vis spectrometer was kept at 25 ^oC.

MALDI-TOF mass spectral measurement of the oxidized naproxen

After an enzymatic (*S*)-naproxen oxidation by the myoglobin H64D/T67R/V68I mutant, an adequate amount of 50 mM potassium phosphate buffer (pH 2.0-3.0) was added to the reaction solution. The reaction mixture was extracted with chloroform. The extracted compounds and 2,5-dihydroxybenzoic acid as a matrix were applied on a plate and a MALDI-TOF-MS spectrum was measured in the positive ion mode.

Comparison of oxidation activities between (S)-naproxen and (R)-naproxen

The reaction was carried out in 50 mM potassium phosphate buffer (pH 7.0) containing 10 mM of substrate, 10% EtOH, and 3.0 μM of myoglobin mutants in a final volume of 3 mL at room temperature. After the addition of 100 mM hydrogen peroxide (final concentration of 1 mM), the time course of absorbance change at 560.0 nm was recorded for 30 minute. The cell temperature in the UV-vis spectrometer was kept at 20 ^{o}C.

Binding constants of (S)-naproxen for myoglobin mutants

The binding constants were determined from the slopes of the plots of (*S*)-naproxen concentration versus the absorbance change of myoglobin mutants at 395.5 nm (H64D/V68I) and 403.0 nm (H64D/T67R/V68I). The binding constants were calculated based on Equation 1. The binding constant K_{11} was calculated by curve fitting with Igor. Pro. 5.04B.

$$\Delta A_{obs} = \frac{b\Delta\varepsilon_{11}}{2K_{11}} [1+K_{11}[H]_0+K_{11}[G]_0-\{(1+K_{11}[H]+K_{11}[G]_0)^2-4K_{11}^2[H]_0[G]_0\}^{1/2}] \qquad \text{(Eq. 1)}$$

ΔA_{obs} is the absorbance change at 395.5 nm (H64D/V68I) or 403.0 nm (H64D/T67R/V68I) upon substrate binding to myoglobin mutants, $[H]_0$ is the concentration of naproxen (mM) as a host molecule, $[G]_0$ is the fixed concentration of

myoglobin mutants (mM) as a guest molecule, *b* is the optical path length (cm), and K_{11} is the binding constant of 1:1 complex. $\Delta\varepsilon_{11}$ is the difference in the molar absorptivity between the free and complexed substrate.

Michaelis constant in (S)-naproxen oxidation

The reaction was carried out in 50 mM potassium phosphate buffer (pH 7.0) containing (*S*)-naproxen, 10% EtOH, and 3.0 μM of myoglobin mutants in a final volume of 1 mL at room temperature. After addition of 100 mM of hydrogen peroxide (final concentration of 1 mM), the time course of absorbance change at 560.0 nm was recorded for 30 minute. The cell temperature in the UV-vis spectrometer was kept at 20 ^{o}C.

For steady state kinetic analysis, initial rates of the reaction were estimated from the slopes of the plots of the final product concentration versus the reaction time. The equation 2 is an equation of Michaelis-Menten kinetics.

$$v_0 = \frac{V_{max}[\mathrm{S}]}{K_\mathrm{m} + [\mathrm{S}]} \qquad \text{(Eq. 2)}$$

where v_0 and V_{max} are the initial rate and the maximum velocity, respectively. [S] is the substrate concentration and K_m is the Michaelis constant. Because the mol absorption coefficient of the purple product is unknown, the equation was converted into the equation 3.

$$A = \frac{A_{max}[\mathrm{S}]}{K_\mathrm{m} + [\mathrm{S}]} \qquad \text{(Eq. 3)}$$

A is the absorbance at 560.0 nm after the 30 minutes reaction. A_{max} is an expected maximum absorbance. The value of K_m was calculated by curve fitting with Igor. Pro. 5.04B.

Calculation of Hill coefficient

The Hill coefficient was estimated by a linear fit of the data to a logarithmic form of the equation 4.

$$\log_{10}\left(\frac{A}{A_{max} - A}\right) = n \log_{10}[S] - \log_{10}K' \qquad \text{(Eq. 4)}$$

where K' is a constant including interaction factor and intrinsic dissociation constant. A and A_{max} are the absorbance at 560.0 nm after the 30 minutes reaction and the expected maximum absorbance at 560 nm, respectively. n and [S] are the number of substrate binding sites and substrate concentration. The equation 4 is based on the Hill equation (equation 5).

$$\log_{10}\left(\frac{v}{V_{max} - v}\right) = n \log_{10}[S] - \log_{10}K' \qquad \text{(Eq. 5)}$$

where v and V_{max} refer to the rate and the maximum velocity, respectively.

Reference

[1] H. Kawai, H. Nishino, Y. Nishida, K. Masuda, S. Saito, *Muscle Nerve* **1987**, *10*, 144-149.

[2] G. A. Ordway, D. J. Garry, *J. Exp. Biol.* **2004**, *207*, 3441-3446.

[3] J. B. Wittenberg, B. A. Wittenberg, *J. Exp. Biol.* **2003**, *206*, 2011-2020.

[4] B. A. Wittenberg, J. B. Wittenberg, P. R. Caldwell, *J. Biol. Chem.* **1975**, *250*, 9038-9043.

[5] J. Vojtechovsky, K. Chu, J. Berendzen, R. M. Sweet, I. Schlichting, *Biophys. J.* **1999**, *77*, 2153-2174.

[6] R. E. Brantley, S. J. Smerdon, A. J. Wilkinson, E. W. Singleton, J. S. Olson, *J. Biol. Chem.* **1993**, *268*, 6995-7010.

[7] J. S. Olson, A. J. Mathews, R. J. Rohlfs, B. A. Springer, K. D. Egeberg, S. G. Sligar, J. Tame, J. P. Renaud, K. Nagai, *Nature* **1988**, *336*, 265-266.

[8] K. Shikama, A. Matsuoka, *Crit. Rev. Biochem. Mol. Biol.* **2004**, *39*, 217-259.

[9] J. C. Kendrew, G. Bodo, H. M. Dintzis, R. G. Parrish, H. Wyckoff, D. C. Phillips, *Nature* **1958**, *181*, 662-666.

[10] T. Matsui, S. Ozaki, E. Liong, G. N. Phillips, Y. Watanabe, *J. Biol. Chem.* **1999**, *274*, 2838-2844.

[11] K. K. Khan, M. S. Mondal, L. Padhy, S. Mitra, *Eur. J. Biochem.* **1998**, *257*, 547-555.

[12] T. Matsui, S. Ozaki, Y. Watanabe, *J. Am. Chem. Soc.* **1999**, *121*, 9952-9957.

[13] S. I. Rao, A. Wilks, P. R. O. Demontellano, *J. Biol. Chem.* **1993**, *268*, 803-809.

[14] S. Kato, T. Ueno, S. Fukuzumi, Y. Watanabe, *J. Biol. Chem.* **2004**, *279*, 52376-52381.

[15] N. Yeung, Y. W. Lin, Y. G. Gao, X. Zhao, B. S. Russell, L. Y. Lei, K. D. Miner, H. Robinson, Y. Lu, *Nature* **2009**, *462*, 1079-U1144.

[16] G. H. Loew, D. L. Harris, *Chem. Rev.* **2000**, *100*, 407-419.

[17] M. Sundaramoorthy, J. Terner, T. L. Poulos, *Structure* **1995**, *3*, 1367-1377.

[18] S. Adachi, S. Nagano, K. Ishimori, Y. Watanabe, I. Morishima, T. Egawa, T. Kitagawa, R. Makino, *Biochemistry* **1993**, *32*, 241-252.

[19] T. L. Poulos, *J. Biol. Inorg. Chem.* **1996**, *1*, 356-359.

[20] W. R. Patterson, T. L. Poulos, D. B. Goodin, *Biochemistry* **1995**, *34*, 4342-4345.

[21] M. Wirstam, M. R. A. Blomberg, P. E. M. Siegbahn, *J. Am. Chem. Soc.* **1999**, *121*, 10178-10185.

[22] V. Guallar, R. A. Friesner, *J. Am. Chem. Soc.* **2004**, *126*, 8501-8508.

[23] M. Newcomb, R. Zhang, R. E. P. Chandrasena, J. A. Halgrimson, J. H. Horner, T. M. Makris, S. G. Sligar, *J. Am. Chem. Soc.* **2006**, *128*, 4580-4581.

[24] T. L. Poulos, J. Kraut, *J. Biol. Chem.* **1980**, *255*, 8199-8205.

[25] C. Zazza, A. Palma, N. Sanna, S. Tatoli, M. Aschi, *J. Phys. Chem. B* **2010**, *114*, 6817-6824.

[26] T. Deemagarn, B. Wiseman, X. Carpena, A. Ivancich, I. Fita, P. C. Loewen, *Proteins: Struct. Funct. Bioinform.* **2007**, *66*, 219-228.

[27] Y. Watanabe, H. Nakajima, T. Ueno, *Account. Chem. Res.* **2007**, *40*, 554-562.

[28] H. J. Yang, T. Matsui, S. Ozaki, S. Kato, T. Ueno, G. N. Phillips, S. Fukuzumi, Y. Watanabe, *Biochemistry* **2003**, *42*, 10174-10181.

[29] H. J. Yang, T. Matsui, S. Ozaki, S. Kato, T. Ueno, G. N. Phillips, S. Fuku-Zumi, Y. Watanabe, *Biochemistry* **2008**, *47*, 2700-2700.

[30] J. Xu, O. Shoji, T. Fujishiro, T. Ohki, T. Ueno, Y. Watanabe, *Catal. Sci. Technol.* **2012**, *2*, 739-744.

[31] T. D. Pfister, T. Ohki, T. Ueno, I. Hara, S. Adachi, Y. Makino, N. Ueyama, Y. Lu, Y. Watanabe, *J. Biol. Chem.* **2005**, *280*, 12858-12866.

[32] T. W. Ost, C. S. Miles, J. Murdoch, Y. Cheung, G. A. Reid, S. K. Chapman, A. W. Munro, *FEBS Lett.* **2000**, *486*, 173-177.

[33] H. Li, T. L. Poulos, *Nat. Struct. Biol.* **1997**, *4*, 140-146.

[34] O. Shoji, T. Fujishiro, S. Nagano, S. Tanaka, T. Hirose, Y. Shiro, Y. Watanabe, *J. Biol. Inorg. Chem.* **2010**, *15*, 1331-1339.

[35] O. Shoji, T. Fujishiro, H. Nakajima, M. Kim, S. Nagano, Y. Shiro, Y. Watanabe, *Angew. Chem. Int. Ed.* **2007**, *46*, 3656-3659.

[36] F. Russig, *J. Praktische Chemie* **1900**, *62*, 30-60.

[37] S. Goldschmidt, H. Wessbecher, *Ber. Dtsch. Chem. Ges.* **1928**, *61*, 372-377.

[38] S. Ozaki, H. J. Yang, T. Matsui, Y. Goto, Y. Watanabe, *Tetrahedron Asymmetry* **1999**, *10*, 183-192.

[39] S. Ozaki, H. J. Yang, T. Matsui, Y. Goto, Y. Watanabe, *Tetrahedron Asymmetry* **2006**, *17*, 3192-3192.

[40] T. J. Atkinson, J. Fudin, H. L. Jahn, N. Kubotera, A. L. Rennick, M. Rhorer,

Pain Med. **2013**, *14*, S11-S17.

[41] C. Redaelli, E. Monzani, L. Santagostini, L. Casella, A. M. Sanangelantoni, R. Pierattelli, L. Banci, *ChemBioChem* **2002**, *3*, 226-233.

[42] T. Ohki, Master Thesis and Unpublished Data.

[43] S. Kato, H. J. Yang, T. Ueno, S. Ozaki, G. N. Phillips, S. Fukuzumi, Y. Watanabe, *J. Am. Chem. Soc.* **2002**, *124*, 8506-8507.

[44] S. Ozaki, I. Hara, T. Matsui, Y. Watanabe, *Biochemistry* **2001**, *40*, 1044-1052.

[45] O. Shoji, C. Wiese, T. Fujishiro, C. Shirataki, B. Wunsch, Y. Watanabe, *J. Biol. Inorg. Chem.* **2010**, *15*, 1109-1115.

Chapter III

Capture of Artificial Metal Complexes by a Heme Acquisition Protein of *Pseudomonas aeruginosa* and Its Effect for Living Cells

Chapter III. Capture of artificial metal complexes by a heme acquisition protein of *Pseudomonas aeruginosa* and its effect for living cells

Introduction

Iron is an abundant mineral on the earth and it is an essential nutrient for nearly all organisms including bacteria. In the aerobic environment, iron exists mainly as Fe^{3+} that tends to form insoluble hydroxide and oxyhydoxide in water, making the iron ion largely unavailable to bacteria.[1] To acquire the iron ion, bacteria have developed systems using small organic compounds called siderophores as high-affinity ferric iron chelators.[2] However, the systems using siderophores are not sufficient to get the iron ion under low-iron ion conditions. Because levels of iron ion concentration and its tissue distribution in the mammal bodies are regulated strictly, several pathogens have systems using not only siderophores but also heme acquisition proteins to acquire the iron ion.[3] In mammals, the majority of the iron ion is stored as a heme iron,[4] thus, heme acquisition from their hosts is an effective strategy for pathogens to acquire the iron ion.

A heme acquisition system called Has (Heme acquisition system) has been developed in several Gram-negative bacteria to acquire the iron ion from their host mammal.[5, 6] In this system, a hemophore protein HasA is secreted to the extracellular medium under low-iron ion conditions.[7, 8] HasA scavenges free heme and/or heme from hemoproteins (hemoglobin, hemopexin, etc.) of their hosts, and then, it interacts with a specific outer membrane receptor, HasR. Eventually, the heme captured by HasA is transported to HasR by utilizing an interaction between HasA and HasR.[9, 10] It is suggested that the heme passes through HasR using energy derived from proton motive force transduced by inner membrane proteins.[5] Finally, the heme is transported to cytoplasm, and it is degraded by heme oxygenase to release the iron ion in the cytoplasm.[6] The genes of Has proteins exist in one operon called *has*, and several pathogenic bacteria, e.g. *Serratia marcescens*, *Yersinia pestis*, *Pseudomonas fluorescens* and *Pseudomonas aeruginosa* have such *has* operons.[6, 11-14]

In 1999, Arnoux *et al*. determined the first crystal structure of *S. marcescens* HasA ($HasA_{sm}$) binding heme.[15] $HasA_{sm}$ binds heme using two loops with coordination of Tyr-75 and His-32 to the heme iron. The overall structure of the heme-binding form (holo-form) of $HasA_{sm}$ resembles "a fish biting the heme."[15] Subsequently, Alontaga *et al*. reported the crystal structure of the hemophore from *P. aeruginosa* ($HasA_p$) shown in Fig. 3-1.[16] The structures of these two hemophores are essentially identical. The crystal structures of two HasA proteins in their holo-forms show that captured hemes are highly exposed to the solvent; not only the propionate groups, but also the edges of three pyrrole rings of the heme can be seen from outside. This unique feature of heme binding suggests that metal complexes having different structures from heme could also be accommodated by HasA proteins. Due to a heme free-form (apo-form) of HasA (Fig. 3-1) exhibiting an "open conformation" with a large rearrangement of the His-32 loop,[17, 18] even relatively bulky metal complexes could enter the heme binding pocket. These considerations led the author to investigate whether HasA could capture metal complexes other than heme. The author is also interested in how the addition of synthetic metal complexes to HasA might affect the transportation of exogenous compounds including heme in bacterial cells. The author reports herein that the hemophore from *P. aeruginosa* ($HasA_p$) can capture several artificial metal complexes. In addition, the author also reports effects of HasA carrying artificial metal complexes against living bacterial cells.

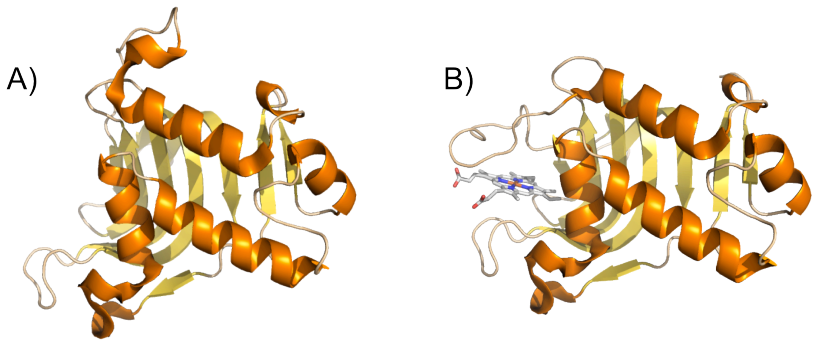

Fig. 3-1 Crystal structures of A) apo-$HasA_p$ (PDB ID: 3MOK) and B) holo-$HasA_p$ ($HasA_p$ binding heme; PDB ID: 3ELL). These are side views of all over structures.

Result and Discussion

Capture of artificial metal complexes by $HasA_p$

At first, interactions between $HasA_p$ and several metal complexes were examined by measuring electrospray ionization-time of flight mass spectra (ESI-TOF-MS) of a simple mixture of apo-$HasA_p$ (3.5 μM) and a methanolic solution of metal complexes (2.7 eq.). Among the artificial complexes examined, Fe-mesoporphyrin IX (Fe-MPIX), Fe-2,3,7,8,12,13,17,18-octaethyl 21H,23H-porphyrin (Fe-OEP), and *N,N'*-disalicylal- 1,2-phenylenediamine (Fe-salophen) gave a clear peak, related to the holo-protein formation under the conditions of $HasA_p$ loaded heme (Fig. 3-2). On the other hand, Fe-tetraphenylporphyrin (Fe-TPP) and protoporphyrin IX (PPIX) showed only the peak corresponding to apo-$HasA_p$. UV-vis spectra of samples used for ESI-TOF-MS are shown in Fig. 3-3, and UV-vis spectra changes upon the addition of methanol solutions of synthetic molecules indicate that $HasA_p$ accepts artificial compounds, Fe-MPIX, Fe-OEP, and Fe-salophen as it there were the heme. The intensity of the peaks in ESI-MS spectra for holo-$HasA_p$ with synthetic metal complexes was comparable to that of heme, suggesting that $HasA_p$ complexed with Fe-MPIX, Fe-OEP, or Fe-salophen is relatively stable.[19] Fortunately, purification of $HasA_p$ accommodating these metal complexes has succeeded with column chromatography, and UV-vis spectra of $HasA_p$ with metal complexes after purification are shown in Fig. 3-4. In addition, titration experiments showed 1:1 complexation of $HasA_p$ and metal complexes (Fig. 3-5). These results indicate that $HasA_p$ forms 1:1 complexes with Fe-MPIX, Fe-OEP, and Fe-salophen, respectively.

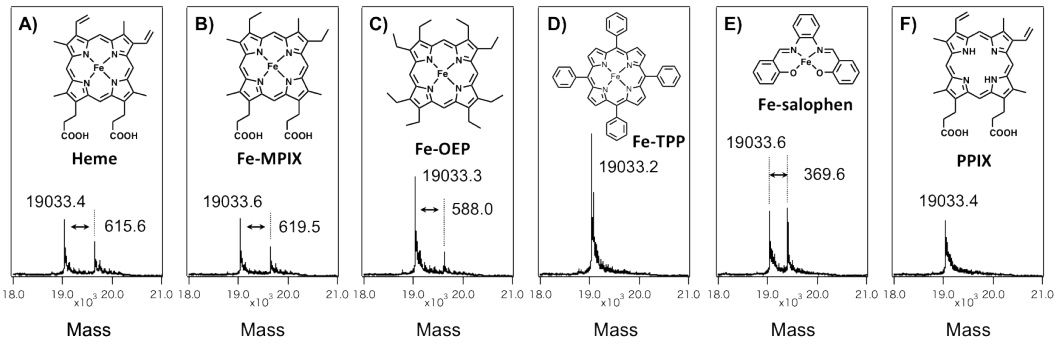

Fig. 3-2 Positive mode ESI-TOF mass spectra of the mixtures of apo-$HasA_p$ and metal complexes: A) hemin; B) Fe-MPIX·Cl; C) Fe-OEP·Cl; D) Fe-TPP·Cl; E) Fe-salophen·Cl; and F)PPIX. The sample mixture was prepared by adding 100 μL (2.7 eq.) of metal complexes dissolved in methanol to a solution of purified apo-HasAp in 5 mM ammonium acetate buffer (3.5 nmol, 900 μL). Cone voltage was fixed at 45 V in all measurements. The molecular weight of apo-$HasA_p$ was calculated to be 19034.77 Da based on its amino acid sequence. The exact masses of the metal complexes are 616.18 Da (heme), 620.21 Da (Fe-MPIX), 588.29 Da (Fe-OEP), 668.17 Da (Fe-TPP), 370.04 Da (Fe-salophen), 562.26 Da (PPIX), respectively.

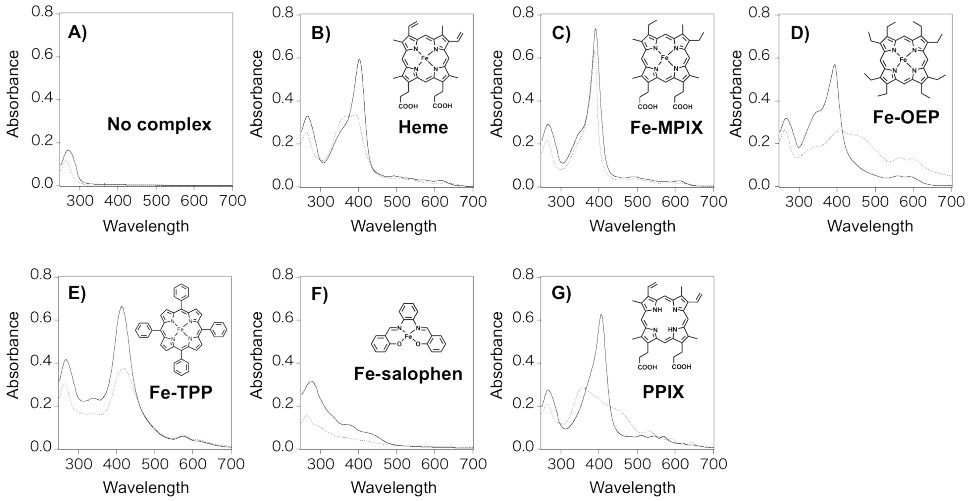

Fig. 3-3 UV-vis spectra of the samples used for ESI-TOF mass measurements (Fig. 1): A) No complex (only methanol); B) Heme; C) Fe-MPIX; D) Fe-OEP; E) Fe-TPP, F) Fe-salophen, and G) PPIX. The sample mixture was prepared by adding 100 μL (2.7 eq.) of metal complexes dissolved in methanol to a solution of purified apo-$HasA_p$ in 5 mM ammonium acetate buffer (3.5 nmol, 900 μL). The spectra of the same samples without $HasA_p$ are shown as dotted lines.

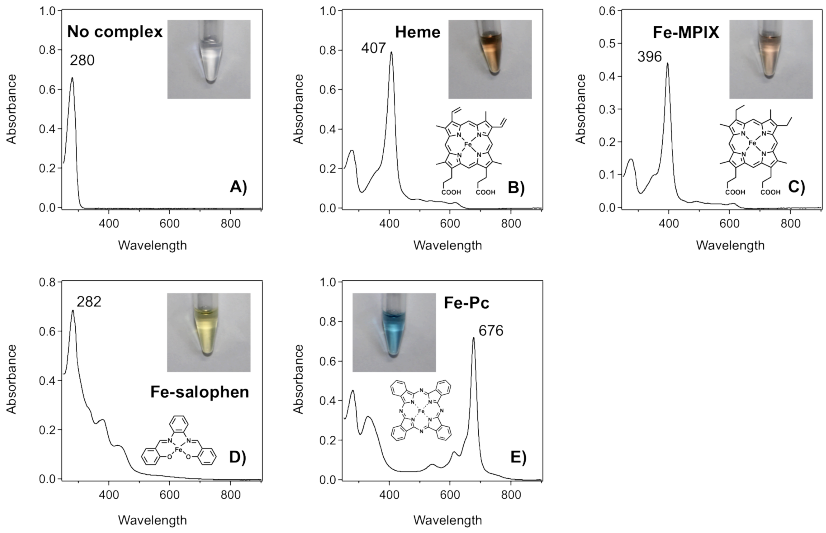

Fig. 3-4 UV-vis spectra of various conditions of $HasA_p$. The UV-vis spectrum of purified apo-$HasA_p$ in PBS solution is shown in A). UV-vis spectra of the purified $HasA_p$ harboring: B) heme; C) Fe-MPIX; D) Fe-salophen; and E) Fe-Pc in PBS solution. The structures of the metal complexes and pictures of the protein solutions in plastic containers are shown as insets. The concentrations of the solution used for UV-vis measurements are different from those for the pictures of protein solutions.

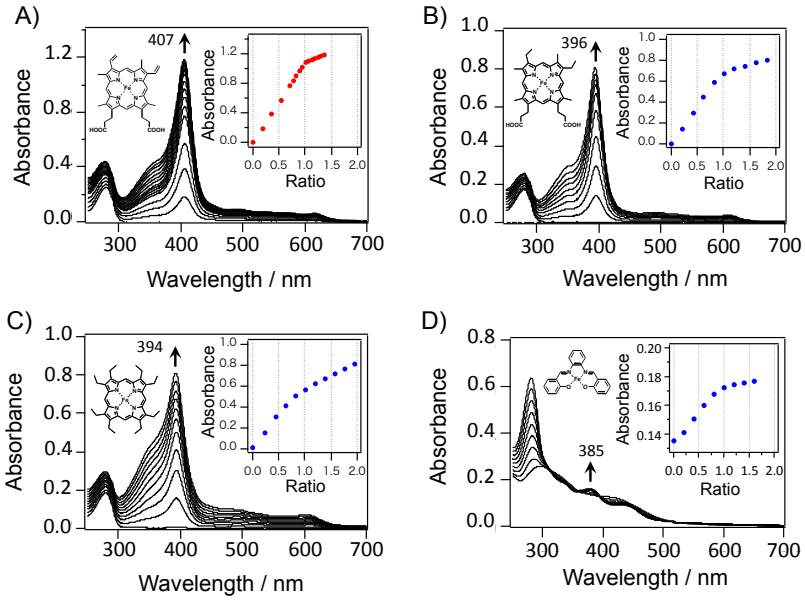

Fig. 3-5 Spectrophotometric titration of apo-$HasA_p$ with: a) heme; b) Fe-MPIX; and c) Fe-OEP. Titration of Fe-salophen with apo-$HasA_p$ is shown in d). The insets display the profiles of the titration curves plotted against the increasing peak indicated by the arrows.

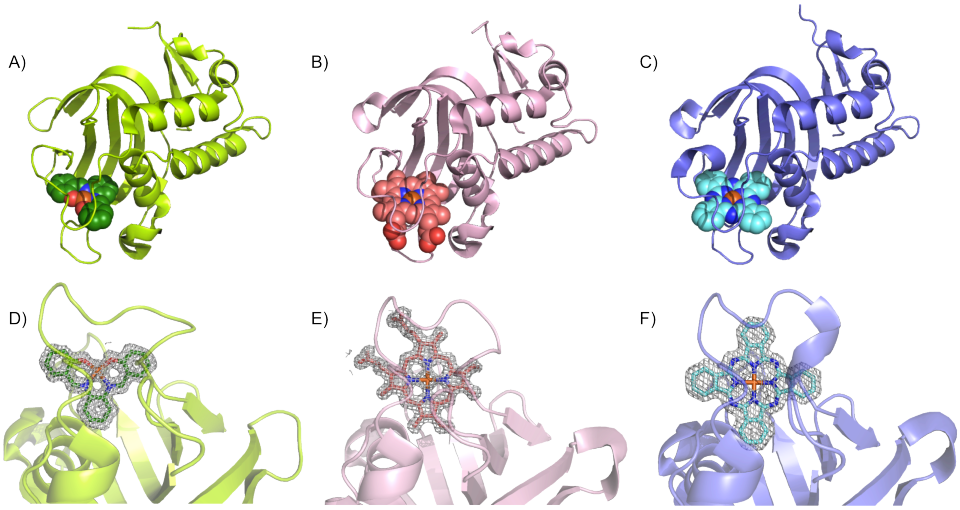

Fig. 3-6 X-ray crystal structures of $HasA_p$ with synthetic metal complexes: A) and D), Fe-salophen (Green); B) and E), Fe-MPIX (Pink); and C) and F), Fe-Pc (Blue). The overall structures (top row, A–C) are shown as ribbon models. In D–F, 2Fo-Fc electron-density maps of the metal complexes contoured at the 1.0 σ level are shown in gray mesh.

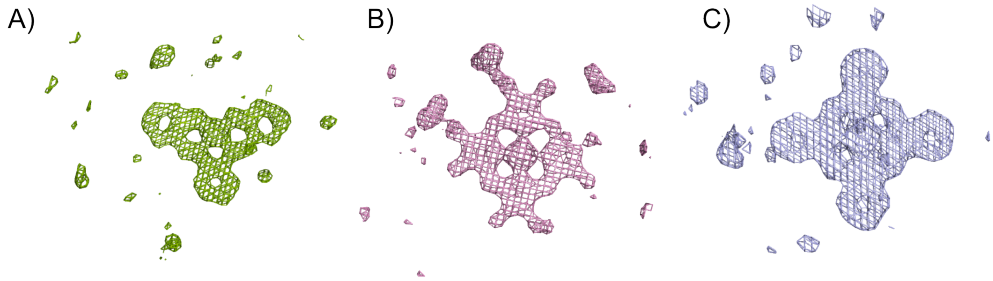

Fig. 3-7 Electron density, contoured at 3 σ, derived from a *Fo*-*Fc* Fourier synthesis omitting the A) Fe-salophen, B) Fe-MPIX, and C) Fe-Pc.

We have further succeeded in crystalizing $HasA_p$ with Fe-salophen and Fe-MPIX (Fig. 3-6, 3-7, 3-8), respectively. The crystal structures showed clear electron densities assignable to Fe-salophen (Fig. 3-6D, 3-7A) and Fe-MPIX (Fig. 3-6E, 3-7B) at the heme-binding position. The overall structures of $HasA_p$ with Fe-salophen and Fe-MPIX are essentially identical to that of $HasA_p$ with heme (root-mean-square deviation (RMSD) over 2-184 amino acid residues of Ca atoms: 0.810 for Fe-salophen and 0.443 for Fe-MPIX), whereas the His-32 loop in the $HasA_p$ with Fe-salophen clearly

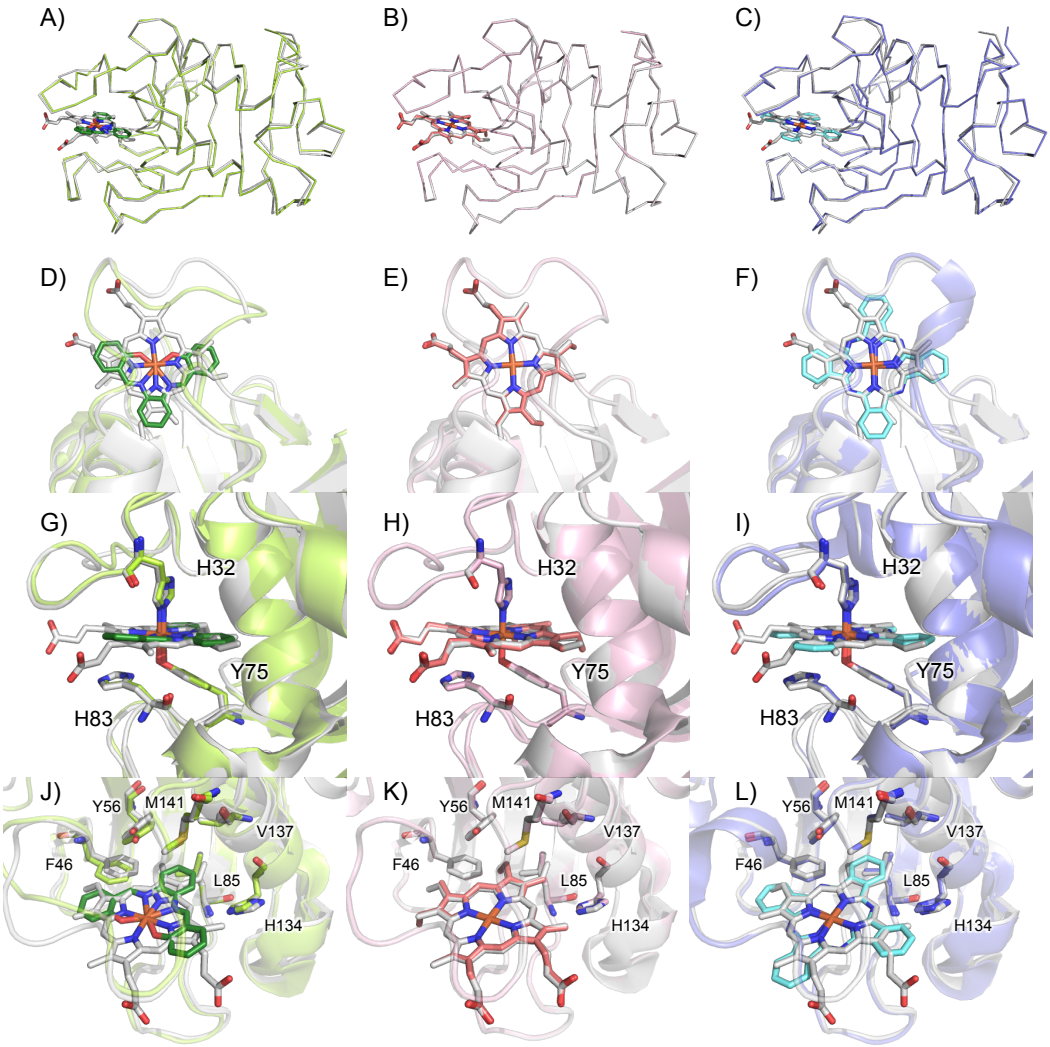

Fig. 3-8 Comparison of X-ray crystal structures of HasAp harboring synthetic metal complexes with heme bound form: A), D), G), J) Fe-salophen (Green); B), E), H), K) Fe-MPIX (Pink); and C), F), I), L) Fe-Pc (Blue). Superimposed crystal structures shown light gray models are $HasA_p$ harboring heme (light gray, PDB ID: 3ELL). The top row (A–C) shows the side views of overall structures. The second row (second row, D–F) shows the top views of the binding sites, which are shown as ribbon models. In the third row (G–I), close-up views of the ligand residues His32, Tyr75 and His83 that is helps coordination of the tyrosinate. These amino acid residues and the metal complexes areshown as stick models. In the bottom row (J–L), close-up views corresponding to those from the propionate side of the heme are shown, in which the metal complexes and the hydrophobic amino acid residues located in the depth of the binding pocket are depicted as stick models.

moved towards the inside because of the induced fit binding to accommodate a small metal complex. Both Tyr-75 and His-32 bind to the iron of Fe-salophen as well as that of Fe-MPIX (Fig. 3-8). His-83, that stabilizes the tyrosinate of Tyr-75 through a hydrogen bonding, showed no structural perturbation among crystal structures of $HasA_p$ with metal complexes (Fig. 3-8). The location of Fe-MPIX is identical to that of heme but Fe-MPIX is captured in a reverse fashion to that of heme (minor orientation) (Fig. 3-8E), possibly due to a steric repulsion of two ethyl groups of Fe-MPIX protruding out of the porphyrin plane. This observation indicates that the heme binding to $HasA_p$ is regulated by recognizing the vinyl groups of the heme, so that the heme can only be complexed in a single orientation. Although the structure of Fe-salophen is largely different from heme, Fe-salophen was similarly captured by $HasA_p$. The central phenyl ring in the salophen ligand was accommodated in the hydrophobic pocket composed of Phe-46, Tyr-56, Leu-85, His-134, Val-137, and Met-141 located in the depth of the heme binding site (Fig. 3-8J). This hydrophobic interaction seems to be a key in fixing Fe-salophen, leading to a single orientation of Fe-salophen in $HasA_p$. The UV-vis spectrum of a mixture of $HasA_p$ and PPIX are clearly different from that of PPIX alone (Fig. 3-3G), suggesting that $HasA_p$ interacts with PPIX. The hydrophobic interaction and π-π stacking contribute the metal complex binding by $HasA_p$.[20]

Given the crystal structure of $HasA_p$ with Fe-salophen, it is intriguing to examine complexation of Fe-phthalocyanine (Fe-Pc) and $HasA_p$ because the structure of Fe-Pc is partially similar to that of Fe-salophen and the crystal structure shown in Fig. 3-8A, D, G and J suggested that there is enough space to accommodate Fe-Pc, which bears a large π plane. Phthalocyanine is a highly hydrophobic molecule with a large planer structure and is thus insoluble in water. It is even difficult to dissolve Fe-Pc in methanol, mainly because of a strong stacking interaction among Fe-Pc molecules. Thus, the author must use other polar organic solvents to dissolve Fe-Pc. Because apo-$HasA_p$ did not form any aggregate even in 50% DMSO, the author examined the complex formation of apo-$HasA_p$ by adding a DMSO solution of Fe-Pc. After the complex

formation, $HasA_p$ with Fe-Pc was stable even after removal of DMSO by dialysis. The ESI-MS spectrum of purified $HasA_p$ bound to Fe-Pc is shown in Fig. 3-9. The crystal structure of $HasA_p$ harboring Fe-Pc showed clear electron density for Fe-Pc (Fig. 3-6, 3-7). Its binding fashion is similar to $HasA_p$ harboring Fe-salophen. As was observed for the Fe-salophen binding, one of the phenyl rings of Fe-Pc was accommodated in the hydrophobic pocket in the depths of the heme-binding site. The RMSD over 2-184 amino acid residues of Cα atoms against $HasA_p$ harboring heme was estimated to be 0.915. The data collection and refinement of the crystal structural analysis is shown in Table 3-1.

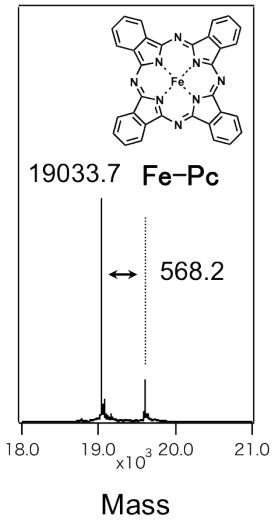

Fig. 3-9 Positive mode ESI-TOF mass spectrum of purified $HasA_p$ harboring Fe-Pc in 5 mM ammonium acetate buffer. The concentration of HasAp with Fe-Pc was 4.5 μM. The exact masses of Fe-Pc is 568.08 Da (Fe-Pc).

Effects of $HasA_p$ harboring artificial metal complexes on bacterial cells

To examine whether *P. aeruginosa* can use artificial metal complexes as an iron source, *P. aeruginosa* PAO1 strain was cultured in the presence of $HasA_p$ bound to an artificial metal complex and monitored bacterial growth by observing OD_{600}. *P. aeruginosa* did not grow in a M9-based medium in the presence of 40 mM EDTA as an iron chelator (Fig. 3-10A, green line). However, the bacterial growth was observed by addition of both 40 mM EDTA and $HasA_p$ bound to heme (Fig. 3-10A, red line). While

the concentration of EDTA is high, the growth of *P. aeruginosa* under the conditions was not much different from the growth under the conditions without EDTA (Fig. 3-11). The growth of *P. aeruginosa* in the presence of EDTA was also observed upon the addition of Fe-MPIX bound $HasA_p$, indicating *P. aeruginosa* can use Fe-MPIX as an iron source (Fig. 3-10A, pink line). These results indicate that the transfer of heme from $HasA_p$ to HasR as well as the heme degradation processes to acquire iron are not much affected by the substitution of the two vinyl groups for ethyl groups. On the other hand, the same experiments were carried out for $HasA_p$ with Fe-salophen and Fe-Pc, respectively, and no OD_{600} change observed in both cases (Fig. 3-10A, yellow line and blue line). The result suggests that Fe-salophen and Fe-Pc were either not transferred to HasR, or that they were transferred to HasR, but subsequent transportation steps did not proceed accurately (Steps III, IV, V in Fig 3-12).

Table 3-1 Data collection and refinement of $HasA_p$ binding synthetic metal complexes.

$HasA_p$ with complex (PDB code)	$HasA_p$ with Fe-salophen (3W8M)	$HasA_p$ with Fe-mesoporphyrineIX (3WAH)	$HasA_p$ with Fe-phthalocyanine (3W8O)
Data collection			
Wavelength (Å)	1	1	1
Space group	P63	P31	P61
Cell dimensions			
a, b, c (Å)	98.212, 98.212, 32.662	47.518, 47.518, 140.893	153.868, 153.868, 36.699
α, β, γ (ϒ)	90.000, 90.000, 120.000	90.000, 90.000, 120.000	90.000, 90.000,120.000
Resolution (Å)	50.00–1.46 (1.46-1.51)	50.0–1.54 (1.54–1.60)	50.00–1.85 (1.85–1.92)
No. of total observed reflections	202223	242758	365118
No. of unique reflections	30551	51545	43201
R_{merge} [a, b] (%)	5.1 (24.7)	6.7 (27.0)	8.8 (36.6)
Completeness [a] (%)	96.7 (82.0)	97.7 (85.7)	100.0 (99.9)
$I/\sigma(I)$ [a]	31.2 (3.8)	20.01 (3.81)	25.0 (6.4)
Redundancy [a]	6.6 (3.1)	4.7 (2.4)	8.5 (8.2)
Refinement statistics			
Resolution range (Å)	19.63–1.46	19.70–1.54	19.23–1.85
No. of monomer/asymmetric unit	1	2	2
R_{work}/R_{free} [c, d] (%)	18.18/20.59	17.53/19.38	18.54/21.79
RMSD bond length [e] (Å)	0.008	0.014	0.012
RMSD bond angles [e] (º)	1.261	1.350	1.661
No. of atoms	1588	2983	3131
Average *B*-factor (Å^2)	19.6	19.2	24.7

[a] The values in parentheses are for the highest resolution shell.

[b] $R_{merge} = \Sigma_{hkl}\Sigma_i|I_i(hkl)-\langle I(hkl)\rangle| / \Sigma_{hkl}\Sigma_i I_i(hkl)$ where $\langle I(hkl)\rangle$ is the average intensity of the *i* observations.

[c] $R_{work} = \Sigma_{hkl}|F_{obs}(hkl) - F_{calc}(hkl)|/\Sigma_{hkl}F_{obs}(hkl)$, where F_{obs} and F_{calc} are observed and calculated structure factors, respectively.

[d] R_{free} was calculated with 5% of the reflections that were not included in the refinement.

[e] r. m. s. d. = root mean square deviation

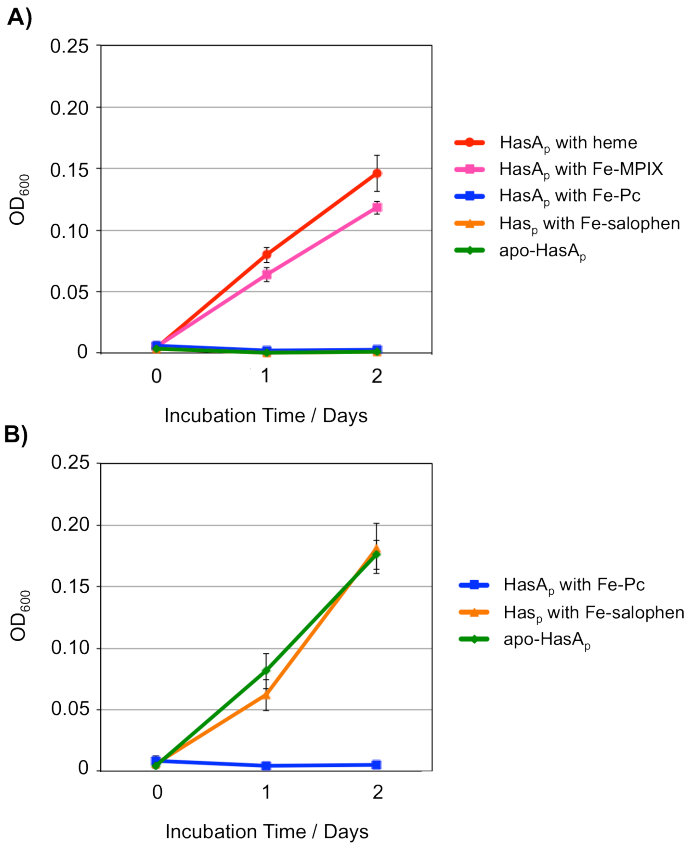

Fig. 3-10 Growth behavior of *P. aeruginosa* in iron-limited medium containing EDTA as an iron ion scavenger. Cell growth was monitored by optical density at 600 nm (OD_{600}). A) Growth of *P. aeruginosa* in the presence of 0.25 μM of holo-$HasA_p$ with heme or $HasA_p$ with synthetic metal complexes. As a control experiment, apo-$HasA_p$ was also added (green line). B) Effect of $HasA_p$ with synthetic metal complexes as inhibitors on the growth of *P. aeruginosa*. A solution of $HasA_p$ with synthetic metal complexes or apo-$HasA_p$ (as a negative control) was added to a suspension of *P. aeruginosa* (the final concentrations were 0.25 μM, respectively) provided with 0.5 μM holo-$HasA_p$ with heme as an iron source. Uncertainty is given as the standard deviation from at least three measurements in A) and B).

To examine the influences of Fe-salophen and Fe-Pc on the growth of *P. aeruginosa*, the bacterial cultures were incubated in the co-presence of EDTA, $HasA_p$ harboring heme, and either $HasA_p$ harboring Fe-salophen, or Fe-Pc (Fig. 3-10B). The bacterial growth was observed in the presence of both Fe-salophen bound to $HasA_p$ and

heme bound to $HasA_p$, however, OD_{600} did not increase in the presence of both Fe-Pc bound to $HasA_p$ and heme bound to $HasA_p$. In the absence of EDTA, OD_{600} increased despite the addition of $HasA_p$ bound to Fe-Pc, implying Fe-Pc did not affect on the growth of *P. aeruginosa* (Fig. 3-13). These results indicate that $HasA_p$ bound to Fe-Pc inhibits the heme acquisition through the Has system. The half-maximal (50%) inhibitory concentration (IC_{50}) was estimated to be 24 nM (Fig. 3-14), showing that $HasA_p$ with Fe-Pc efficiently inhibited heme transportation. It has been known that *P. aeruginosa* has two heme acquisition systems, Has system and Phu system.[11] Because *P. aeruginosa* has Phu system, *P. aeruginosa* can use free heme to get iron as a nutrient. Therefore, *P. aeruginosa* was incubated in the presence of EDTA, hemin, and $HasA_p$ bound to Fe-Pc. Then, the growth of this bacterium was examined to check the toxicity of $HasA_p$ with Fe-Pc (Fig. 3-15, green line and pink line). There was no effect of $HasA_p$ bound to Fe-Pc upon the growth, indicating $HasA_p$ bound to Fe-Pc has no toxicity for bacterial cells under the conditions. These results support a possible specific interaction between HasR and $HasA_p$ bound to synthetic metal complexes.

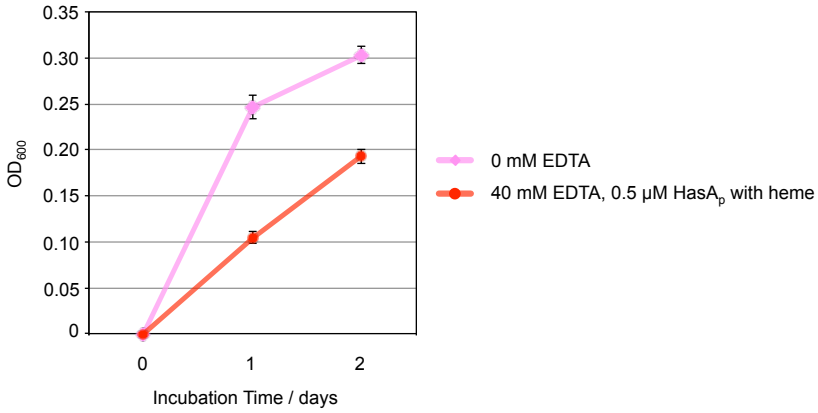

Fig. 3-11 Comparison of growth behavior of *P. aeruginosa* in the presence and absence of 40 mM EDTA. Cell growth was monitored by optical density at 600 nm (OD_{600}). *P. aeruginosa* PAO1 was cultured in M9-based media in the presence (red) and absence (pink) of 40 mM EDTA. To the culture solution including 40 mM EDTA, $HasA_p$ with heme was added as an iron source. Uncertainty is given as the standard deviation from at least three measurements.

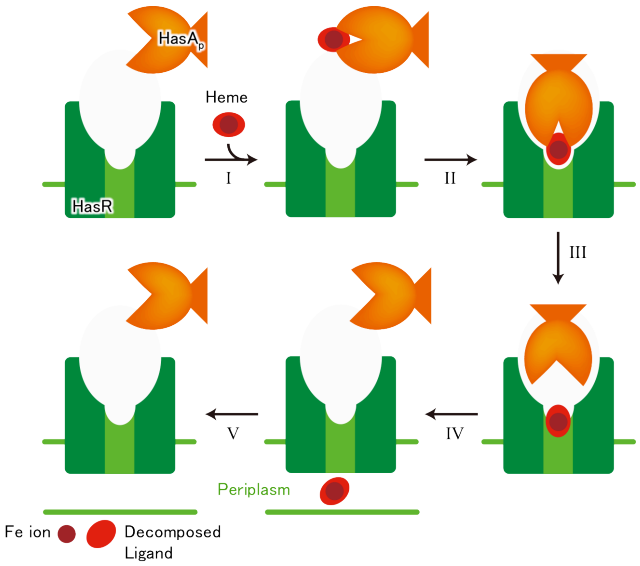

Fig. 3-12 Steps of the expected general heme uptake process by HasA. I) HasA captures a heme molecule. II) The holo-HasA interacts with a specific receptor called HasR. III) The heme is transferred from HasA to HasR. IV) The heme passes through HasR and is transported into the periplasm. V) The heme is degraded by heme oxygenase to release an iron cation in the cytoplasm.

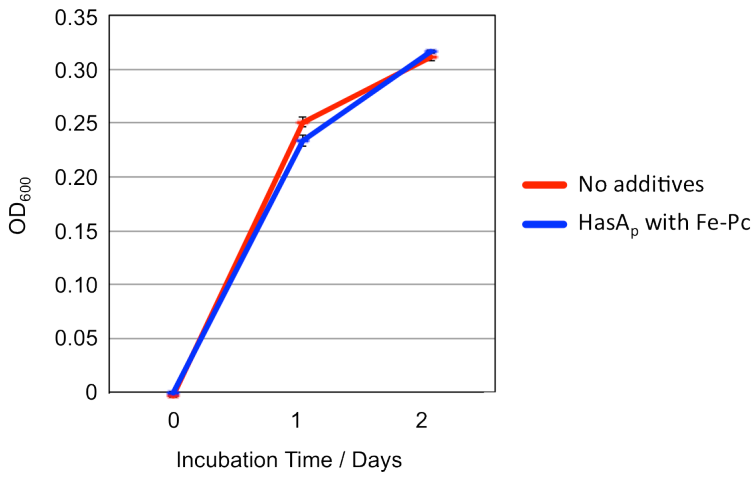

Fig. 3-13 Growth behavior of *P. aeruginosa* without EDTA as an iron scavenger monitored by optical density at 600 nm (OD_{600}). *P. aeruginosa* PAO1 was cultured in M9-based media in the absence (red) and presence (blue) of 0.25 µM $HasA_p$ with Fe-Pc. Uncertainty is given as the standard deviation from at least three measurements.

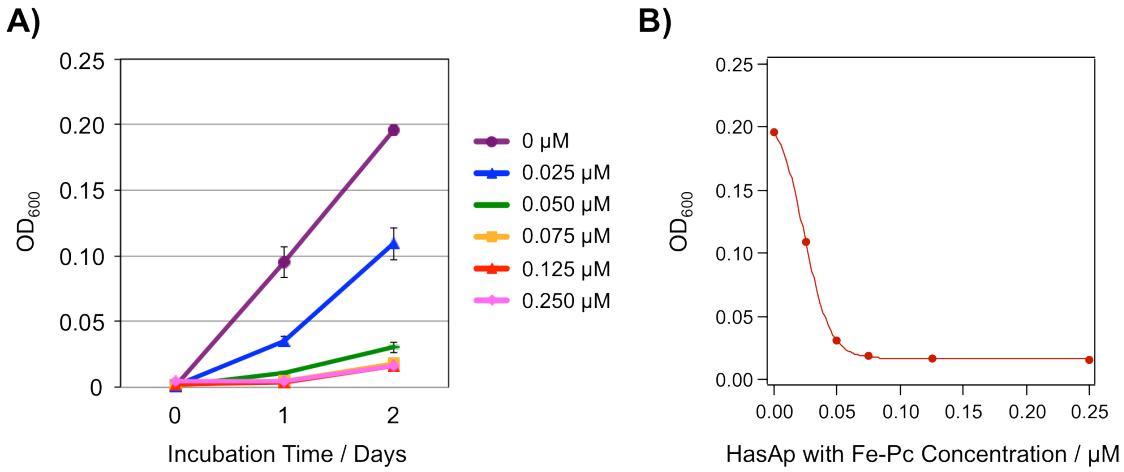

Fig. 3-14 Growth inhibition of *P. aeruginosa* under different concentrations of $HasA_p$ with Fe-Pc. Experiments were carried out in the same manner as the experiment shown in Fig. 3-10B. A) Growth curves of *P. aeruginosa* under different concentrations of $HasA_p$ with Fe-Pc. Uncertainties are given as the standard deviation from at least three measurements. The concentration of $HasA_p$ with Fe-Pc is shown in the right part of this figure. The initial number of cells used for *in vivo* inhibition experiments was estimated to be $3.4 \times 10^5 \pm 0.7 \times 10^5$ CFU/mL. (CFU: Colony Forming Unit) B) An average of absorbance at 600 nm after 2 days incubation is plotted against the concentration of $HasA_p$ with Fe-Pc. The half-maximal (50%) inhibitory concentration (IC_{50}) was estimated to be 24 nM. Uncertainty is given as the standard deviation from at least three measurements.

There are two possibilities on the inhibition of the bacterial growth by $HasA_p$ harboring Fe-Pc: 1) $HasA_p$ bound to Fe-Pc strongly interacts with HasR due to high hydrophobicity of Fe-Pc, and blocks the specific interaction site of HasR, thus, $HasA_p$ with heme cannot interact with HasR and *P. aeruginosa* cannot get iron (Fig. 3-16A); 2) Fe-Pc transported to HasR blocks the passage of metal complexes in HasR due to high hydrophobicity of Fe-Pc (Fig. 3-16B). Not only $HasA_p$ bound to Fe-Pc but also $HasA_p$ bound to Fe-OEP inhibited the heme acquisition by the Has system (Fig. 3-17). On the other hand, Fe-salophen bound to $HasA_p$ did not inhibit the heme acquisition of *P. aeruginosa* (Fig. 3-10B). These results show that their size and hydrophobicity of metal complexes are important for the inhibition of heme acquisition.

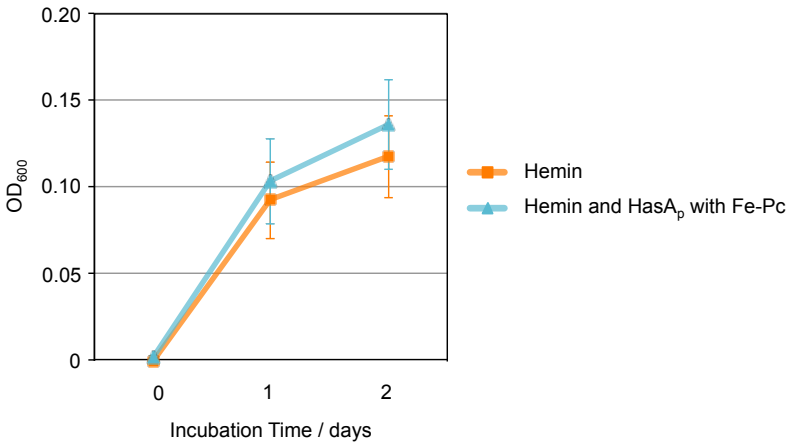

Fig. 3-15 Growth behavior of *P. aeruginosa* in iron-limited media containing EDTA as an iron scavenger. Cell growth was monitored by optical density at 600 nm (OD_{600}). *P. aeruginosa* PAO1 was cultured in M9-based media including 40 mM EDTA in the absence (yellow) and presence (light blue) of 0.25 µM $HasA_p$ with Fe-Pc. Hemin was added as an iron source (0.5 µM). Uncertainty is given as the standard deviation from at least three measurements.

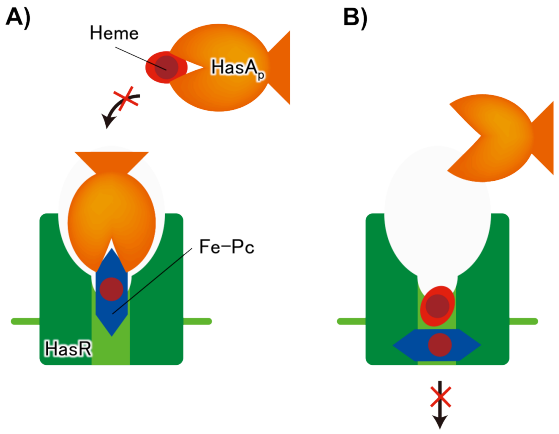

Fig. 3-16 Schematic representations of plausible mechanisms to explain the inhibition by HasAp with Fe-Pc: A) $HasA_p$ with Fe-Pc strongly interacts with HasR and blocks the specific interaction domain of HasR; B) Fe-Pc transferred to HasR blocks the access channel of HasR.

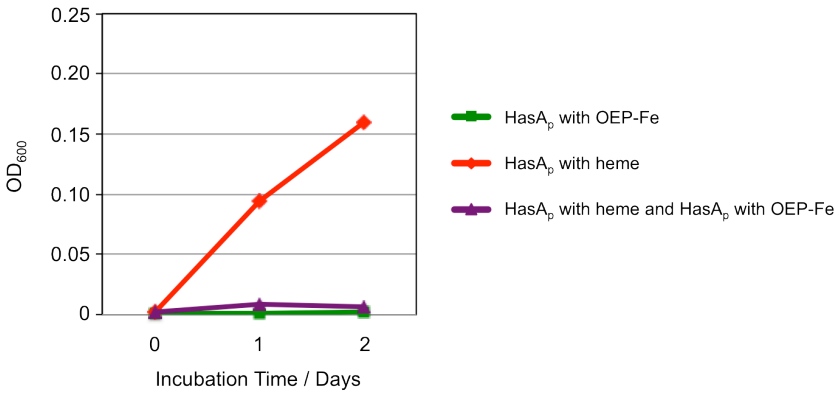

Fig. 3-17 Effect of $HasA_p$ with Fe-OEP as an inhibitor on the growth of *P. aeruginosa*. This bacterium was incubated in a medium including 0.25 μM $HasA_p$ with Fe-OEP (green), 0.5 μM $HasA_p$ with heme (red), or both (purple). Experiments were carried out in the same manner as the experiment shown in Fig. 3-10B.

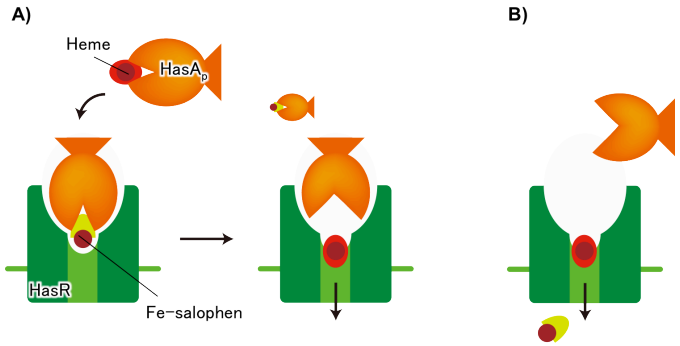

Fig. 3-18 Schematic representations of plausible mechanisms to explain the inhibition by $HasA_p$ with Fe-salophen: A) $HasA_p$ harboring Fe-salophen not so strongly interacts with HasR, and it is replaced by $HasA_p$ harboring heme; B) Fe-salophen can be transported and can pass through HasR, then Fe-salophen does not block the access channel of HasR, resulting heme is transported to inside.

The author presumes that the interaction of HasAp harboring Fe-salophen with HasR were week (Fig. 3-18A) or the interaction of Fe-salophen with HasR is insufficient to block the transportation of heme (Fig. 3-18B).

Conclusion

In conclusion, the author has demonstrated that $HasA_p$ can capture several synthetic metal complexes other than heme. The crystal structure of $HasA_p$ bound to Fe-MPIX, Fe-salophen, and Fe-Pc showed that $HasA_p$ captures these artificial metal complexes in the same fashion as it does for heme without any structural perturbation. Further, $HasA_p$ bound to Fe-Pc inhibited the growth of *P. aeruginosa* in the presence of $HasA_p$ harboring heme as an iron source and EDTA as an iron ion scavenger. These findings would contribute to understanding the heme transportation from HasA to HasR. Moreover, it is expected that these observations could lead to the development of a *P. aeruginosa*-elimination system without using antibiotics.

Materials and Methods

Construction of expression system of the truncated $HasA_p$

As $HasA_p$ secreted by *Pseudomonas aeruginosa* has lost 21 amino acid residues at the C-terminal (truncated $HasA_p$),[16, 21, 22] we used truncated $HasA_p$ in our research. A gene encoding the full length of $HasA_p$ in *P. aeruginosa* PAO1 was synthesized by PCR and subcloned into pQE30 (QIAGEN). Using the pQE30 harboring the full length of the $HasA_p$ gene as a template, truncated $HasA_p$ was synthesized and subcloned into pQE-30t using BamHI and HindIII restriction sites.[23] Two primers for PCR are designed to introduce a HindIII restriction site and a stop codon that prevents translation of the 21 amino acids at the C-terminal. The primers used are 5′-CCCGAAAAGTGCCACCTG-3′ and 5′-TATAAGCTTTTACGCAGCCGGGGTGGC-3′. The recombinant plasmid pQE-30t harboring the truncated $HasA_p$ gene was then transferred into *E. coli* M15 [pREP4] cells (QIAGEN).

Expression and Purification of the truncated $HasA_p$

The truncated $HasA_p$ was expressed and purified as follows. A single colony of *E. coli* was cultured in 3 mL of a Luria-Bertani (LB) medium containing ampicillin (0.1

g/mL or 0.05 g/mL) and kanamycin (0.025 g/L). An aliquot amount of the cultured solution was added to 100 mL of the LB medium including ampicillin and kanamycin and cultured overnight. The *E. coli* were further cultivated in 1 L of the LB medium supplemented with ampicillin and kanamycin using a 5 L baffled flask. After 4 h incubation at 37 °C, isopropyl β-d-1-thiogalactopyranoside (IPTG) was added to a final concentration of 0.1 mM. After being cultured for 20 h at 28 °C, the cells were harvested by centrifugation and stored at -80 °C. The frozen cells were resuspended in an H buffer (20 mM sodium phosphate, 15 mM 2-mercaptoethanol, 20 mM imidazole, 0.5 M NaCl, pH 7.4). The cells were disrupted by sonication. The cell debris was removed by centrifugation and the supernatant was applied to a Ni-affinity column equilibrated with the H buffer. After washing the column with the H buffer, the bound proteins were eluted with the H buffer containing 200 mM imidazole. The resulting protein solution was treated with thrombin to remove any His-tag and dialyzed against a phosphate-buffered saline (PBS; 140 mM NaCl, 2.7 mM KCl, 10 mM Na_2HPO_4, 1.8 mM KH_2PO_4, pH 7.3) solution overnight. This sample was further purified by Ni-affinity column chromatography followed by dialysis against a PBS solution. The purified protein solution was frozen by liquid nitrogen and stored at -80 °C.

Preparation of apo-HasA$_p$

The purified truncated $HasA_p$ solution was dripped into cooled acetone including 0.2% (w/v) HCl to remove heme. The precipitate was collected by centrifugation and dissolved in a solution of 7 M urea (adjusted to pH 7.5 with Tris-HCl). The resulting solution was dialyzed against a PBS solution. After overnight dialysis, the solution was concentrated using Amicon Ultra (Merck Millipore). The concentrated solution of apo-$HasA_p$ was further purified by a gel filtration column (Sephacryl S-200 column; GE Healthcare) equilibrated with a PBS solution. The concentration of apo-$HasA_p$ in the PBS solution was determined by UV absorption at 280 nm. (ε_{280} = 28.6 mM^{-1} cm^{-1}).[24]

Measurements

UV-vis spectra were recorded on a Shimadzu UV-2450 or UV-2500 spectrophotometer (Shimadzu). The optical path length of the UV-cell (Tosoh or GL Science) was 1 cm. The ESI-MS spectra were recorded on a micromass LTC-OPT (Waters).

UV-vis titration

Spectrophotometric titration of apo-$HasA_p$ with metal complexes was performed by adding an aliquot amount of a hemin, Fe(III) Mesoporphyrin IX chloride (Fe-MPIX·Cl), or 2,3,7,8,12,13,17,18-octaethyl-21H,23H-porphine iron chloride (Fe-OEP·Cl) solution to 600 μL of apo-$HasA_p$ in PBS solution (for hemin, and Fe-MPIX·Cl) or apo-$HasA_p$ in a 1:1 mixture of PBS solution and MeOH (for Fe-OEP·Cl). The concentration of apo-$HasA_p$ was 5.4 nmol for heme and 3.6 nmol for Fe-MPIX and Fe-OEP, respectively. The absorption change was plotted against [metal complex]/[apo-$HasA_p$]. With Fe-salophen, a titration experiment was carried out by adding a PBS solution of apo-$HasA_p$ to a PBS solution of Fe-salophen (3 mL, 32. 4 nmol) including 10% EtOH. The absorption change was corrected with a dilution factor and plotted against [apo-$HasA_p$]/[metal complex].

Preparation of $HasA_p$ with Fe-MPIX

Fe(III) Mesoporphyrin IX chloride (Fe-MPIX·Cl) was purchased from Frontier Science and used without further purification. An aqueous solution of Fe-MPIX·Cl in 0.1 M NaOH. was added to a PBS solution of apo-$HasA_p$ and gently stirred at room temperature. The mixture was passed through a DEAE cellulose column (DE52; Whatman) equilibrated with the same buffer to remove the excess Fe-MPIX·Cl. The eluent was further purified by a gel filtration column (Sephacryl S-200) equilibrated with the PBS solution. The sample buffer was changed to 0.1 M KPi buffer (pH 7.0) and

concentrated by using Amicon Ultra (Merck Millipore). The molar extinction coefficient at 395.5 nm of $HasA_p$ with Fe-MPIX was estimated to be 113 mM^{-1} cm^{-1}. The solution of $HasA_p$ with Fe-MPIX used to estimate the molar extinction coefficient was prepared by adding 1.0 eq. of Fe-MPIX to the solution of apo-$HasA_p$, whose concentration was determined in advance by UV absorption at 280 nm.

Preparation of $HasA_p$ with Fe-salophen

The salophen ligand and its iron complex were prepared according to a method described in the literature.[25-27] A methanol solution of Fe-salophen·Cl was added to apo-$HasA_p$ in a PBS solution on ice and gently stirred at 4 °C. The mixture was passed through a DE52 column equilibrated with the same buffer and eluted with 20 mM Tris/HCl buffer (pH 8.0) containing 100 mM NaCl. The eluent was applied to an anion exchange (Q column, GE Healthcare) column and eluted with 20 mM Tris-HCl buffer (pH 8.0) containing 600 mM NaCl. The colored fractions were collected, concentrated, and further purified by a gel filtration column (Sephacryl S-200) equilibrated with the PBS solution. The sample buffer was changed to 0.1 M KPi buffer (pH 7.0) and concentrated by using Amicon Ultra (Merck Millipore). The molar extinction coefficient at 281.5 nm of $HasA_p$ with Fe-salophen was estimated to be 48.9 mM^{-1} cm^{-1}. The solution of $HasA_p$ with Fe-salophen used to estimate the molar extinction coefficient was prepared by adding 1.0 eq. of apo-$HasA_p$ to the solution of Fe-salophen. The concentration of apo-$HasA_p$ solution which is used for the estimation was determined in advance by UV absorption at 280 nm.

Preparation of $HasA_p$ with Fe-Phthalocyanine

Fe(II) Phthalocyanine (Fe-Pc) was purchased from TCI and used without further purification. A DMSO solution of Fe-Pc with imidazole as a ligand (imidazole was added until Fe-Pc being dissolved completely) was added to a PBS solution of apo-$HasA_p$ including DMSO (25-50 %). The total amount of DMSO in the resulting

mixture reached to ca. 50 %. After 1 h incubation at 4 ˚C, the mixture was dialyzed against the PBS solution or 20 mM Tris-HCl (pH 8.0) overnight to remove DMSO. To remove nonspecifically bound Fe-Pc, the sample solution was loaded onto a DE-52 column equilibrated with 20 mM Tris-HCl buffer (pH 7.3) and then washed with the same buffer. The target protein was eluted with 20 mM Tris-HCl (pH 7.3) buffer with a linear gradient of NaCl ranging from 0 - 0.4 M. The colored fractions were collected and concentrated using Amicon Ultra. After changing the sample buffer to 0.1 M KPi buffer (pH 7.0), the target protein was further purified by a gel filtration column (Sephacryl S-200) equilibrated with PBS buffer. The concentration of $HasA_p$ with Fe-Fc was estimated by a bicinchoninic acid (BCA) method using apo-$HasA_p$ as a standard. The molar extinction coefficient at 676.0 nm was estimated to be 98.0 mM^{-1} cm^{-1}.

Crystallization of $HasA_p$ with Fe-MPIX

The conditions for crystallization of $HasA_p$ with Fe-MPIX were the same as those for $HasA_p$ with heme. A solution of $HasA_p$ with Fe-MPIX in 0.1 M KPi buffer pH 7.0 was concentrated to 4.96 mM using Amicon Ultra filter units (Merck Millipore). Of the concentrated $HasA_p$ with Fe-MPIX solution, 5 μL was mixed with an equal volume of the reservoir solution composed of 80% PEG400, 100 mM MES, and 100 mM ammonium chloride (pH 6.0). Crystals were grown by a hanging-drop vapor-diffusion method at 20 °C for 1 week.

Crystallization of $HasA_p$ with Fe-Salophen

A 2.5 μL aliquot of the concentrated $HasA_p$ with a Fe-salophen solution (0.90 mM protein in 0.1 M KPi buffer at pH 7.0) was mixed with 2.5 μL of the reservoir solution composed of 50 mM MES buffer (pH 5.25), 1.7 M lithium sulfate, and 12 mM magnesium sulfate. The drop was equilibrated against 700 μL of the reservoir solution. Crystals of $HasA_p$ with Fe-salophen were grown by a sitting-drop vapor-diffusion method at 20 °C for 1 week.

Crystallization of $HasA_p$ with Fe-Phthalocyanine

A 1.5 μL aliquot of the concentrated $HasA_p$ with Fe-Pc solution (0.84 mM in 0.1 M KPi buffer at pH 7.0) was mixed with 1.5 μL of the reservoir solution composed of 0.1 M MES (pH 6.0) and 1.6 M magnesium sulfate. The drop was equilibrated against 100 μL of the reservoir solution. Crystals of $HasA_p$ with Fe-salophen were grown by a sitting-drop vapor-diffusion method at 20 °C for 1 week.

Data Collection and Refinement

Crystals were flash-cooled by liquid nitrogen. X-ray diffraction data sets were collected on beam lines ($HasA_p$ with Fe-MPIX: BL26B1 equipped with an ADSC Quantum 210 CCD detector; $HasA_p$ with Fe-salophen: BL26B2 equipped with an ADSC Quantum 210 CCD detector, and $HasA_p$ with Fe-Pc: BL41XU equipped with an ADSC Quantum 315 CCD detector) at SPring-8 (Hyogo, Japan) with a 1.0 Å wavelength at 100 K. Program HKL2000 was used for integration of diffraction intensities and scaling.[28] The structures of $HasA_p$ with Fe-MPIX, Fe-salophen and Fe-Pc were solved by molecular replacement with MolRep.[29] Model building and refinement were performed by using COOT and REFMAC5.[30, 31] The synthetic metal complex models were generated by using JLigand,[32] and used in the refinement with COOT and REFMAC5. All protein figures were depicted by using PyMOL.[33] The final refinement statistics are summarized in Table 3-1.

RMSD Calculation

For RMSD calculation, each crystal structure data of molecule A was used. All RMSD values were calculated against the crystal structure of HasAp harboring heme (PDB ID: 3ELL, molecule A) by CCP4.

Evaluation of an effect of synthetic metal complexes on the growth of Pseudomonas aeruginosa under Iron-limited Conditions

A single colony of *P. aeruginosa* PAO1 was cultured in 2 mL of M9-based media (1.2% (w/v) $Na_2HPO_4 \cdot 12H_2O$, 0.6% (w/v) KH_2PO_4, 0.1% (w/v) NaCl, 0.2% (w/v) NH_4Cl, 0.2% (w/v) casamino acids, 22 mM glucose, and 0.0002% (w/v) vitamin B1) at 37 °C with shaking at 150 rpm overnight. To 4 mL of an M9-based medium including 40 mM EDTA (ethylenediaminetetraacetic acid, iron ion scavenger) in a glass test tube was added 30 μL of $HasA_p$ with heme or synthetic metal complexes in a PBS solution (33 μM). To this solution, 10 μL of an overnight culture of *P. aeruginosa* PAO1 was added and grown at 37 °C with shaking at 150 rpm for 48 h. To monitor cell growth, 600 μL of the cultured solution was taken every 24 h and its optical density at 600 nm (OD_{600}) was measured. The concentration of the solution of $HasA_p$ with heme used in the experiments was estimated from UV-vis absorption at 406.5 nm. The molar extinction coefficient at this wavelength of $HasA_p$ with heme was estimated to be 120.9 mM^{-1} cm^{-1}. The solution of $HasA_p$ with heme used to estimate the molar extinction coefficient was prepared by adding 1.0 eq. of heme to the solution of apo-$HasA_p$, whose concentration was determined in advance by UV absorption at 280 nm.

Evaluation of Inhibitory Effect of $HasA_p$ with Fe-salophen and Fe-Pc on the Growth of Pseudomonas aeruginosa under Iron-limited Conditions

To 4 mL of an M9-based medium including 40 mM EDTA in a glass test tube was added 20 μL of HasAp with heme (0.1 mM) in a PBS solution and 10 μL of $HasA_p$ with Fe-salophen or Fe-Pc in a PBS solution (0.1 mM). The overnight culture of *P. aeruginosa* PAO1 (10 μL) obtained in the previous section was added to this solution. In the presence of both $HasA_p$ with heme and $HasA_p$ with Fe-salophen or Fe-Pc, *P. aeruginosa* PAO1 was grown at 37 °C with shaking at 150 rpm for 48 h. The cell growth was monitored in the manner described in the previous section.

Evaluation of Toxicity of $HasA_p$ with Fe-Pc in medium without EDTA

To 4 mL of an M9-based medium without EDTA in a glass test tube was added 30 μL of $HasA_p$ with Fe-Pc in a PBS solution (33 μM). As a control experiment, a PBS solution was added in place of a solution of HasAp with Fe-Pc. An overnight culture of *P. aeruginosa* PAO1 (10 μL) obtained in the previous section was added to this solution. In the presence of $HasA_p$ with Fe-Pc, *P. aeruginosa* PAO1 was grown at 37 °C with shaking at 150 rpm for 48 h. The cell growth was monitored in the manner described in the previous section.

Evaluation of Toxicity of $HasA_p$ with Fe-Pc in iron-limited medium containing EDTA

To 4 mL of an M9-based medium including 40 mM EDTA in a glass test tube was added 20 μL of hemin in a PBS solution (0.1 mM) and 10 μL of $HasA_p$ with Fe-Pc in a PBS solution (0.1 mM). As a control experiment, a PBS solution was added in place of a solution of $HasA_p$ with Fe-Pc. An overnight culture of *P. aeruginosa* PAO1 (10 μL) obtained in the previous section was added to this solution. *P. aeruginosa* PAO1 was grown at 37 °C with shaking at 150 rpm for 48 h. The cell growth was monitored in the manner described in the previous section. *P. aeruginosa* can uptake hemin using another heme acquisition system, Pseudomonas heme uptake (Phu) system.[11]

Evaluation of Effect of EDTA on the Growth of Pseudomonas aeruginosa

To 4 mL of an M9-based medium including 40 mM EDTA in a glass test tube was added an overnight culture of *P. aeruginosa* PAO1 (10 μL) obtained in the previous section was added to this solution. *P. aeruginosa* PAO1 was grown at 37 °C with shaking at 150 rpm for 48 h. The cell growth was monitored in the manner described in the previous section.

Estimation of the Cell Number

The overnight culture of *P. aeruginosa* PAO1 obtained in the previous section was diluted 10^5 times. Then, 50 μL of this diluted sample was applied on to a plate and incubated at 37 °C for 18 h. The number of cells in the culture was estimated by simply counting the number of colonies. The initial number of cells used for in *vivo* inhibition experiments was estimated to be $3.4\times10^5\pm0.7\times10^5$ CFU/mL.

CFU: Colony Forming Unit

Reference

[1] M. Rajkumar, N. Ae, M. N. V. Prasad, H. Freitas, *Trends Biotechnol.* **2010**, *28*, 142-149.

[2] M. Miethke, M. A. Marahiel, *Microbiol. Mol. Biol. Rev.* **2007**, *71*, 413-+.

[3] T. E. Clarke, L. W. Tari, H. J. Vogel, *Curr. Top. Med. Chem.* **2001**, *1*, 7-30.

[4] I. J. Schultz, C. Y. Chen, B. H. Paw, I. Hamza, *J. Biol. Chem.* **2010**, *285*, 26753-26759.

[5] S. Cescau, H. Cwerman, S. Letoffe, P. Delepelaire, C. Wandersman, F. Biville, *BioMetals* **2007**, *20*, 603-613.

[6] C. Wandersman, P. Delepelaire, *Annu. Rev. Microbiol.* **2004**, *58*, 611-647.

[7] S. Letoffe, J. M. Ghigo, C. Wandersman, *Proceedings of the National Academy of Sciences of the United States of America* **1994**, *91*, 9876-9880.

[8] S. Letoffe, J. M. Ghigo, C. Wandersman, *J. Bacteriol.* **1994**, *176*, 5372-5377.

[9] N. Izadi-Pruneyre, F. Huche, G. S. Lukat-Rodgers, A. Lecroisey, R. Gilli, K. R. Rodgers, C. Wandersman, P. Delepelaire, *J. Biol. Chem.* **2006**, *281*, 25541-25550.

[10] S. Krieg, F. Huche, K. Diederichs, N. Izadi-Pruneyre, A. Lecroisey, C. Wandersman, P. Delepelaire, W. Welte, *Proc. Natl. Acad. Sci. USA* **2009**, *106*, 1045-1050.

[11] U. A. Ochsner, Z. Johnson, M. L. Vasil, *Microbiol.* **2000**, *146*, 185-198.

[12] M. S. Rossi, J. D. Fetherston, S. Letoffe, E. Carniel, R. D. Perry, J. M. Ghigo, *Infect. Immun.* **2001**, *69*, 6707-6717.

[13] A. Idei, E. Kawai, H. Akatsuka, K. Omori, *J. Bacteriol.* **1999**, *181*, 7545-7551.

[14] S. Letoffe, K. Omori, C. Wandersman, *J. Bacteriol.* **2000**, *182*, 4401-4405.

[15] P. Arnoux, R. Haser, N. Izadi, A. Lecroisey, M. Delepierre, C. Wandersman, M. Czjzek, *Nat. Struct. Biol.* **1999**, *6*, 516-520.

[16] A. Y. Alontaga, J. C. Rodriguez, E. Schonbrunn, A. Becker, T. Funke, E. T. Yukl, T. Hayashi, J. Stobaugh, P. Monne-Loccoz, M. Rivera, *Biochemistry* **2009**, *48*, 96-109.

[17] N. Wolff, N. Izadi-Pruneyre, J. Couprie, M. Habeck, J. Linge, W. Rieping, C. Wandersman, M. Nilges, M. Delepierre, A. Lecroisey, *J. Mol. Biol.* **2008**, *376*, 517-525.

[18] G. Jepkorir, J. C. Rodriguez, H. A. Rui, W. Im, S. Lovell, K. P. Battaile, A. Y.

Alontaga, E. T. Yukl, P. Moenne-Loccoz, M. Rivera, *J. Am. Chem. Soc.* **2010**, *132*, 9857-9872.

[19] Y. Satake, S. Abe, S. Okazaki, N. Ban, T. Hikage, T. Ueno, H. Nakajima, A. Suzuki, T. Yamane, H. Nishiyama, Y. Watanabe, *Organometallics* **2007**, *26*, 4904-4908.

[20] R. Kumar, H. Matsumura, S. Lovell, H. L. Yao, J. C. Rodriguez, K. P. Battaile, P. Moenne-Loccoz, M. Rivera, *Biochemistry* **2014**, *53*, 2112-2125.

[21] S. Letoffe, V. Redeker, C. Wandersman, *Mol. Microbiol.* **1998**, *28*, 1223-1234.

[22] C. Arevalo-Ferro, M. Hentzer, G. Reil, A. Gorg, S. Kjelleberg, M. Givskov, K. Riedel, L. Eberl, *Environ. Microbiol.* **2003**, *5*, 1350-1369.

[23] I. Matsunaga, A. Ueda, T. Sumimoto, K. Ichihara, M. Ayata, H. Ogura, *Arch. Biochem. Biophys.* **2001**, *394*, 45-53.

[24] E. T. Yukl, G. Jepkorir, A. Y. Alontaga, L. Pautsch, J. C. Rodriguez, M. Rivera, P. Moenne-Loccoz, *Biochemistry* **2010**, *49*, 6646-6654.

[25] M. Gerloch, J. Lewis, F. E. Mabbs, A. Richards, *J. Chem. Soc. A* **1968**, 112-&.

[26] B. W. Fitzsimmons, A. W. Smith, L. F. Larkwort, K. A. Rogers, *J. Chem. Soc. Dalton* **1973**, 676-680.

[27] H. Y. Chen, J. A. Cronin, R. D. Archer, *Macromolecules* **1994**, *27*, 2174-2180.

[28] Z. Otwinowski, D. Borek, W. Majewski, W. Minor, *Acta Crystallogr. A* **2003**, *59*, 228-234.

[29] A. Vagin, A. Teplyakov, *J. Appl. Crystallogr.* **1997**, *30*, 1022-1025.

[30] G. N. Murshudov, P. Skubak, A. A. Lebedev, N. S. Pannu, R. A. Steiner, R. A. Nicholls, M. D. Winn, F. Long, A. A. Vagin, *Acta. Crystallogr. D* **2011**, *67*, 355-367.

[31] P. Emsley, K. Cowtan, *Acta. Crystallogr. D* **2004**, *60*, 2126-2132.

[32] A. A. Lebedev, P. Young, M. N. Isupov, O. V. Moroz, A. A. Vagin, G. N. Murshudov, *Acta. Crystallogr. D* **2012**, *68*, 431-440.

[33] W. L. DeLano, **2002**, http://www.pymol.org

Chapter IV

Conclusion

Chapter IV. Conclusion

In this thesis, the author aimed to further understand the relationship between protein structures and functions. She also tried to derive a novel function from the artificial metal proteins.

Chapter II describes enzymatic hydroxylation reactions of aromatic rings by myoglobin mutants. Because the aromatic C-H bond hydroxylation is one of difficult oxidations, it is challenging to perform the aromatic C-H bond hydroxylation by myoglobin. In this study, the author succeeded to the aromatic ring hydroxylation of methoxynaphthalene and naproxen by rationally designed myoglobin mutants. The author also found that the H64D/T67R/V68I myoglobin mutant showed higher hydroxylation activity for (*S*)-naproxen over (*R*)-naproxen while H64D/V68I mutant oxidize both isomers at the same rates, indicating that the H64D/T67R/V68I mutant recognized the chirality of naproxen. In addition, it was shown that naproxen is a useful substrate to examine the activity of aromatic hydroxylation and the selectivity of substrate chirality catalyzed by enzymes. The author believes that the result obtained hereby would contribute to further improvement of the catalytic activity of man-made enzymes and to understanding the relationship between protein structures and functions.

Chapter III describes that artificial metal complexes can be captured by a heme acquisition protein of *Pseudomonas aeruginosa*, $HasA_p$. This chapter describes effects of the $HasA_p$ carrying artificial metal complexes other than heme upon the growth of *P. aeruginosa*. $HasA_p$ can capture synthetic metal complexes having a planner structure without any remarkable structural perturbation of $HasA_p$. The crystal structures of Fe-mesoporphyrin IX (Fe-MPIX), Fe-salophen, and Fe-phthalocyanine (Fe-Pc) bound to $HasA_p$ were determined by X-ray structure analysis at atomic resolution, respectively. The author found that $HasA_p$ harboring Fe-Pc inhibited heme

acquisition of *P. aeruginosa*. It is suggested that high hydrophobicity of the artificial metal complex would contribute to inhibition of the heme acquisition by *P. aeruginosa*. *P. aeruginosa* is one of bacteria causing hospital infection due to multi-antibiotics resistant. The author expects that these findings regarding the growth inhibition of *P. aeruginosa* by $HasA_p$ harboring Fe-Pc could lead to the development of elimination systems for multi-drug resistance and contribute to further understanding the acquisition mechanisms of foreign substrates. The author also expects that the growth inhibition by $HasA_p$ harboring Fe-Pc could be applicable to include other pathogenic bacteria, such as *Serratia marcescens*, *Pseudomonas fluorescens*, and *Yersinia pestis* having Has system.

Through the research described in this thesis, the author demonstrated that artificial metal proteins can be rationally prepared based on crystal structures of the target proteins. Furthermore, not only the artificial metal enzymes but also the artificial metal protein with ability to block heme acquisition of bacteria can be developed by rational design of proteins. While the author focused on myoglobin and $HasA_p$, both of them utilize heme, molecular design of artificial metalloproteins and metalloenzymes other than heme proteins based on the target protein structures as well as their reaction mechanisms can be possible.

Acknowledgement

The research presented in this thesis has been carried out at the Department of Chemistry, Graduate School of Science, Nagoya University under the supervision of Professor Yoshihito Watanabe. He has provided me with the opportunity to work professionally in the field of chemistry. I am incredibly thankful to Prof. Watanabe for his continuous guidance, stimulating discussions, and hearty encouragement. I am greatly indebted to Associate professor Osami Shoji for his persistent coaching, constant encouragement, support and guidance on the details of my doctorate. I would also like to express my utmost gratitude to Prof. Bernhard Wünsch for his affectionate support and guidance during my study in Germany from September 2011 to December 2011, continuing even after my stay. I am deeply grateful to Dr. Dirk Schepmann for his kind and gentle instruction in Münster.

I would like to express my heartfelt thanks to Associate professor Hiroshi Nakajima for his many constructive discussions during my doctorate. I am grateful to Prof. Takafumi Ueno, Dr. Takashi Fukushima, Dr. Yusuke Takezawa, Dr. Norifumi Kawakami, and Dr. Takashi Fujishiro for their invaluable guidance and helpful suggestions during the primary steps of my chemistry research. I am indebted to all members of the Watanabe laboratory, especially Ms. Yoshiko Morimoto, Mr. Mitsuyoshi Terada, Mr. Yusuke Iwai, and Ms. Ayaka Nakashima for their cooperation, productive discussions and loving encouragement. Moreover, I am thankful to Dr. Christian Wiese, Dr. Xu Jiakun and Mr. Takahiro Ohki for their kind support on my myoglobin research. I am grateful to Ms. Makiko Mizuno and Ms. Chie Kasai for their efficient management of the research group. The assistance of Mr. Joshua Kyle Stanfield on all matters English is highly appreciated. To all members of Prof. Wünsch group, I would like to express my sincere gratitude, especially Dr. Andre Benner, Dr. Stefanie Brune, Dr. Anna Junker, and Mr. Bastian Frehland, which due to their kindhearted support, enabled me to spend a wonderful time in Münster.

I would like to express my gratitude to Prof. Shin-ichi Ozaki for his invaluable discussions and his generous offer of $HasA_p$ expression systems. I am thankful to Prof. Yoshitsugu Shiro and Dr. Hiroshi Sugimoto for their helpful assistance and discussions on collection of X-ray crystallographic analysis data. I would like to sincerely thank Dr. Kin-ichi Oyama for his meticulous machine maintenance and other support offered pertaining the use of chemical instruments at the Research Center for Materials Science at Nagoya University. I am deeply thankful to Dr. Nobuyuki Takatani for his kind assistance with several biological experiments.

This study was supported by the Global COE program in chemistry of Nagoya University “Elucidation and Design of Materials and Molecular Functions” and the program for Leading Graduate Schools “Integrative Graduate Education and Research Program in Green Natural Sciences” by MEXT Japan. The IRTG programme Münster-Nagoya enabled my research in the Prof. Wünsch group and provided me with the financial support for my life in Münster.

Finally, I am wholeheartedly thankful to all my friends and teammates for their loving encouragement; and I genuinely appreciate my family's faith in me at all times. In addition, I appreciate the financial support offered to me by my parents during my study over the years.

July 8th 2014 Chikako Shirataki

白瀧 千夏子

List of Publications

[1] Inhibition of Heme Uptake in *Pseudomonas aeruginosa* by its Hemophore ($HasA_p$) Bound to Synthetic Metal Complexes
C. Shirataki, O. Shoji, M. Terada, S. Ozaki, H. Sugimoto, Y. Shiro, and Y. Watanabe
Angew. Chem. Int. Ed. **2014**, *53*, 2862–2866. (selected as the inside cover of the issue)

[2] Aromatic C–H bond hydroxylation by P450 peroxygenases: a facile colorimetric assay for monooxygenation activities of enzymes based on Russig's blue formation
O. Shoji, C. Wiese, T. Fujishiro, C. Shirataki, B. Wünsch, and Y. Watanabe
J. Biol. Inorg. Chem. **2010**, *15,* 1109–1115.

[3] GluN2B-Selective N-Methyl-d-aspartate (NMDA) Receptor Antagonists Derived from 3-Benzazepines: Synthesis and Pharmacological Evaluation of Benzo[7]annulen-7-amines
A. Benner, A. Bonifazi, C. Shirataki, L. Temme, D. Schepmann, W. Quaglia, O. Shoji, Y. Watanabe, C. Daniliuc, and B. Wünsch
ChemMedChem **2014**, *9*, 741–751.